University of Alberta

High Sensitivity Surface Enhanced Raman Scattering Detection of Tryptophan

by

Archana Kandakkathara

A thesis submitted to the Faculty of Graduate Studies and Research in partial fulfillment of the requirements for the degree of

Doctor of Philosophy

in

Photonics and Plasmas

Department of Electrical and Computer Engineering

Fall 2012
Edmonton, Alberta

To my parents

Abstract

Raman spectroscopy has the capability of providing detailed information about molecular structure, but the extremely small cross section of Raman scattering prevents this technique from applications requiring high sensitivity. Surface enhanced Raman scattering (SERS) on the other hand provides strongly increased Raman signal from molecules attached to metallic nanostructures. SERS is thus a promising technique for high sensitivity analytical applications. One particular area of interest is the application of such techniques for the analysis of the composition of biological cells. However, there are issues which have to be addressed in order to make SERS a reliable technique such as the optimization of conditions for any given analyte, understanding the kinetic processes of binding of the target molecules to the nanostructures and understanding the evolution and coagulation of the nanostructures, in the case of colloidal solutions. The latter processes introduce a delay time for the observation of maximum enhancement factors which must be taken into account for any given implementation of SERS.

In the present thesis the goal was to develop very sensitive SERS techniques for the measurement of biomolecules of interest for analysis of the contents of cells. The techniques explored could be eventually be applicable to microfluidic systems with the ultimate goal of analyzing the molecular constituents of single cells. SERS study of different amino acids and organic dyes were performed during the course of this thesis. A high sensitivity detection system based on SERS has been developed and spectrum from tryptophan (Trp) amino acid at very low concentration (10^{-8} M) has been detected. The concentration at

which good quality SERS spectra could be detected from Trp is 4 orders of magnitude smaller than that previously reported in literature. It has shown that at such low concentrations the SERS spectra of Trp are qualitatively distinct from the spectra commonly reported in literature. These distinctions are attributed to the unique binding geometry of Trp molecules to the small silver nanoclusters at these low concentrations.

Background electrolytes in the solution can have a significant role in SERS experiment as it helps in the binding of molecules to the metallic structures and stabilizes the colloid in some cases We performed a study of effects of different electrolytes and an optimization of electrolytes has been carried out, which leads to the high enhancement reported in this thesis. The SERS detection has also been performed in microfluidic and flow cell geometries which enable a combination of high sensitivity of the SERS with the low volume requirements of microfluidic devices. A Teflon AF capillary was used for performing liquid core waveguide (LCW) SERS measurements. With this geometry the enhancement obtained was about a factor of 10 compared to that from cuvette so the detection limit could be further decreased by a factor of 10 in LCW reaching 10^{-9} - 10^{-10}M for Trp amino acid. The enhanced sensitivity and better understanding of the optimum conditions for SERS developed in the thesis are important since they now could allow the possibility of assays of the chemical constituents of single cells in future microfluidic systems.

Acknowledgements

I would like to express my sincere gratitude to my supervisor Dr. Robert Fedosejevs for giving me the opportunity to work in his group. I am thankful for his encouragement, guidance and support throughout the project. I would like to thank Dr. Ilya Utkin for his valuable suggestions and help. I really appreciate the countless discussions we had during the project. I thank Professors Ying Tsui, James McMullin, Chris Backhouse, Wofgang Jaeger, Roger Zemp, Zubin Jacob and Alexandre Brolo for being part of my thesis and candidacy committee. I am thankful for the great technical support from Blair Harwood, Rick Conrad, Steve Drake at numerous stages during the course of the thesis. I am also thankful to other group members, Zahid, Yogesh, ,Christina, Chin-Kuei Wen, Lei Pan, Henry, Shyama, Raj, Sunita, Fatema and all the rest for their help and valuable support. I would like to acknowledge Dr. Saneej's help with Monte- Carlo simulation and Abhay for his help with LATEX.

I thank all my friends for their encouragement and support. Special thanks to Vitna and her family for their help during my final exam and Swaroop and Esha for their help and guidance. I would like to express my special gratitude to my parents, brother, and sister. Thank you all for the love and selfless support. I also would like to thank my parents in law for their support and understanding, specially my mother in law, Jayanthi Sadasivan for her help. Finally, I would like to thank my husband Saji for his love, understanding and patience and my little one Shanku for bringing me so much joy.

Table of Contents

List of Tables

List of Figures

List of Symbols and Abbreviations

SERS	Surface Enhanced Raman Scattering
NRS	Normal Raman scattering
P	Electric dipole moment
EM	Electromagnetic
SP	Surface Plasmons
LUMO	Lowest unoccupied molecular orbital
HOMO	Highest occupied molecular orbital
CCD	Charged coupled device
Trp	Tryptophan
Phe	Phenylalanine
Gly	Glycine
LCW	Liquid core waveguide
DI	Deionized water
AO	Acridine Orange
RhB	Rhodamine B
Rh6G	Rhodamine 6G
TEM	Transmission electron microscopy
SEM	Scanning electron micrscopy
UV	Ultra violet
SM	Single molecule

TERS	Tip enhanced Raman spectroscopy
AFM	Atomic force microscopy
STM	Scanning tunneling microscopy

Chapter 1

Introduction

1.1 Motivation

When light is scattered from an atom or a molecule, most photons are elastically scattered such that the scattered photons have the same energy and wavelength as the incident photons. However, a small fraction of the scattered photons have a frequency (energy) different from, and usually lower than, the frequency of the incident photons. This phenomenon of inelastic scattering of light was first postulated by A. Smekal in 1923 [7] and first observed experimentally in 1928 by C. V Raman and K.S Krishnan [8]. In 1930, Sir C. Venkata Raman received the Nobel Prize for this observation and Raman spectroscopy soon became an important source of information on molecular structure and dynamics. The advent of laser light sources with monochromatic photons at high flux densities resulted in dramatically improved scattering signals and Raman Spectroscopy became a more powerful technique [9]. Availability of lasers with a wide range of frequencies from near ultraviolet to near infrared region, allows the selection of optimum excitation conditions for each sample of interest. Measuring a Raman spectrum does not require special sample preparation techniques in contrast with infrared absorption spectroscopy. The main

advantage of Raman spectroscopy is its capability to provide rich information about the molecular structure of the sample.

Despite all these favorable aspects, Raman spectroscopy is not considered as a powerful tool for ultra-sensitive detection, because of the extremely small cross section of Raman scattering, typically 10^{-31}-10^{-29} cm^2/molecule [2]. Surface enhanced Raman scattering (SERS) is a phenomenon of strongly increased Raman signal from molecules attached to metallic nano structures. SERS was observed about 50 years after the discovery of the Raman effect by Fleischman et al. [10]. The basic motivation for SERS is its potential to overcome the low sensitivity problems inherent in Raman spectroscopy [11]. SERS combines laser spectroscopy with the optical properties of metallic nano structures resulting in strongly increased Raman signals when molecules are attached to nanometer sized metal substrates. SERS overcomes the low sensitivity problems in Raman spectroscopy and has become an intense area of research by providing a high sensitivity equivalent of fluorescence and the structural information of Raman spectroscopy. SERS soon became a promising analytical technique and now SERS has applications in various disciplines. With enhanced Raman signals, SERS offers increased sensitivity and detection limits, this improves the existing Raman applications and even can apply to systems which can not be analyzed with conventional Raman spectroscopy.

Recently there has been considerable interest in studying biologically important molecules like amino acids and peptides using SERS [12–17]. These studies are important as amino acids and peptides are the basic building blocks of proteins and a fundamental knowledge of their interactions with metal nanoparticles can help in the understanding of the SERS effect of more

complicated biological molecules which would be useful for the development of bio sensors. Therefore it is important to carry out SERS studies of these amino acids and peptides and establish sensitive detection limits.

The SERS technique has also been used in microfluidic and flow cell geometries which enable a combination of high sensitivity SERS with the low volume requirement of microfluidic devices [18–20]. Lab on a chip technology has recently been developed to perform a variety of biological analyses [21,22]. This technology has several advantages compared with conventional bench-top techniques like minimal sample requirement, reduced reaction time etc. The optimization of detection systems is a key issue in determining the applicability of a microfluidic system. Because of the extremely small volume in a microfluidic channel, a highly sensitive system is required for the detection of analytes. Fluorescence spectroscopy has been the most widely used detection technique because of its high sensitivity and low detection limits for biologically relevant species [23]. However many biological/ chemical species do not fluoresce and therefore need to be treated with fluorescence tags to allow on-chip detection. Furthermore the broad fluorescence spectrum can cause the overlapping of peaks in multiplexed biological detection. SERS is a promising technique for lab on a chip detection with its enhanced sensitivity also its capability to simultaneously detect multiplexed analytes because of its narrower spectral features [24].

In the present thesis the goal was to develop very sensitive SERS techniques for the measurement of biomolecules of interest for analysis of the contents of cells. In particular, techniques were explored which could eventually be appli-

cable to microfluidic systems with the ultimate goal of analysing the molecular constituents of single cells. In order to do this, in the present thesis different amino acids have been studied with SERS and conditions for observing reproducible SERS spectra have been obtained. The lowest concentration at which we detected tryptophan (trp) amino acid is 3 to 4 orders of magnitude smaller than that previously reported in the literature [1, 25, 26] and the Raman enhancement observed is about 10^8, which is several orders of magnitude stronger than reported before [1]. We have also studied amino acid Trp in a microfluidic chip geometry to explore this capability. Laser micro machining has been employed to increase the scattering length in a standard microfluidic chip to enhance the signals obtained. SERS detection in a Teflon AF capillary was also performed. This liquid core waveguide geometry provides longer excitation and collection lengths and requires much smaller volumes of samples compared to the case of a standard cuvette [27–29]. The detected SERS signal from a Teflon AF waveguide was increased by a factor of 10 compared to that from a cuvette. To our knowledge this is the first observation of SERS in a Teflon AF capillary [30].

The observed enhanced spectra in SERS is due to contributions from different factors. The factors can be case specific and it is almost impossible to separate them into well defined components. Therefore it is important to closely analyze the variables involved in observation of SERS spectra. Background electrolytes in the solution can have a significant role in the observation of SERS signal from molecules and so the selection of electrolyte is important. The electrolytes help with the binding of molecules to the substrate and helps in colloid aggregation. We performed a study of effects of different electrolytes

and made comparison of the enhancement factors we observed using different electrolytes. A composite electrolyte has been developed which gives reproducible SERS spectra with high enhancement for tryptophan amino acid and also for some of the other samples studied.

1.2 Outline

The background of Raman scattering and SERS are outlined in chapter 2. Raman scattering mechanism and surface enhanced Raman scattering are explained along with the details of SERS enhancement mechanisms and SERS active substrates. Application of SERS in different areas is also discussed in this chapter.

Chapter 3 describes the experimental methodologies, including the experimental set up and its calibration. A schematic diagram of the experimental setup is given here. Absorption spectrum measurements and the silver colloid preparation method also are described.

Detection of different amino acids and peptides is described in chapter 4. The conditions for obtaining SERS spectrum from, tryptophan (Trp), phenylalanine (Phe), glycine (Gly), Trp-Trp and Gly-Gly-Gly are described and the SERS spectrum from these are explained, also the enhancement factors observed for different samples are given.

Chapter 5 describes the SERS detection in a microfluidic system and in a liquid core waveguide. The experimental layout is described. A comparison is made between the the SERS spectrum observed in these systems to that observed in cuvette.

A sensitive detection technique for low concentration measurement of Trp amino acid is described in chapter 6. The high enhancement factor observed

and the concentration range studied are described.

Chapter 7 gives the details of the various electrolytes we tested and used for SERS measurements. The conditions for observing SERS spectra with each electrolyte is explained. A comparison of the enhancement factors observed using different electrolytes is also made .

A numerical simulation based on Monte-Carlo method has developed to better understand the process of colloid aggregation and the time of evolution of SERS signals. The details of this are given in chapter 8.

Chapter 9 is the summary of the thesis. This chapter also discusses further issues that might be interesting for future investigation.

Chapter 2

Theory and Background of Surface Enhanced Raman Scattering

2.1 Introduction

The first observation of SERS was reported in 1974 by Fleischmann et al. [10] for pyridine adsorbed on an electrochemically roughened silver electrode and it was proposed that the the enhanced signal is due to the increased surface area. The idea of increased surface area was appealing because of its simplicity and seemed to be the natural explanation for observed signal enhancements. However many questions could not be answered by this hypothesis. In some cases the signals would actually weaken when the roughness of the surface was increased. Two independent and simultaneous works by Jeanmaire and Van Duyne [11] and Albrecht and Creighton [31] recognized that the large intensities observed could not be accounted for simply by the increase in number of scatterers and proposed that the enhancement must be caused by a true enhancement in the Raman scattering efficiency itself. Jeanmaire and Van Duyne tentatively proposed an electric field enhancement mechanism and Albrecht and Creighton proposed that resonance Raman scattering from molec-

ular electronic states broadened by their interaction with metal surface might be responsible. Soon after that strongly enhanced Raman signals were verified for many molecules attached to metallic nano structures which have sizes on the order of tens of nanometers and these nano structures are called SERS active substrates [32]. The metallic nano structures used were rough metal surfaces or colloidal nanoparticles. These experiments showed that SERS is not so much a surface effect as it is a nano structure effect.

SERS was an active research field in the 1980's and most of the theoretical aspects of SERS developed in this early stage. The initial SERS studies have been well summarized by Moskovits in 1985 [33]. The research activities in SERS appear to have faded in the following decade. The ongoing improvements in Raman instrumentation made this technique available to researchers in various fields of science and engineering and with the development of advanced nano science and nano technology techniques SERS again became an active field of research in the last decade; the demonstration of single molecule detection with SERS also has stimulated this technique. Raman enhancement factors on the order of 10^3- 10^6 have been reported in the first reports on SERS. Later, enhancement factors in the range of 10^8-10^{11} have been claimed for many molecules [34–36] and for single molecule detection the enhancement factors reported were 10^{14}-10^{15} [37, 38]. Recently it has been reported that enhancement in the order of 10^6 to 10^8 is sufficient for single molecule detection [39, 40]. Work is still going on in the fundamental understanding of SERS but most of the research is on its applications. The multi-disciplinary nature and the high specificity of Raman technique together with improved sensitivity of SERS made this an attractive and a promising technique. Today SERS is

an active area of research. SERS provides a unique fingerprint of molecules and its signatures can be easily distinguished from the background signals. Also it allows the possibility to simultaneously monitor many samples. SERS can be directly applied to any molecule unlike fluorescence spectroscopy, which requires the presence of a fluorophore and it can work at any excitation wavelength with proper substrates. Infrared excitation has important applications in living tissues, which are not possible with fluorescence spectroscopy which is limited to the visible wavelength range.

2.2 Raman Scattering

The Raman effect, a scattering process between a photon and a molecule is an important spectroscopic technique for studying the vibrational, rotational and other low frequency modes in a system. Incident photons of energy $h\nu_L$ are inelastically scattered from a molecule and shifted in frequency by the energy of characteristic molecular vibrations $h\nu_M$. The scattered photons can occur at lower and higher energies relative to the incoming photons, depending on whether they interacted with a molecule in the vibrational ground state or an excited vibrational state. When interacting with vibrational ground state, photons lose energy by exciting a vibration and the scattered light appears at a lower frequency ν_S, called Stokes scattering. By interacting with a molecule in an excited vibrational state, the photons gain energy from the molecular vibrations and the scattered signal appears at higher frequency ν_{aS} called anti-Stokes scattering. Raman scattering is illustrated schematically in Fig. 2.1

The energy difference between the initial and final vibrational levels or

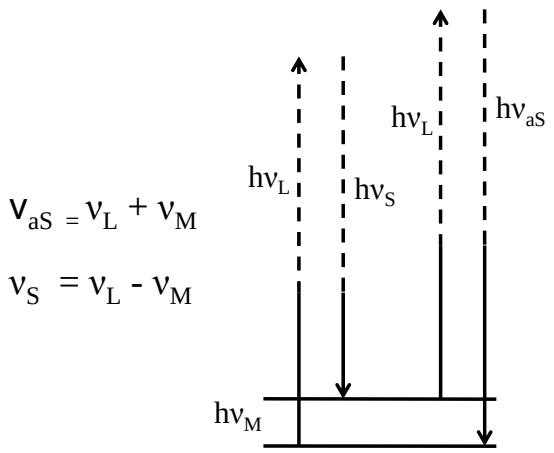

Figure 2.1: Schematic diagram of Raman scattering.

Raman shift in wavenumber (cm^{-1}) is calculated as,

$$\overline{\nu} = \frac{1}{\lambda_{inc}} - \frac{1}{\lambda_{sc}} \tag{2.1}$$

Where λ_{inc} and λ_{sc} are the wavelengths (in cm) of the incident and Raman scattered photons respectively.

Raman scattering can be explained using classical theory as follows [41]. The electric field strength of an electromagnetic wave is given by,

$$E = E_0 cos 2\pi\nu_0 t, \tag{2.2}$$

Where E_0 is the amplitude and ν_0 is the frequency of the incident electromagnetic wave. If a diatomic molecule is irradiated by this wave, an electric dipole moment P is induced,

$$P = \alpha E = \alpha E_0 cos 2\pi\nu_0 t, \tag{2.3}$$

Where α, the proportionality constant is called polarizability. If the molecule

is vibrating with a frequency ν_m, the nuclear displacement is,

$$q = q_0 cos 2\pi\nu_m t, \tag{2.4}$$

Where q_0 is the vibrational amplitude. For a small amplitude of vibration, α is a linear function of q. Thus,

$$\alpha = \alpha_0 + \left(\frac{\partial\alpha}{\partial q}\right)_0 q + ... \tag{2.5}$$

where α_0 is the polarizability at the equilibrium position and $\left(\frac{\partial\alpha}{\partial q}\right)_0$ is the rate of change of α with respect to the change in q evaluated at the equilibrium position. Combining Eqs. 2.3, 2.4 and 2.5

$$P = \alpha E_0 cos 2\pi\nu_0 t$$

$$= \alpha_0 E_0 cos 2\pi\nu_0 t + \left(\frac{\partial\alpha}{\partial q}\right)_0 q E_0 cos 2\pi\nu_0 t$$

$$= \alpha_0 E_0 cos 2\pi\nu_0 t + \left(\frac{\partial\alpha}{\partial q}\right)_0 q_0 E_0 cos 2\pi\nu_0 t cos 2\pi\nu_m t$$

$$= \alpha_0 E_0 cos 2\pi\nu_0 t + \frac{1}{2}\left(\frac{\partial\alpha}{\partial q}\right)_0 q_0 E_0 [cos 2\pi(\nu_0 + \nu_m)t + cos 2\pi(\nu_0 - \nu_m)t]. \tag{2.6}$$

The first term represents an oscillating dipole that radiates light of frequency ν_0, called Rayleigh scattering, the second term corresponds to Raman scattering of frequency ν_0+ν_m called anti-stokes and the third represents Raman scattering at frequency ν_0-ν_m called Stokes scattering. If $\left(\frac{\partial\alpha}{\partial q}\right)_0$ is zero , the vibration is not Raman active. Because the change in polarizability with nuclear displacement is small the effective cross section for Raman scattering is

small which is the major disadvantage of Raman scattering as an analytical technique. Typical Raman cross sections are between 10^{-31} and 10^{-29} cm^2 per molecule [2], which is many orders of magnitude smaller than that of the fluorescent cross section (10^{-16} cm^2 per molecule). This small scattering cross section of Raman scattering spectroscopy is a major issue and this prevents this spectroscopic technique from high sensitivity applications in spite of its advantages. The enhancement of Raman intensity obtained in SERS increases the detection limit or sensitivity therefore the SERS technique combines the specificity of Raman with high sensitivity and is a promising technique for analytical applications.

2.3 Surface Enhanced Raman scattering

Surface enhanced Raman scattering is a phenomenon of enhanced Raman signals, when the molecules are close to some metallic nano structures. SERS combines modern laser spectroscopy with the optical properties of metallic nano structures, resulting in strongly increased Raman signals. SERS is relatively new technique which has been used successfully to enhance the Raman signals.

In normal Raman scattering , the total Stokes Raman signal is proportional to the Raman cross section ${\sigma^R}_{free}$, the excitation laser intensity I(ν_L) and the number of molecules N in the probe volume [42].

$$I_{NRS}(\nu_S) = NI(\nu_L)\sigma^R_{free} \tag{2.7}$$

In SERS the molecules are attached to metallic nano structures, the surface enhanced Stokes Raman signal I_{SERS} is proportional to the Raman cross

section of adsorbed molecules ${\sigma^R}_{ads}$, the excitation laser intensity I(ν_L) and the number of molecules involved in the SERS process N_{SERS} [42].

$$I_{SERS}(\nu_L) = N_{SERS} I(\nu_L) \mid A(\nu_L) \mid^2 \mid A(\nu_S) \mid^2 \sigma^R_{ads} \tag{2.8}$$

where A(ν_L) and A(ν_S) are the field enhancement factors at the incident and scattered frequency, respectively. The enhancement mechanisms and the substrates used in SERS are discussed in the following sections.

2.3.1 Enhancement mechanisms in SERS

Many mechanisms were proposed for SERS in its early days and some of them turned out to be wrong. There are mainly two mechanisms which contribute to the enhancement, the first one is the electromagnetic mechanism which contributes to a major part of the enhancement in SERS and the second is the chemical mechanism. As their name indicates the electromagnetic mechanism focuses on the enhanced electric fields supported on the metallic nano surfaces and the chemical mechanism deals with the changes in the electronic structure of the molecules which occur due to their adsorption on the metal surfaces. Most studies show that the chemical enhancement is much lower than electrical enhancement [2, 43].

The electromagnetic mechanism(EM) explains that the enhancement is primarily due to localized surface plasmon resonance. Surface plasmons (SP) are light waves trapped on the surface of a conductor because of their interaction with the free electrons of the conductor. While interacting, the free electrons oscillate collectively in resonance with the light wave. The resonant interaction between the surface charge oscillation and electromagnetic field of light

constitutes SPs [44]. Surface plasmon resonance causes the formation of high electric field at the surface of the metal particle and this field decays rapidly away from the surface. For analyte molecules adsorbed on the surface of metallic nano structures or in the close proximity to the metallic nano structures the incident field is enhanced due to surface plasmon resonance. In the same way the scattered field also will be enhanced if it is in resonance with the surface plasmons of the metallic surface [2]. A schematic diagram for understanding the concept of electromagnetic enhancement is shown in Fig. 2.2.

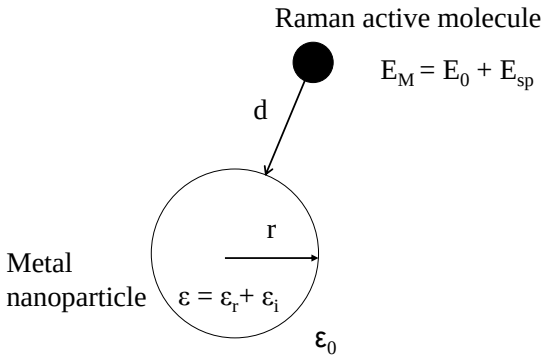

Figure 2.2: Schematic diagram for understanding the concept of electromagnetic SERS enhancement. Adapted from Kneipp et al. [2].

The EM mechanism can be explained as described by Kneipp el al [2]. In the schematic digram shown for understanding EM mechanism, the SERS substrate is a small metal sphere with complex dielectric constant $\epsilon(\nu) = \epsilon_r + \epsilon_i$, where ν is the frequency and ϵ_r , ϵ_i are the real and imaginary part of the dielectric constant of metal. The dielectric constant of the surrounding medium is ϵ_0. The diameter of the sphere 2r is assumed to be much smaller than the wavelength of light λ (Rayleigh limit). A Raman active molecule is placed at a distance d from the metal nano particle and is irradiated with an incident electromagnetic filed E_0. The incident field induces a dipole moment

in the metal nano particle with a field E_{SP}. The field experienced by the molecule E_M is then the superposition of incident field and the field of the dipole induced in the metal particle, given by:

$$E_M = E_0 + E_{SP} \tag{2.9}$$

$$E_{SP} = r^3 \frac{\epsilon - \epsilon_0}{\epsilon + 2\epsilon_0} E_0 \frac{1}{(r+d)^3} \tag{2.10}$$

The enhancement experienced by the molecule is represented as the field enhancement factor $A(\nu)$ and is the ratio of the field at the position of molecule in the presence of metal nanoparticle and the incident field.

$$A(\nu) = \frac{E_M(\nu)}{E_0(\nu)} \sim \frac{\epsilon - \epsilon_0}{\epsilon + 2\epsilon_0} \frac{r^3}{(r+d)^3} \tag{2.11}$$

Eq.2.11 shows that the enhancement factor $A(\nu)$ is strong when the real part of dielectric constant, $\epsilon(\nu)$ is equal to -$2\epsilon_0$. In addition the imaginary part of dielectric constant needs to be small for strong electromagnetic enhancement. These conditions describe the resonant excitation of surface plasmons of the metal sphere. In addition to the incident laser field the scattered Stokes or anti stokes field also will be enhanced if it is in resonance with the surface plasmons of the metal sphere. The SERS enhancement factor is defined as the ratio of the Raman scattered intensity in the presence of the metal particle to its value in the absence of the metal particle [45]. Taking into account these enhancement effects of the laser field and the Stokes field, the total electromagnetic enhancement factor $G_{em}(\nu_S)$ can be written as

$$G_{em}(\nu_S) =\mid A(\nu_L) \mid^2 \mid A(\nu_S) \mid^2 \sim \mid \frac{\epsilon(\nu_L) - \epsilon_0}{\epsilon(\nu_L) + 2\epsilon_0} \mid^2 \mid \frac{\epsilon(\nu_S) - \epsilon_0}{\epsilon(\nu_S) + 2\epsilon_0} \mid^2 (\frac{r}{(r+d)})^{12} \tag{2.12}$$

where $\mid A(\nu_L)\mid^2$ and $\mid A(\nu_S) \mid^2$ are the enhancements factors for the incident laser field at frequency ν(L) and the Raman scattered field at frequency ν(S) respectively. The enhancement scales as fourth power of the local field of the metallic nano particle and is strong when the excitation and scattered fields are in resonance with the surface plasmons. The electromagnetic enhancement does not require direct contact between molecule and metal, but is strongly dependent on the distance between them as shown in Eq.2.12. The enhancement decreases with growing distance as $(1/d)^{12}$ for d>r. Maximum values of electromagnetic enhancement for single silver colloidal particles and gold spheroids which have been reported are on the order of 10^6 - 10^7 [2,46,47]. Stronger enhancements have been predicted for sharp features and large curvatures on metal surfaces [35]. An enhancement of the order of 10^{11} has been reported for closely spaced interacting particles [35, 36]. This strong increase in the enhancement for dimers is due to the coupling of plasmon resonance and also due to the presence of two interfaces which localize the potential drop to a confined region which localize the enhanced field to the confined region between the two nanoparticles forming the dimer [35].

Different models have been used for the investigation of electromagnetic fields induced by optical excitation of localized surface plasmon resonance of metallic nanoparticles [48–52]. These models have studied the shape, size and arrangement of particles which leads to the increased local field enhancements. Recently the details of electric field enhancement caused by nano particle ag-

gregates has been investigated by a few groups [3, 53, 54]. Mock et al. studied the effect of gold nano particle clusters on SERS intensity. They studied both spherical and cylindrical nanoparticles. According to their experimental and theoretical results; for spherical particles when the cluster size increases from 2 to 5 the SERS enhancement remained approximately the same, on the order of 4×10^4 for a probe wavelength of 632nm. For cylindrical particles they experimentally observed higher enhancement than spherical particles and the enhancement increase with cluster size [3]. The calculated fields for a single gold particle and nano clusters of varying number and geometry reproduced from [3] are given in Fig. 2.3.

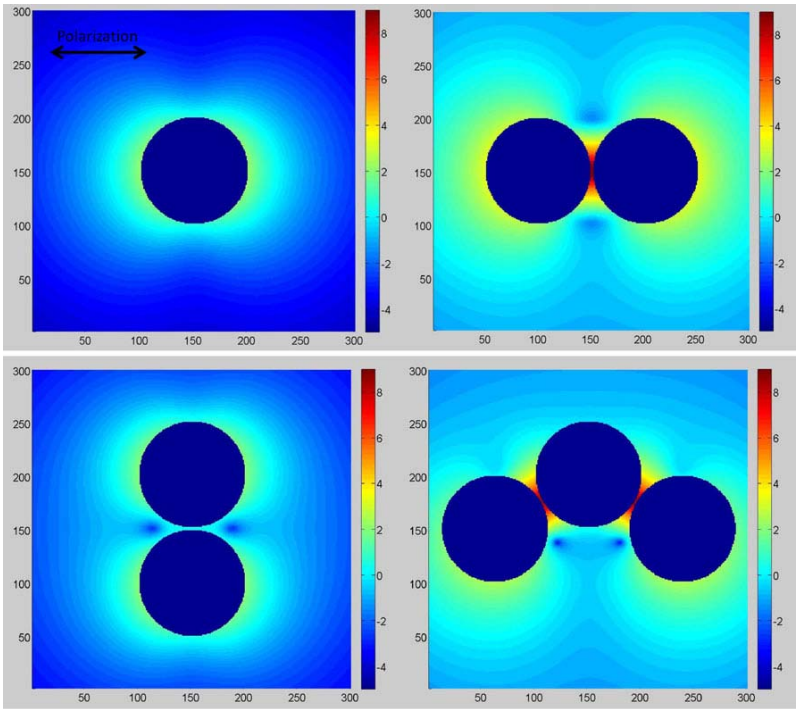

Figure 2.3: Calculated E field intensity for a single gold particle and gold nanoparticle aggregates with 2 nm spacing for linearly polarized incident light. Reproduced from Mock et al [3](Reproduced by permission of Springer).

Xu et al. [51] reported calculation of EM enhancement factors of spherical and nano crystal shaped particles composed of silver and gold. They predicted

a maximum electromagnetic enhancement on the order of 10^{11} for dimer configurations of silver particles with inter particle separation of 1nm and sharp protrusions in nano structures. They observed lower enhancement for gold nanoparticles than for silver. Single spherical and nano crystal shaped particles produce comparatively weak EM enhancement effects. The enhancement shown in Fig. 2.3 for the case of gold nanoparticles separated by 2 nm spacing is lower than estimated in [51]. This can be due to the difference in inter particle separation and particle sizes in both cases. The use of discrete dipole approximation to study the electromagnetic field induced by silver nanoparticles is described by Hao et al. [52]. They calculated the electromagnetic enhancement factor for isolated silver nanoparticles and pairs of nanoparticles separated by a few nanometers. Spherical and triangular particles were considered. According to their findings for individual particles the electromagnetic enhancement factor is always less than 10^8. For dimer particles the enhancement factor is close to 10^{10} for structures with particle separation of 2 nm and the enhancement factor is a strong function of separation distance. They state that the largest enhancement occurs for separations that are very small. They also found that other structural properties of dimers such as local curvature, play a less important role in determining the E-field enhancements. A two dimensional electromagnetic model described by Brown et al. [55] for Raman enhancement around two silver nanoparticles shows that there is strong dependence of Raman enhancement on the separation between particles. The smaller the distance between the nanoparticles the larger the observed enhancement. The difference in predicted Raman enhancement for two nanoparticles 1 nm apart and 25nm apart can be as much as six orders of magnitude. The predicted maximum enhancement is in the order of $\sim 10^9$ and

they state that the predicted enhancement agrees within an order of magnitude of that has been observed experimentally in literature. The authors also state that clusters of more than two particles modeled did not produce significantly large enhancements. This result suggests that the hot spots have more to do with extremely close location of two nanoparticles of optimum geometry rather than clusters of large number of particles. Brown et al. [56] also reported a 2 dimensional electromagnetic model to study the relative performance of four generic SERS substrates. In their study two nanoparticles, structured surfaces with hemispherical features, structured surfaces with cuboid features and tip surfaces were considered. A review on EM mechanism of surface enhanced spectroscopy has written by Schatz et al. [57].

Experimental findings confirm the presence of strong electromagnetic enhancement in SERS, however there is evidence to conclude that SERS is not exclusively an electromagnetic mechanism. If it were only an electromagnetic mechanism strong enhancement would be expected for any Raman active molecule in close proximity to a silver or gold metallic nano structure, but that is not the case. Methanol does not show any SERS enhancement though it has a strong Raman signature [2]. Another experimental observation of Raman scattering from CO_2 and N_2 molecules adsorbed on a particular surface differ by a factor of 200 in their SERS intensities under the same experimental conditions [4]. This result is hard to explain by electromagnetic enhancement. Also the best electromagnetic enhancement factors leave a gap of two orders magnitude to the best experimentally observed SERS enhancement factors on the order of 10^{14}, suggesting the existence of additional enhancement mechanisms accounting for the missing factors [58]. These experimental findings

predict a strong dependence of SERS effect on molecular selectivity and the chemical nature of molecule and these indicate the presence of an additional chemical enhancement mechanism in SERS.

While the EM enhancement applies to all analytes the chemical enhancements are analyte dependent and require some kind of bonding to the metal substrate. Different mechanisms were proposed for explaining the chemical enhancement mechanism in SERS. The chemical mechanism is also known as a first layer effect as it requires direct contact between the molecule and metal [4] . A possible mechanism is electronic coupling between the molecule and metal and the formation of an adsorbate-surface complex resulting in an increased Raman cross section of an adsorbed molecule compared to that of free molecule in normal Raman scattering. Another possible mechanism is a resonance Raman effect in which either (a) the electronic levels in the adsorbed molecules are shifted and broadened compared with the free molecule because of their interaction with the metal surface or (b) new electronic states arise due to chemisorption and serve as resonant intermediate state in Raman scattering [4]. The evidence to date support the later hypothesis. When the adsorbate strongly binds to the metallic surface, the Raman scattering can be considered to emanate from an adsorbate- metal complex rather than from the adsorbate molecules alone [33]. Fig. 2.4 shows a typical energy level diagram for a metal molecule system.

The highest occupied molecular orbital(HOMO) and the lowest unoccupied molecular orbital (LUMO) of the adsorbed molecules are approximately symmetric relative to the Fermi level of the metal. In this case charge transfer excitations between molecule and metal can occur at about half the energy of

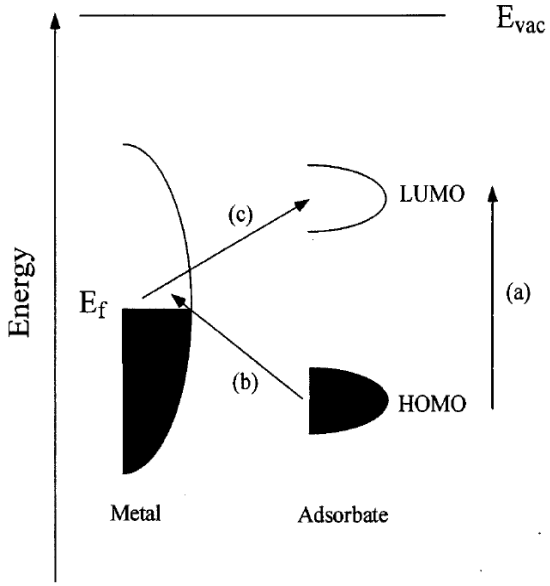

Figure 2.4: Energy level diagram for a molecule-metal system. Resonant Raman processes involving molecular(path(a)) and molecular and metallic states (path (b),(c))are shown. Reproduced from Campion et al. [4](Reproduced by permission of The Royal Society of Chemistry).

the intrinsic intra - molecular excitations of the adsorbate with possible resonant Raman process involving molecular states (Path (a)) and molecular and metallic states (path (b) and (c)) [4]. Another approach to first layer effect called dynamic charge transfer involves the following steps (a) photon annihilation, excitation of an electron into a hot electron state, (b) transfer of the hot electron to the LUMO of the molecule, (c) transfer of an electron from LUMO back to the metal with slightly altered energy due to interactions with internal molecular vibrations, (d) return of the electron to its initial state and Stokes photon creation [2]. Otto et al. [59] discussed surface roughness as a prerequisite for chemical enhancement in SERS based on dynamic charge transfer. Chemical enhancement mechanisms in SERS are limited to very short range and only the first mono layer of the adsorbate can experience it [33]. The

enhancement factor from chemical mechanism is on the order of 10- 10^2 [4,60].

2.3.2 SERS active substrates

Any plasmon resonance supporting structure that provides amplification of Raman signal is known as a SERS substrate. A good SERS substrate is the key in SERS applications. SERS substrates can be mainly classified into three categories: 1) metallic particles in solution, such as metal colloids, 2) metal electrodes and 3) planar metallic structures, such as arrays of metallic nanoparticles supported on a planar substrate. Metal electrodes as SERS substrate have received attention as they have played an important role in the development of SERS [4, 33], but its importance has been diminishing because of the low enhancement factors achievable. As the SERS enhancement occurs due to the resonance response of the substrate, it is wavelength dependent. A given substrate can exhibit good enhancement only for a limited excitation wavelength range. Most of the substrates are designed to operate in visible / near infrared excitation (∼400-1000 nm), which is the range of interest for many Raman scattering experiments.

Silver and gold are the most widely used SERS substrates because of their optical properties (see appendix A). These metals can support good plasmon resonance in the visible and near infrared excitation wavelengths which is of interest to SERS [43]. Silver is the most promising material for SERS since it has the lowest absorption especially at wavelengths below $\sim$ 600 nm and can be used for large enhancement applications. Gold is suitable at longer wavelengths ($>$ 600nm); at such wavelengths optical absorption of gold be-

comes comparable to that of silver. The wavelength range above 600 nm is often used for many biological applications. Gold has the advantage of greater chemical stability and better bio compatibility with many molecules of interest and so is of interest for applications based on near infra red lasers. SERS has also been observed with other metals like copper and platinum but with less enhancements than that observed with silver and gold. The dimensions of typical SERS substrates are in the sub-wavelength range and typically less than 100nm. Rough metallic structures can be used as SERS substrates and these structures have characteristic dimensions down to $\sim$1nm [43].

Methods for fabrication of nanostructures with SERS activity is a very active field of research. Most common types of substrates that give high enhancement in SERS are silver and gold nanoparticles in 10-100nm range, these nanoparticles can be used either in colloidal form or dry on surfaces. Colloidal solutions of silver and gold can be prepared by different chemical reduction processes [61, 62] or by laser ablation [63, 64]. Planar metallic structures can be fabricated in a simple way by drying colloids or by attaching them to a suitable substrate. Other approaches are roughening metallic surfaces by chemical means or by evaporation of metallic islands on surfaces. Recently with the advent of nano-technologies a new class of ordered planar metallic structures has been developed. Self organization is one of the approaches used in nano-fabrication of SERS substrate; island lithogrpahy [65] where Ag islands, which can adopt the shapes of pillars and nano sphere lithography developed by Van Duyne and co workers [34] are examples of self organization method and are some of the highly desirable substrates for SERS applications. Nano-lithography is another way to obtain uniform and reproducible SERS

substrates, where structure of the substrate is controlled by lithographic techniques. Due to the high degree of control of substrate geometry nano- lithographic techniques provide the opportunity to match the experimental findings with theoretical predictions [66]. Electron-beam nano-lithography and focused ion beam (FIB) milling are the most used nano-lithographic techniques [67,68]. Gold nano particle arrays of well defined size and shape were fabricated by electron beam lithography and used in SERS by Felidj et al. [67, 69]. Brolo et al. have fabricated arrays of sub-wavelength holes in Au films using focused ion beam (FIB) milling and used that for enhanced Raman scattering [68, 70]. Another recent development is the fabrication of tunable SERS substrates and temperature controlled substrates [71]. Another aspect is nano particles of different shapes. Different methods have been introduced for production of metal nanostructures with different shapes. Nanoparticles geometries such as nano rings, nano rods, nano holes and nano shells support well defined Plasmon resonances [68, 72–76]. Nano shells with a dielectric core and metallic shell are widely used as SERS substrates [77, 78]. Successful fabrication of SERS substrate is still an important step in the practical application of SERS as the application mainly depends on the activity and reproducibility of substrate. A recent review article from Brolo's group [79], who have developed several structured SERS substrates [68, 76, 80, 81] describes the recent developments on three general types of SERS substrates (1) metallic nanoparticles immobilized in planar solid supports; (2) metallic nano structures fabricated using nano lithographic methods; and (3) metallic nano structures fabricated using template techniques and their use in analytical applications [79].

Among the various SERS substrates, metal colloidal nano particles are the

most used SERS substrates. The main attractions of colloidal nanoparticles are their ease of preparation and low cost. Some of the inexpensive and simple preparation methods for silver colloids are chemical reduction, laser ablation and photo-reduction. Silver colloids are prepared by reduction reactions in solution either by using silver nitrate and trisodium citrate called the Lee and Meisel method [62] or using borohydride as the reducing agent called the Creighton method [61]. In the laser ablation method a pulsed laser is used to ablate metal plates or foils in distilled water or NaCl solution, the properties of the metal colloids formed will depend on the laser pulse energy, laser beam focusing, time of ablation and the presence of additional ions [64]. For the photo reduction method light (gamma or UV irradiation) is used to reduce a metal salt [82]. Silver colloids provide larger electromagnetic SERS enhancement in the visible range. Metallic colloids are used in the recent developments of single molecule detection, both in colloidal form in [38] and deposited on a planar substrate [37]. One of the drawbacks of colloidal nanoparticles is that their aggregation makes reproducibility more challenging. On the other hand in some cases aggregation is required for the observation of SERS. SERS substrates can be characterized by different methods such as scanning electron microscopy(SEM), transmission electron microscopy(TEM) and also by using extinction or UV/visible spectroscopy.

2.3.3 Applications of SERS

SERS overcomes the sensitivity problems of Raman scattering technique and increases the detection limit. The main analytical advantages of SERS are enhanced sensitivity, surface specificity and fluorescence quenching by metal

nano particles. As the SERS signals are much narrower than fluorescence bands it is possible to detect multiple analytes simultaneously using SERS. SERS has potential applications in analytical chemistry, biochemistry, forensic sciences etc, where identification and structural characterization of molecules play a central role. In addition to its various advantages SERS technique has its own limitations. One of the main issues in SERS is the the problem of reproducibility [43]. The poor reproducibility of this technique prevents it from many practical applications. One can see complementarity between SERS enhancement and reproducibility. The large enhancement factors are difficult to reproduce. This thesis will address some of the issues of reproducibility and discuss the conditions where we have reproducible signal with high enhancements. Another issue is the time delay in observing the SERS signals. For example for Trp, Aliaga et al. reported the observation of reproducible spectra only a few hours after preparation of the sample solution, they also observed a large variation in the SERS of Trp [25]. Another limitation is selectivity of SERS technique to the analyte. In order to observe the enhancement the analyte has to bind to the substrate. Background electrolytes help the binding of analyte molecule to substrate and are an important factor in SERS studies.

SERS has been used for the analysis of biofluidic like glucose monitoring as reported by Lyandres et al. [83]. SERS has been extensively used for the analysis of many biomolecules like DNA [18, 84], protein [85, 86], bacteria [87, 88], virus [89] etc, it provides ultra sensitve detection, monitoring, and characterization of bio medically relevant molecules and is one of the fastest growing techniques in bioscience. Applications of SERS in biophysics and biomedical spectroscopy has been discussed by Kneipp et al. [2] in their review. Envi-

ronmental and biomedical applications with new developments in fiber -optic SERS monitors, SERS-based bio assaays and near field nanoprobes are discussed by Vo-Dinh [90]. Structural investigation and limit of detection analysis of several widely used pharmaceutical compounds by SERS has been described in [91]. With better understanding of the basic experimental requirements and the theoretical knowledge from electromagnetic interpretation, applications of SERS are growing at a fast pace. One of the promising applications is associated with the single molecule detection capabilities of SERS. In 1997, two groups independently claimed single molecule (SM) detection under SERS conditions [37, 38] and an enhancement factor as large as 10^{14}. Single molecule detection opens up new possibilities in bio-sensing applications due to the ability to analyse molecules at the ultimate sensitivity limit and this area is the subject of intense fundamental research. SM-SERS detection meets with same problems as that of SERS, like fluctuations in the signals, lack of reproducibility and lack of understanding of the conditions and lack of control over the magnitude and spatial location of the hot spots. The authors on the first reports on SM-SERS in their discussion [92] pointed out that the deduction of SM-SERS from their result was not straightforward although much evidence supported the claim. Single molecule detection has started to be believed after large amount of evidence has been gathered over the years [43]. Another promising recent development in SERS is tip enhanced Raman spectroscopy (TERS), which is a combination of SERS and enhancement produced by a metallic tip. Atomic force microscopy (AFM) and scanning tunneling microscopy (STM) use metallic tips, the combination of SERS together with AFM and STM is interesting where hot spots can be produced at controlled positions. It has the additional advantage of imaging capabilities of AFM and

STM. One of the first reports on TERS with AFM has been reported in [93]. Pettinger et al. has described TERS with STM tip [94]. Development of new substrates from nano technology is another active research area which contributes to the development and applications of SERS.

In this thesis the goal was to develop a very high sensitivity SERS technique for detection of biomolecules which eventually could be incorporated in microfluidic analysis systems. The ultimate goal would be to achieve sensitivities high enough for analysis of the protein content of a single cell. In order to develop such techniques, in the present thesis we focused on SERS studies of different amino acids, peptides and dyes in silver colloid. The high sensitive detection of amino acids and peptides is important as they are the basic building blocks of proteins. Other methods used in protein detections are ELISA (enzyme-linked immunosorbent assay), Immunofluorescence etc. In ELISA the presence of antibodies or antigens in a sample are detected based on antibody-antigen immunoreactions. Immunofluorescence uses the specificity of antibodies to their antigen to tag fluorescent dyes to specific biomolecule targets within a cell, and thereby visualize the distribution of the target molecule through the sample. Though SERS has the capability to detect even single molecules [39, 40] and for many analytes sub-nanomolar detection limit has been achieved, the detection of amino acids at very low concentrations has not been reported. The lowest concentration detected for Tryptophan amino acid using SERS reported in the literature is 10^{-5} to 10^{-4} M [25]. In our studies we detected SERS signals from Trp amino acid at concentration as low as $\sim 10^{-8}$ M with SERS enhancement of $\sim 10^{8}$. Background electrolyte is an important factor in SERS measurements as they change the aggregation

and binding. In most cases, addition of electrolyte is necessary to observe SERS signal. In the vast majority of experiments sodium chloride was used as the background electrolyte and a few papers deal with other electrolytes. During the course of this thesis we tested different electrolytes. Along with the commonly used electrolyte NaCl, we also used some composite electrolytes and which led to high enhancement of Raman signals. A comparison of the SERS enhancement factors observed with different electrolytes has also been discussed. We performed SERS measurements in a microfluidic chip and in a liquid core waveguide geometry. The low volume requirement of microfluidic chip together with the high sensitivity of SERS technique make it possible to analyze small volume of samples. The amount of sample required for SERS analysis in microfluidic chip is on the order of femto moles as described in chapter 5. It is expected that this can be used for the detection of protein from a single cell. For example the amount of protein in a human retinal pigment epithelial cell is measured to be $\sim$ 100pg/cell [95]. Assuming that the average proteins contain more than 100 amino acids and the average molecular weight of each amino acids is approximately 100 to 125 [96], the average molecular weight of protein can be taken as $\sim$ 10000g/mol and the amount of protein from one cell can be calculated as 10 femto moles. So it may be possible to detect high concentration constituents in single cell in a microfluidic chip with the concentration range we have achieved in SERS. The use of a liquid core waveguide(LCW) can further increase the sensitivity of Raman measurements. A Teflon AF capillary with refractive index 1.29 supports total internal reflection for aqueous solution and can be used as a LCW. Detection of Raman signals in Teflon AF capillary has been reported before, but to the best of our knowledge SERS detection in Teflon AF capillary has not been

reported to date. We detected SERS signal in a Teflon AF capillary, which provides the possibility of additional signal enhancement of up to 100 times which further increases the detection limit of SERS. In principle short waveguides channels on the order of centimeters in length could be incorporated into microfluidic systems for high sensitivity lab on a chip analysis. In addition, a numerical simulation has also been performed to better understand the aggregation process in silver colloid and time of evolution of SERS signal.

Chapter 3

Experimental Methodologies

3.1 Introduction

This chapter gives the details of the the experimental techniques and equipment used in the course of the thesis. In particular details of spectrometers and detectors used and their calibration procedure are described. The measurement of scattering length is explained and the method of preparation of silver colloid is also described.

3.2 SERS Experimental Setup

The SERS spectra were collected in a backscattering geometry using a custom-built laser setup. The schematic diagram of the experimental setup is shown in Fig. 3.1.

A diode pumped second harmonic solid-state laser (Nd:YVO_4, 30 mW, 532 nm) was used, which has a laser beam quality factor (M^2 factor) equal to 1.3. To record spectra we used a 0.35 m McPherson monochromator with a 1200 lines/mm grating, it has an adjustable slit with a slit width which can be varied from 5 to 4000 microns. The wavelength range available is from 190nm to 1300nm. The monochromator has an effective aperture of f/4.8 and dispersion

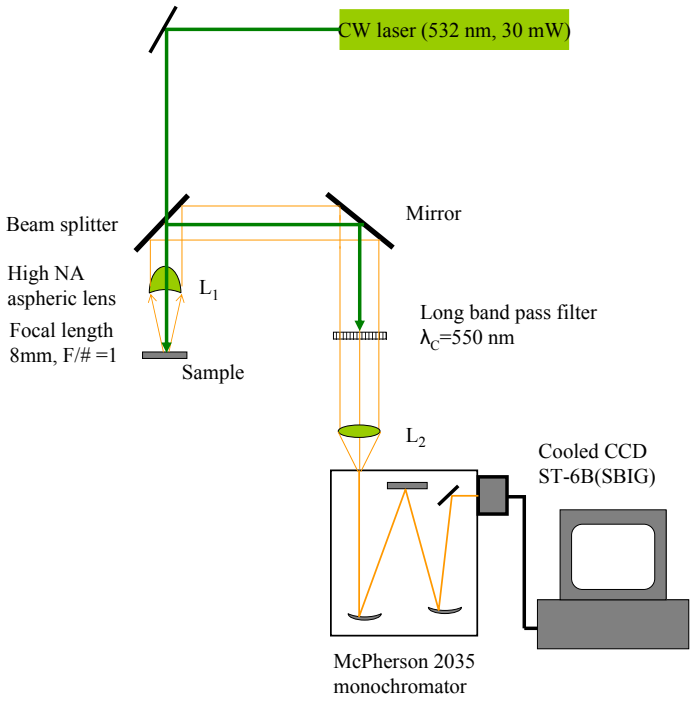

Figure 3.1: Experimental setup.

of 2 nm/mm when using a 1200 lines/ mm grating and was equipped with a model 789A scan controller from McPherson. The detector used was a cooled charge-coupled device (CCD) array (ST6-SBIG, Santa Barbara Instrument Group), the detector size is 8.6x6.5 mm and the pixel size is 23x27 μm. The exposure time of the CCD can be varied from 0.01 to 3600 seconds with a 10ms resolution and the operating temperature was either -20 deg C or -25 deg C. The setup also includes a focusing/collecting aspheric lens (f =8 mm, diameter = 8 mm) and a beam splitter, a 550 nm long pass interference filter (TFI Technologies). The transmission spectrum of filter is shown in Fig. 3.2.

An 8 mm lens was used to collect the scattered light. A second lens L_2 of focal length 8 cm imaged the the collected light onto the monochromator slit, which was set to a width of 150 μm, corresponding to a spectral resolution

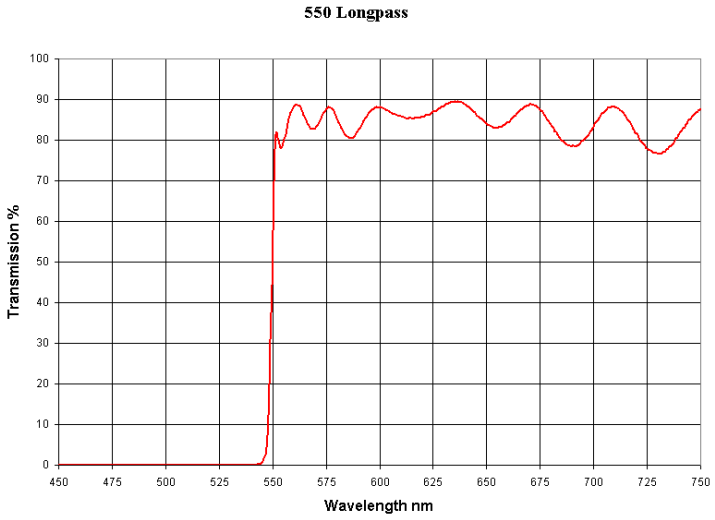

Figure 3.2: Transmission spectrum of filter.

of about 12 cm^{-1}. All the components of the experimental set up except the monochromator and CCD were placed in a light tight box. The picture of experimental set up is shown in Fig. 3.3.

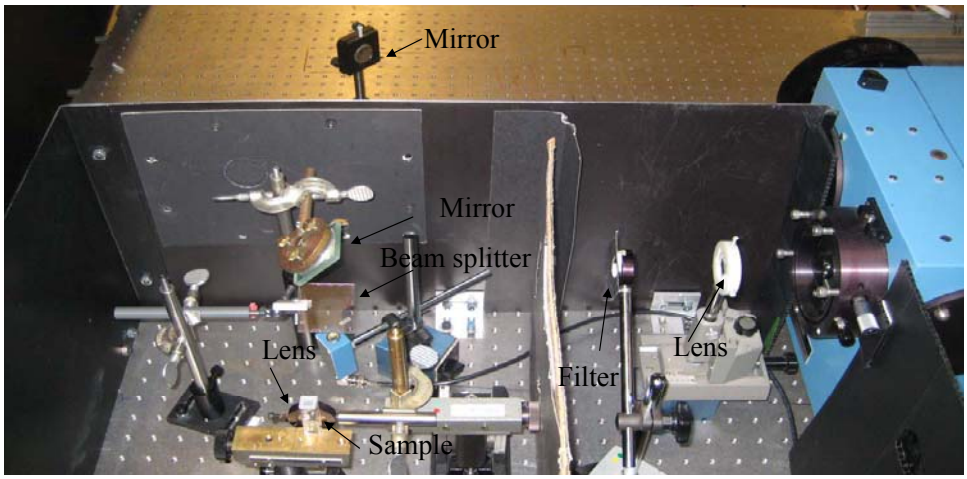

Figure 3.3: Picture of experimental setup.

The spectral calibration was accurate to approximately $\pm$ 5 cm^{-1}. During a single exposure the monochromator observed a 17 nm spectral range when 1200 lines/ mm grating was used. To obtain spectra over a wider range, multiple

exposures with different grating positions were used. Quartz or disposable plastic cuvettes were used during spectral measurements. KestrelSpec software [97] is used for the observation of the spectra. A dark current background subtraction was performed for each measurement.

3.3 Spectrometer Calibration

A mercury light source from Pen Ray Lamp(12011087, B 264738) was used for the calibration of the spectrometer. To take into account a small non linearity of the spectral line value versus its position on the CCD detector the following procedure was used. The spectrometer was set to observe one of the known mercury lines at 579.066 nm at the center of the detector array. First an auto calibration procedure was performed as described in KestrelSpec software manual [97]. Auto calibration updates the spectrograph parameters and links the wavelength of spectral line to its position on the CCD array and grating angle. After autocalibration the pixel position is known for the yellow-orange mercury line at 579.066nm and the wavelengths corresponding to all the other pixel can be determined using the spectrograph parameters. Then we changed the scanning wavelength of the monochromator so that the mercury line moved across the CCD array with 1 nm step size. At each position we measured the difference between the observed value of the spectral line and its database value. The corresponding pixel position is also noted. This difference (correction factor) is shown in Fig. 3.4. The data were interpolated and the correction is applied to the spectra after each measurement.

An example of a test spectra measured using this set up for isopropanol is given in Fig. 3.5. This compares well to the reported literature spectrum for isopropanol in [98].

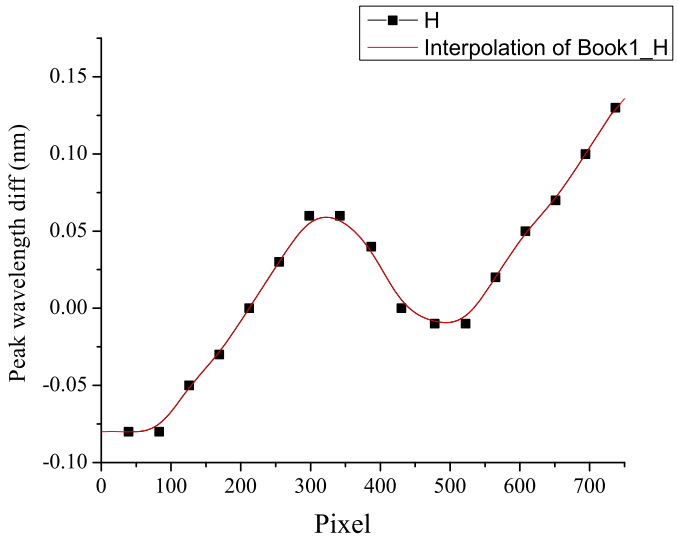

Figure 3.4: Calibration graph.

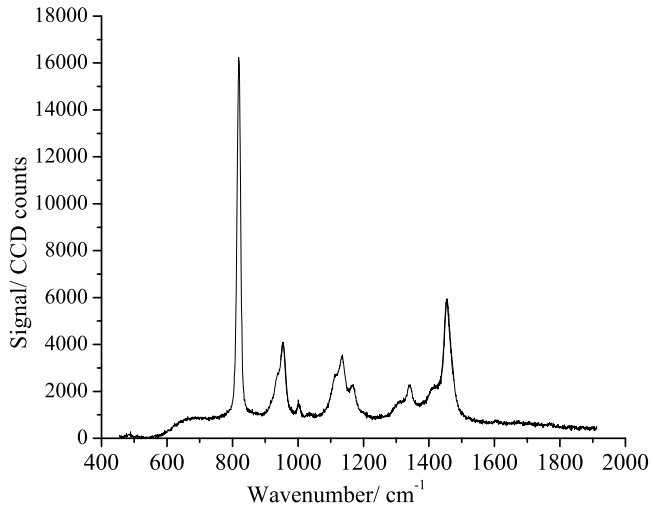

Figure 3.5: Test spectrum measured from 2-Propanol.

A comparison of the peak positions from the spectrum of 2-Propanol measured in our setup with that of the reference spectrum in Spectral Database for Organic Compounds SDBS [98] is shown in Table.3.1.

Peak position(wavenumber, cm^{-1})	
Spectrum measured	Reference spectrum from database
821 ±1.8	820
955 ±2.1	955
1134 ±3	1132
1454 ±1.5	1454

Table 3.1: Comparison of Raman spectrum of 2- Propanol measured in our setup with that in the spectral database. The error bars shows the standard deviation estimated from 9 spectral measurements.

3.4 Estimation of Effective Scattering Length and Scattering Volume

To measure the variation of detected signal versus sample position and the effective scattering length a mylar sheet of thickness 25 μm was used as a test sample. The mylar sheet was mounted on a precision translation stage, (P1-M11-1DG). The sample was moved and spectrum was recorded for different positions with an integration time of 5 seconds. A graph is plotted of the peak signal height as a function of position as shown in Fig. 3.5 and the scattering length is measured at full width at half maximum. The strength of the scattered signal was measured for slit width of 150 μm as shown in Fig. 3.6. The scattering length measured for 150 μm slit width was $\sim$ 400 μm.

In order to measure the scattering volume we need to consider the shape of the beam on the sample. As the scattering length is much larger than the depth of focus, we can use geometrical optics to calculate the scattering volume, in that case the scattering volume is represented by two cones as shown in Fig. 3.7.

The beam diameter ($1/e^2$) measured on the lens is 2 mm and the focal length of the lens is 8 mm. The measured scattering length for 150 μm slit width is 400 μm. Scattering volume is limited by two cones with heights of

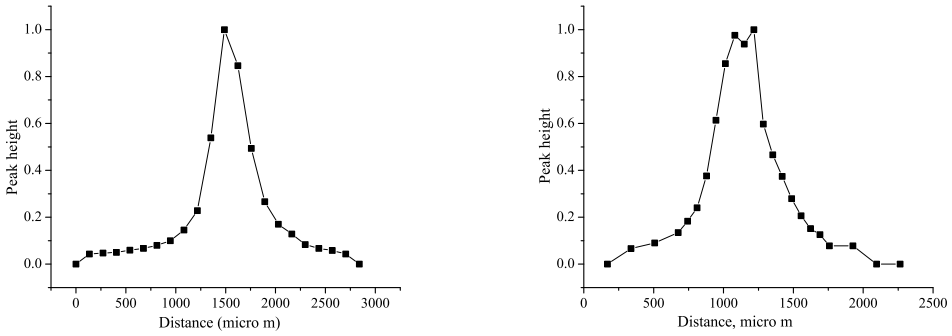

(a) (b)

Figure 3.6: Raman Scattering vs axial position measured for for 150 μm slit width.

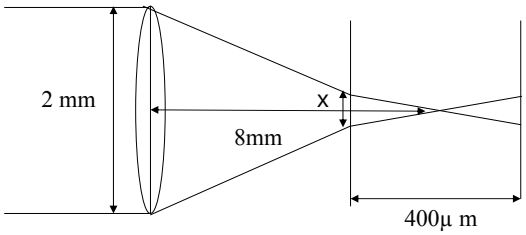

Figure 3.7: Scattering volume measurement.

half of the scattering length. In the air the beam diameter on the surface limiting the scattering length is calculated using the input beam cone angle as, x = $\sim$ 50 μm, (200/8000 = x/2000). The scattering volume consists of two cones. The volume of the cone is calculated using V = 1/3 π r^2 h , with r = x/2 and h =200 μm. The calculated scattering volume in air is 2.6×10^{-7} cm^3. in water the angle of light cone inside the sample is reduced by the refractive index and is calculated as 0.092 radian.

3.5 Resolution vs Slit Width

To measure the resolution vs slit width, the laser line was measured for different slit widths with 0.02 seconds integration time. A plot of observed CCD signal versus slit width is shown in Fig. 3.8 and the resultant value of slit widths are tabulated in Table.3.2

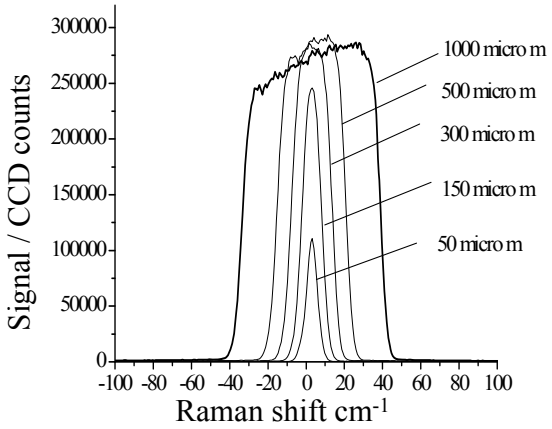

Figure 3.8: Observed CCD signals for different slit widths.

Slit width(μm)	FWHM (cm^{-1})
50	7.3
100	10.6
150	12.2
200	15.5
300	22.0
500	36.9
1000	72.6

Table 3.2: Observed spectral resolution versus slit width.

3.6 Absorbance Spectrum Measurements

A portable (Ocean Optics USB2000) spectrometer was used to measure the absorbance spectra of the colloidal solutions. A schematic digram is shown in

Fig. 3.9. To obtain the spectrum, first the incident light was measured without any sample. Then the sample in a cuvette was inserted into measuring chamber and measured the transmitted light. The spectrum of the incident light was then divided by spectrum of transmitted light and common logarithm of that gives the absorbance. The excitation light source was made by combining different light emitting diodes and it could give absorption spectrum measurements only from 380nm to 800nm.

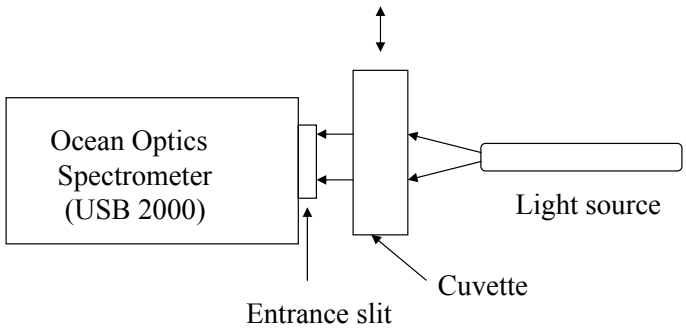

Figure 3.9: Schematic diagram of absorption measurement setup.

3.7 Silver Colloid Preparation

A modified Creighton procedure was used to produce the silver colloid [61]. The colloid was produced by fast syringe injection of 5 mL of silver nitrate ($AgNO_3$) solution (10^{-3} M) into a 5 mL solution of sodium borohydride, $NaBH_4$ (6×10^{-3} M). Fig. 4.5 given below shows the picture of silver colloid solution and a TEM picture of the colloid dried onto a TEM grid. The sample preparation of TEM measurement was done by placing a drop of fresh silver colloid right after preparation on a grid and taking out the excess solution using a filter paper and then drying it.

$6\times\ 10^{-3}$ M $NaBH_4$ + 10^{-3} M $AgNO_3\rightarrow$ Silver colloid

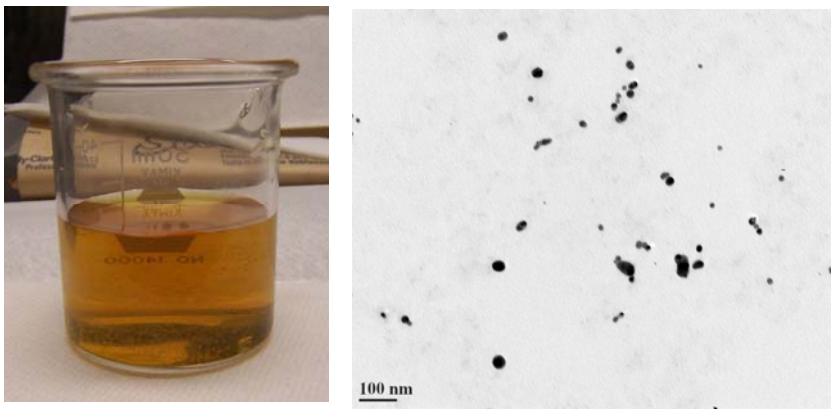

(a) (b)

Figure 3.10: (a) Silver colloid solution (b) TEM image of the silver colloid.

The colloid prepared was six times more concentrated that the colloid in the original procedure [61]. 18 MΩ deionized water was used for solution preparation. We found that colloid formation and its SERS performance are sensitive to the aging of the sodium borohydride solution used, probably due to the decrease of its reduction strength with time, which in turn can influence the size of the colloidal particles generated. To obtain the maximum reproducibility, one day old solution of $NaBH_4$ was used for the experiments . After preparation, the solution of sodium borohydride was kept in a refrigerator at about 10 deg C for one day. Just after mixing, the colloid had a pale yellow color. The reaction was completed in approximately 10 seconds, when the colloid color became deeper yellow and stabilized. The colloid was stable for about 30 minutes. The absorption spectrum of the colloid solution is shown in Fig. 3.11.

The absorption spectrum was measured from a four times diluted silver colloidal solution prepared by the above mentioned method. The spectrum has a sharp plasmon resonance at 390 nm, which is in agreement with the silver colloid absorption spectrum reported in the literature [61, 99, 100]. The

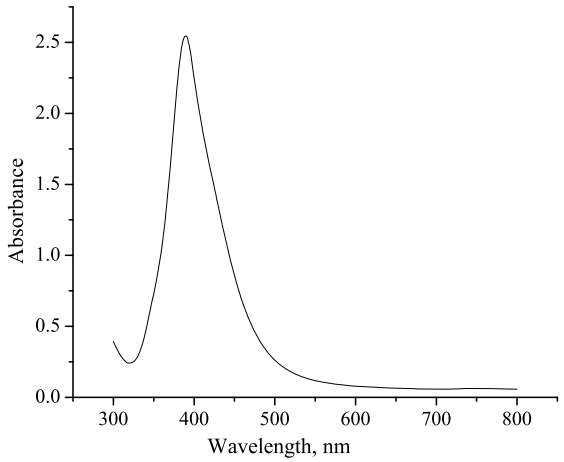

Figure 3.11: Absorption spectrum of silver colloid.

peak at ∼400 nm is well known for silver spheres with small radii ($\leq$ 20 nm) and the absence of any shoulder in this spectrum indicates the presence of mainly single particles [100]. The absorption spectrum was obtained using Perkin-Elmer NIR-UV spectrophotometer. The colloid was used for SERS measurements just after preparation. It was also found during the experiments that the SERS signal strength is affected by the concentration of the colloid solution. In most of the experiments the colloid was used as prepared and in some experiments diluted colloid was used. A diluted colloidal solution was obtained by adding an appropriate amount of deionized water to the concentrated colloid generated by the above described procedure. For colloid activation different electrolytes have been tested as discussed in the following chapters.

Chapter 4

Surface Enhanced Raman Scattering Detection of Amino Acids and Peptides

4.1 Introduction

Surface enhanced Raman scattering (SERS) technique with its high sensitivity is particularly applicable for biological applications of Raman spectroscopy. Since its discovery SERS has been used as a powerful analytical tool for sensitive detection of biomolecules [101–103]. There are many medical and biological applications where detection of molecular compounds at low concentrations is important. The high sensitivity and selectivity of this technique makes it possible to detect even single molecules [38, 104]. SERS studies of different proteins, bacteria and DNA have been reported recently [84, 88, 105]. In order to have a better understanding of the SERS spectra of complex biomolecules, it is essential to analyze SERS spectra of the constituent elements. Amino acids are the basic building block of proteins. Amino acid molecules contain an amine group, a carboxyl group and a side chain. The side chain differs between different amino acids. Peptides are short polymers formed from amino acids, where the amino acids are linked together by amide bonds, a cova-

lent bond formed between the carboxyl group of one molecule with the amino group of the other molecule. The general structural formula of amino acid and a dipeptide is shown in Fig. 4.1, where R represents the side chain, an organic substituent. SERS studies of amino acids and peptides are important because they can be used as a basis for understanding the interaction between proteins and metal surfaces and they can provide useful data for the subsequent studies of larger peptides and proteins. SERS studies of different amino acids like tryptophan (Trp), phenylalanine (Phe), Glycine (Gly), tyrosine (Tyr) , alanine (Ala) , lysine (Lys) etc have been reported in the literature [12–17]. Peptides provide a better model system than amino acids for protein studies because of the presence of amide linkage and decreased role of end group effects in determining both solute-solvent and adsorbate-surface interactions. Additionally, small peptides are closer vibrational spectroscopic analogues to proteins than are amino acids, and so they provide a more useful data base for subsequent studies of larger peptides and proteins [106]. From the vibrational studies of amino acids on metal surfaces, we can learn about the orientation and the binding geometry of different functional groups on metal surfaces ,and get an idea of the surface geometry. The information obtained can then be used for studying the surface interaction of functional groups in more complicated molecules. Even though all amino acids contain carboxyl and amine functional groups, the conditions for observing the SERS spectra are still different for different amino acids.

In this chapter we report SERS studies of several amino acids and peptides using borohydride reduced silver colloid substrate. We studied the SERS signals from the amino acids tryptophan (Trp), phenylalanine (Phe) and glycine (Gly) and from the peptides Trp-Trp and Gly-Gly-Gly. The impact of the

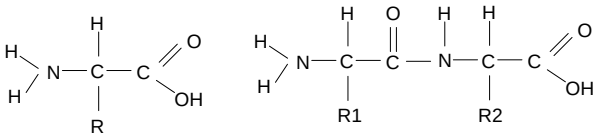

(a) (b)

Figure 4.1: Structural formula of (a) an amino acid and (b) a peptide.

type of electrolyte used for colloid aggregation and the dependence on the experimental procedures for mixing of the components on the amplitude and the stability of the SERS signal have been studied. Some of the results presented here are already published in [30, 107].

4.2 Chemicals

Sodium borohydride (EMD), silver nitrite (EM Science), sodium chloride (Fisher), amino acids: tryptophan (Trp)(Alberta Peptide Institute,Sigma Aldrich), phenylalanine (Phe) and glycine (Gly) (Alberta Peptide Institute) and peptides Trp-Trp (Alberta Peptide Institute) and Gly-Gly-Gly (Sigma Aldrich) were used as received without further purification. Deionized water (18 MΩ) was used for solution preparation. Silver colloid was prepared from Sodium borohydride and silver nitrite as described in the previous chapter.

4.3 SERS study of Tryptophan (Trp) and Trp-Trp

Tryptophan is an important amino acid among the 20 standard amino acids and is an essential amino acid in human diet. Trp has its medicinal use as an antidepressant and a narcotic [108]. The structure of amino acid is shown

in Fig. 4.2. The distinguishing structural characteristic of this amino acid is the presence of an indole ring functional group containing an HN group in the ring.

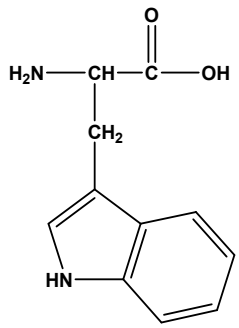

Figure 4.2: Trp Structure.

We have performed a detailed study of Trp amino acid. The SERS spectrum of Trp has been studied in the concentration range 1.4×10^{-8} M to 5×10^{-4} M. Different electrolytes have been tested for the activation of the colloid and optimum conditions have been determined for achieving high sensitivity of detection. In this chapter we present some of the initial results we obtained for this amino acid using sodium chloride (NaCl), sodium bicarbonate ($NaHCO_3$) and a composite electrolyte (bottled drinking water) containing the following ions: HCO_3^-, Ca^{2+}, Cl^-, $SO_4{}^{2-}$, Mg^{2+}, Na^+ (45, 19, 8, 7, 4, 2 ppm) respectively according to the manufacture specification) as the electrolytes. We could also detect SERS spectrum from Trp without using any electrolytes. A more detailed study of low concentration detection of trp amino acid is given in chapter 6 and details of the other electrolytes used and a comparison of enhancement factors are presented in chapter 7.

Normal Raman spectra from Trp pressed solid powder and its aqueous solution (0.03M) are shown in Fig. 4.3.

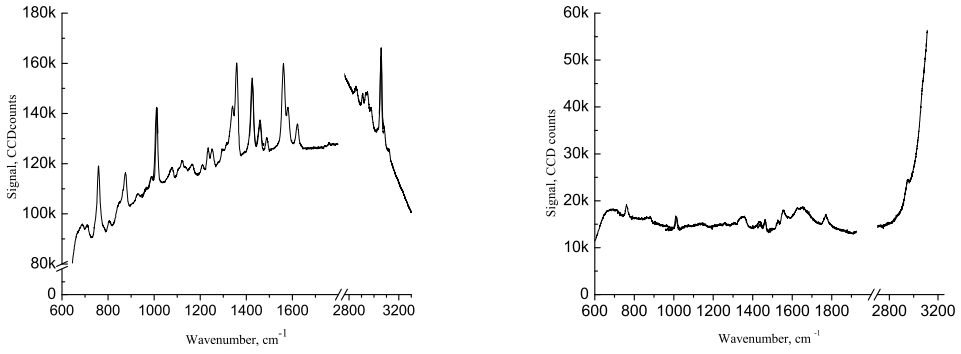

(a) (b)

Figure 4.3: Raman spectra from Trp: (a) solid powder with acquisition time of 10s, (b) 0.03 M aqueous solution with acquisition time of 100s.

4.3.1 SERS study of Trp using sodium chloride electrolyte

Sodium chloride is one of the most commonly used electrolyte in SERS experiments [109, 110]. When we used NaCl electrolyte the solution for SERS measurements was prepared adding 1 ml of 2×10^{-3} M Trp into 10 ml concentrated silver colloid followed by 2ml of 10^{-1} M NaCl, giving a final concentration of 1.5×10^{-4} M Trp in solution. The SERS signal started appearing clearly after a few seconds ($\sim$ 45 seconds) after preparation of the solution and continued to strengthen. The spectrum observed at 30 minutes after the preparation of sample solution is shown in Fig. 4.4.

The yellow color silver colloid remained in the same color after the addition of Trp and NaCl. The strength of the SERS emission remained above 70% of its peak value for a period of 2 days.

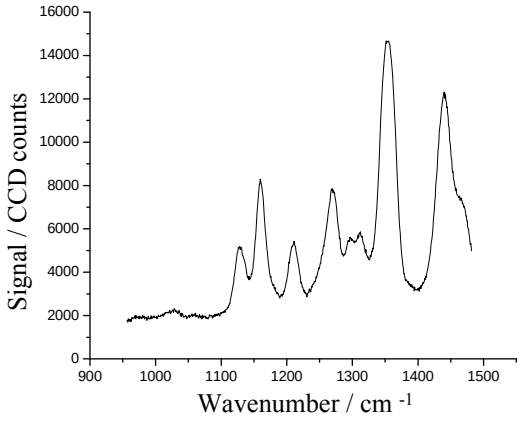

Figure 4.4: SERS signal of Trp with NaCl electrolyte.

4.3.2 SERS study of Trp using aged sodium bicarbonate electrolyte

The solution for SERS measurement using aged sodium bicarbonate $NaHCO_3$ electrolyte was prepared by adding 0.07 ml of 5×10^{-3} M aqueous solution of Trp into 10 ml of concentrated silver colloid solution followed by the addition of 40 ml of DI water and 10 ml of 5×10^{-3} M of sodium bicarbonate. The final concentration of Trp for the SERS measurement was 2.3×10^{-6} M . Before the addition of $NaHCO_3$ the silver colloid was yellow in color. After the electrolyte was added, the solution changed its color from yellow to dark red and then to green-gray. The SERS spectrum started appearing within 1-2 minutes after preparation of the solution and the maximum signal was observed between 10-15 minutes after mixing. An enhancement of about 10^7 was observed relative to the normal Raman spectrum of Trp shown in Fig. 4.2(c). It is important to mention that the order of mixing of components can have a very strong impact on the ability to the level of the observed SERS signal. We could observe the SERS signal from Trp only when the amino acid was introduced

to the colloid before the addition of deionized water and $NaHCO_3$. When the order of mixing was changed by adding the electrolyte into the solution before adding the amino acid, no spectrum was observed. SERS spectrum observed in both the cases and the corresponding absorbance spectra are shown in Fig. 4.5.

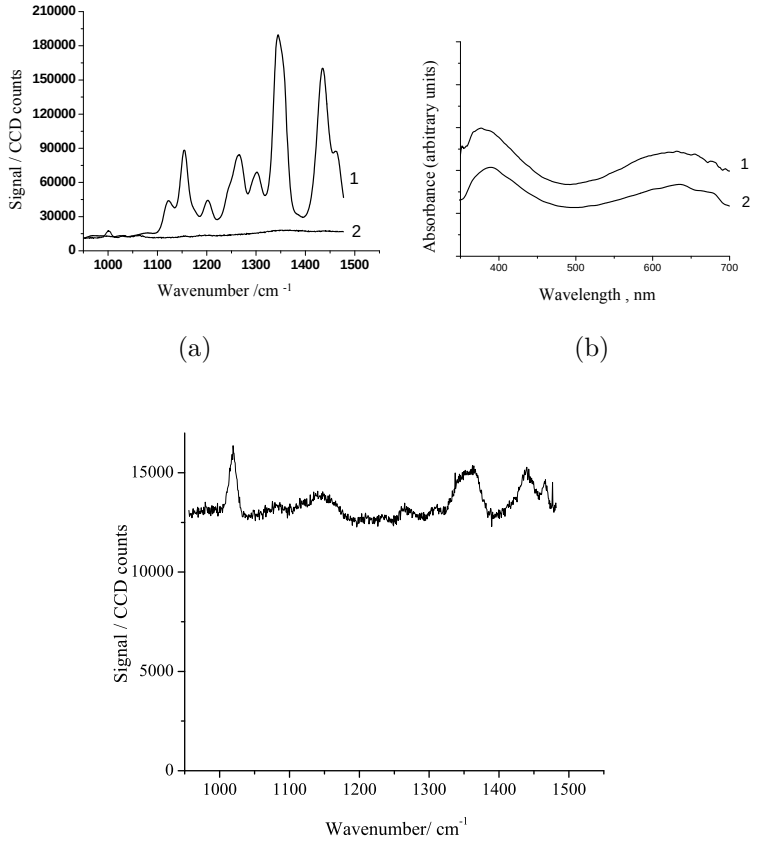

Figure 4.5: (a) SERS spectrum from Trp 2.3×10^{-6} M when electrolyte was added to the colloid after Trp (curve 1) and when electrolyte was added to the colloid before Trp (curve2); (b) Absorbance spectra when electrolyte was added to the colloid after Trp (curve 1) and before Trp (curve 2). The absorbance spectra are offset for better visibility. (c) Raman spectrum of 0.03M aqueous solution of Trp with acquisition time of 100 seconds.

In both the cases a similar change in color was observed and also the

absorbance spectra observed were similar in both cases. Two peaks, which can be seen in the absorbance spectra, are the evidence of the existence of aggregates of elongated shape and or fractal shape [6, 61]. We repeated the experiment 3 times and observed similar spectra using the same $NaHCO_3$ electrolyte. However much weaker and irreproducible spectra were obtained when freshly prepared $NaHCO_3$ was used. This indicated that some subtle change in the solution was important in the enhancement leading to further studies as discussed in chapter 7.

4.3.3 SERS study of Trp using composite electrolyte

Another electrolyte we used for observation of SERS spectra from Trp is a composite electrolyte containing the following ions HCO_3^-, Ca^{2+}, Cl^-, SO_4^{2-}, Mg^{2+}, Na^+ (45, 19, 8, 7, 4, 2 ppm). In fact this electrolyte was a commercial bottled drinking water(Nestle, purelife) and gave higher enhancement of the Raman signal compared to the previously described electrolytes. The solution for SERS measurements was prepared by adding Trp into 10 ml of silver colloid followed by 30 ml of deionized water and 20 ml of composite electrolyte. An example of the SERS spectrum of Trp at a final concentration in the colloid of 4.2×10^{-8} M is shown in Fig. 4.6.

This is one of the electrolytes we tested which gave very high enhancement of the Raman signal with stable and reproducible SERS spectra. A time dependence study of the SERS signal for 4.2×10^{-8} M concentration of Trp is shown in Fig. 4.7. The Raman spectrum of Trp in silver colloid started to appear approximately 2 min after mixing and reached its maximum value at about 30 to 60 min after mixing. After reaching its maximum the signal slowly fell down on the time scale of hours. Fig. 4.7 illustrates the typical temporal

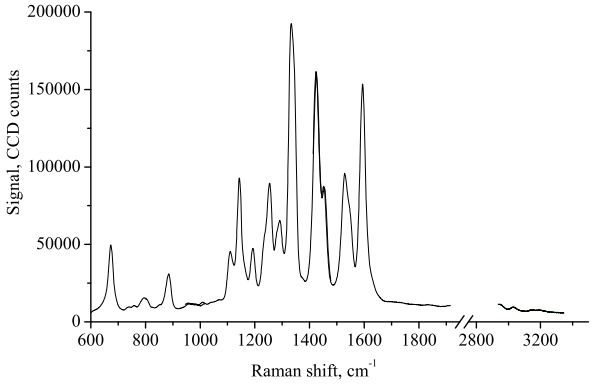

Figure 4.6: SERS spectra from Trp (4.2×10^{-8} M) in the silver colloid with composite electrolyte. The spectrum was taken 10 minutes after addition of Trp to the colloidal solution.

behavior of the SERS signal. The shape of the emission spectra did not change with time as shown in Fig. 4.7. The batch to batch reproducibility was also very good. The peak height at 1350 cm^{-1} varied with a standard deviation of mean of 25% from batch to batch but these variations did not influence the relative intensities and position of the peaks.

Based on the peak to background height at $\sim$ 1350 cm^{-1} from aqueous solution shown in Fig. 4.5(c) and at $\sim$1345 cm^{-1} from the SERS measurement an enhancement of Raman scattering as high as$\sim10^9$ is estimated, which is several orders of magnitude higher than previously reported for Trp in silver colloids [1]. In the case when 5×10^{-3} M solution of aged sodium bicarbonate($NaHCO_3$) was used instead of the composite electrolyte the results did not show as high reproducibility and were weaker in strength. Usually the maximum SERS signal observed under identical conditions was approximately five to ten times smaller for the case of $NaHCO_3$ versus composite

electrolyte. However the shapes of the spectral curves were the same in both cases.

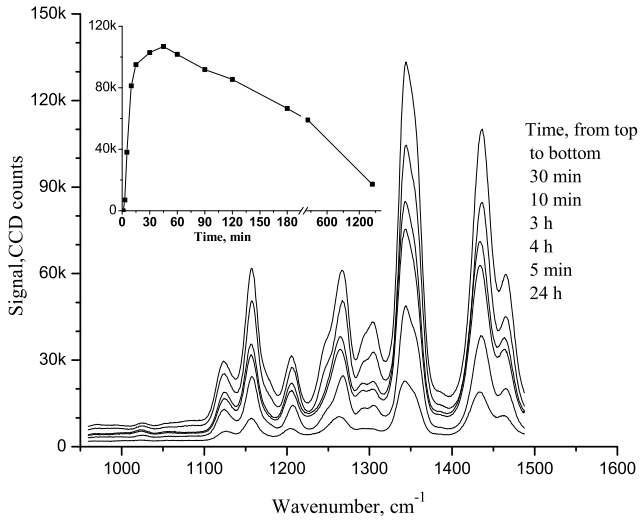

Figure 4.7: (SERS spectra of Trp (4.2×10^{-8} M) in silver colloid solution at different times after mixing. In the insert, the time dependence of the peak height of the peak at $\sim$1345 cm^{-1} above the background at 1393 cm^{-1} is shown.

We also carried out a concentration dependence study of SERS signal from Trp using this electrolyte. Eight samples were prepared by adding different amount of Trp stock solution mixed into 10 ml of silver colloid followed by addition of 30 ml of deionized water and 20 ml of the composite electrolyte. The final concentrations of tryptophan in the solutions were 4×10^{-9} M, 1.4×10^{-8} M, 4.2×10^{-8} M, 1.4×10^{-7} M, 4.2×10^{-7} M, 1.4×10^{-6} M 1.4×10^{-5} M and 1.4×10^{-4} M. The SERS spectrum from each of these solutions was measured over a 2 hour period of time. In Fig. 4.8(a) the spectra taken at 10 min after mixing are shown on a log scale for better demonstration of the invariability of the spectra with concentration. One can see from the figure that the spectral shape stays largely unchanged in the whole range of concentrations studied.

The small peak around 1000 cm^{-1} at low concentration of Trp is attributed to the Raman scattering from the walls of the plastic cuvettes used in the measurements. The concentration dependence of the amplitude of the highest peak (max at $\sim$ 1345 cm^{-1} - min at 1390 cm^{-1}) is shown in Fig. 4.7(b). The intensity of the signal (peak height) increases linearly up to the concentration of $\sim 10^{-7}$ M then it stays constant up to the concentration level of $\sim 10^{-5}$ M, after which it rapidly drops down.

This decrease of the signal strength at high concentration is likely to be caused by a change of the adsorption of the Trp molecules to the nanoparticle surface at high concentration. The strongly pronounced saturation behavior can be explained in terms of the limited number of molecules that can be adsorbed on the surface of a silver particle. Assuming that the silver colloid consists of monodispersed particles with a diameter of 10nm [1] (this value is consistent with our SEM observations) the concentration at which the SERS signal saturates ($\sim 10^{-7}$ M) corresponds to approximately 35 molecules per nanoparticle. Taking into account that the length of the Trp molecule is about 1nm one may conclude that the number of molecules that can be adsorbed on the surface of the nanoparticle is smaller than that for single monolayer coverage. However as will be shown later the largest EM field enhancement effect occurs at the boundary of two nanoparticles forming a dimer and once this limited surface region is covered the SERS signal should saturate. Though the composite electrolyte works well, we can not rely on this electrolyte as it is not well defined and may change with changes in the water source or preparation. We thus produced an electrolyte which works similarly to that of this composite electrolyte and is described in chapter 7.

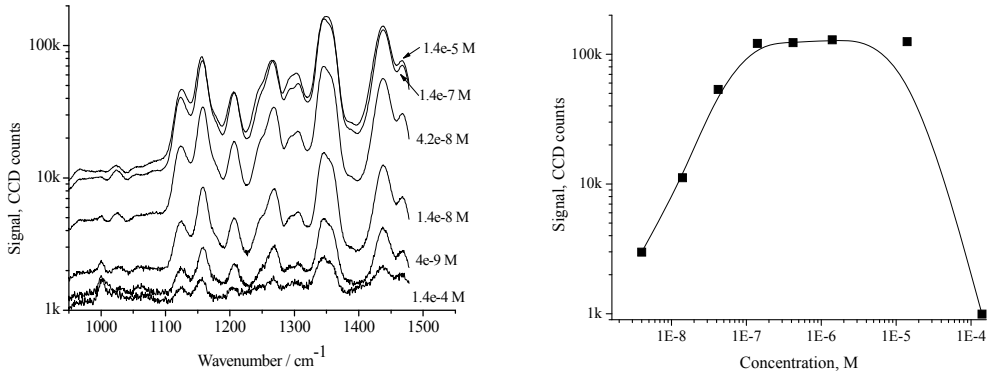

(a) (b)

Figure 4.8: (a) SERS spectra of Trp with composite electrolytes at different concentrations at 10 min after mixing (b) Concentration dependence of the magnitude of SERS peak at $\sim$1345 cm^{-1} of Trp.

4.3.4 SERS spectrum from Trp without electrolyte

We could also observe the SERS signal from Trp even without the addition of any electrolyte. One of the solutions for this measurement was prepared by adding 0.1ml of 2×10^{-3} M solution of Trp into 84 ml of diluted colloid (4 ml of colloid prepared by the method described in chapter 3 diluted by 80 ml of deionized water), giving a final concentration of 2.4×10^{-6} M. The spectrum started appearing almost 1 minute after preparation of solution when the solution color changed from yellow to light pink. Then about 6 minutes later the solution became light green gray in color. The strength of the signal increased with time and then remained stable. Spectrum observed around 20 minutes after preparation of the sample solution is shown in Fig. 4.9. The spectrum was also observed when we changed the order of mixing that is when we added Trp into the concentrated colloid and then diluted the solution. This result indicate that Trp acts similarly to the electrolyte solution by promoting agglomeration of the silver nanoparticles.

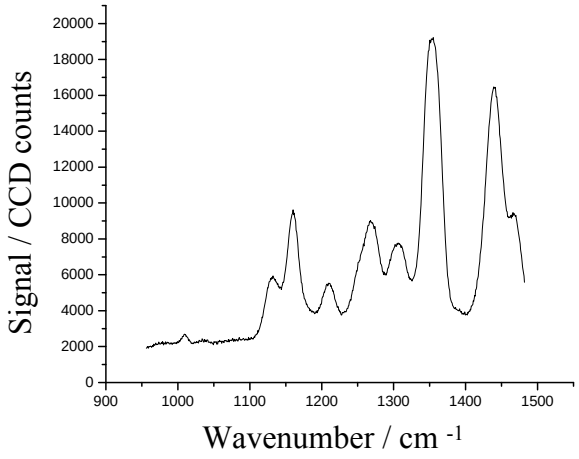

Figure 4.9: SERS spectrum of Trp at concentration of 2.4×10^{-6} M of without any electrolyte at a time of approximately 20 minutes after mixing.

4.3.5 SERS study of Trp-Trp

In the case of dipeptide Trp-Trp, a SERS spectrum could also be observed when the aqueous solution of dipeptide was added to the colloid even without addition of the any electrolyte. The SERS spectrum of Trp-Trp is shown in Fig. 4.10. The final concentration of Trp-Trp in the colloidal solution was 1.3×10^{-6} M. The silver colloid was yellow in color when prepared. After the addition of colloid the solution changed color from yellow to dark red / pink and then green-gray. The spectrum of Trp-Trp is similar to that of Trp except the peaks at 1122 and 1202 cm $^{-1}$ are slightly broader and the peak at 1302 cm $^{-1}$is smaller. As there is no maximum in the spectra around 1400 cm $^{-1}$ which would correspond to the COO- symmetric stretching vibrational lines one may conclude that Trp and Trp-Trp do not bind to the silver surface through the carboxylate group. In general, the peaks observed in the Trp and Trp-Trp are in agreement with the spectra in the literature [26, 106].

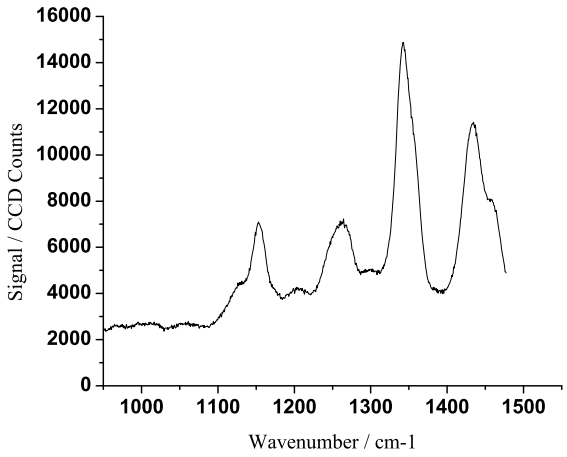

Figure 4.10: SERS spectrum of Trp- Trp.

4.4 SERS study of Phenylalanine(Phe)

Phenylalanine is an essential amino acid and can be readily found in food sources. Phenylalanine helps the brain to produce norepinephrine, a neurotransmitter which conveys information between nerve cells and the brain and is also important for memory, alertness and learning. Phe is used in treatment of depression, bipolar disorder, hyperactivity and can also function as a pain reliever [111]. The structure of Phe is shown in Fig. 4.11 and the Raman spectrum and SERS spectrum are shown in Fig. 4.12.

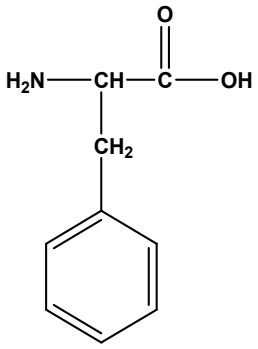

Figure 4.11: Phenylalanine Structure.

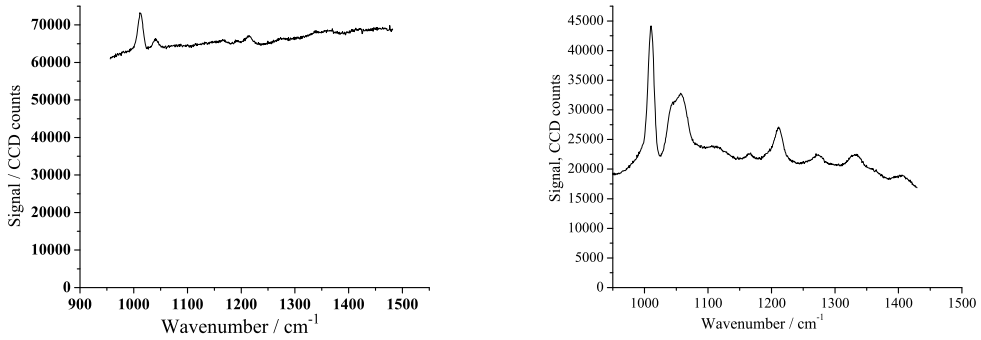

(a) (b)

Figure 4.12: (a) Raman spectra of 0.1M aqueous solution of Phe using a 100s integration time (b) SERS spectra of Phe (1.8×10^{-4} M)using a 50s integration time.

The final concentration of Phe for the SERS measurement was 1.8×10^{-4} M, which was obtained by adding aqueous solution of Phe into concentrated silver colloid. When 1 ml of 2×10^{-3} M Phe was added to the 10 ml of colloid, it changed the color from yellow to dark green in about 10-15 minutes and became dark gray in 30 minutes, the peak SERS signal was observed at that time. No electrolyte was necessary to observe SERS spectrum from Phe. An integration time of 100 seconds was used for the normal Raman spectrum and 50 seconds for SERS measurements. The SERS enhancement factor observed is about 10^4 times. The spectrum is in agreement with the Phe spectra presented in the literature [12]. The peak observed at 1054 cm^{-1} can be attributed to (C-CH_2) and (C-N) stretching and the peak at 1002 cm^{-1} to a benzene ring vibration [12]. A similar SERS spectrum observed for a final concentration of 2.8×10^{-5} M Phe in solution with peak height 1.3 times smaller than that observed with 1.8×10^{-4} M. For the experimental conditions we studied no SERS spectrum could be observed from Phe when the previous composite electrolyte was used with the same sample preparation method as that used

for Trp. One of the possible reasons for lack of spectrum may be the poor binding of Phe to the substrate with composite electrolyte. The orientation of adsorbate on the substrate is also an important factor in SERS.

4.5 SERS study of Glycine(Gly) and Gly-Gly-Gly

Glycine with chemical formula (NH_2CH_2COOH) is the smallest amino acid. Gly helps in the synthesis of hemoglobin. Gly is also useful for detoxifying toxic chemicals in the body and in wound healing [111]. The chemical structure of Gly is shown in Fig. 4.13. In contrast to Trp and Phe, Gly does not have a cyclic group.

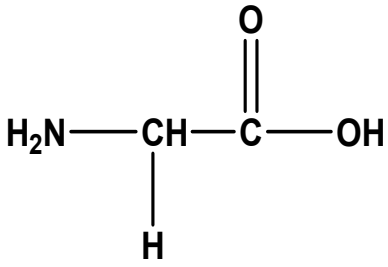

Figure 4.13: Glycine Structure.

In order to observe SERS spectrum from Gly and its tripeptide Gly-Gly-Gly , 0.5 ml of 2×10^{-3} M aqueous solutions of Gly or Gly-Gly-Gly were added to the diluted silver colloid giving a final concentration of 1.8×10^{-4} M analyte in the solution. SERS spectra of amino acid glycine(Gly) and its tripeptide (Gly-Gly-Gly) are shown in Fig. 4.14. In the same figure, the Raman spectrum of 0.1M aqueous solution of Gly is also shown for comparison. An integration time of 5 seconds was used for the SERS measurements and 100s was used for Raman measurements.

No addition of electrolyte was used to observe the SERS spectrum from

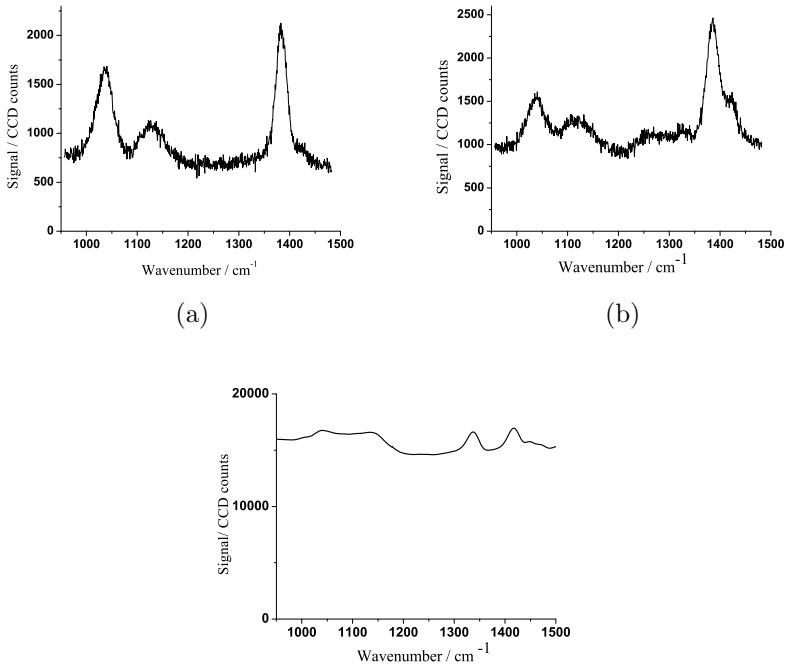

Figure 4.14: (a) SERS spectra of Gly(1.8×10^{-4} M), (b) SERS spectra of Gly-Gly-Gly (1.8×10^{-4} M) and (c) Raman spectrum of an aqueous solution of 0.1M Gly using a 100s exposure time.

glycine and its tripeptide. The SERS signal was measured about 5 minutes after preparation of the solution for both Gly and Gly-Gly-Gly. The peak at 1383 cm^{-1} corresponds to carboxylate group (-COO^-) and the peaks at 1032 cm^{-1} and 1122 cm^{-1}correspond to CN stretching and NH_2 twisting vibrations [13]. This indicates that Gly and Gly-Gly-Gly molecules are more likely attached to the silver surface through both carboxylate and amino groups [13]. The band at 1383 cm^{-1} belongs to the carboxylate group and this indicates that the carboxyl group is ionized on the metal surface [13]. In addition to the peaks observed in Gly, the SERS spectrum of its tripeptide exhibits a shoulder at 1425 cm^{-1}, and two small peaks at 1250 cm^{-1} and 1340 cm^{-1}. The yellow color colloid remained the same after the addition of Gly but in the case of

tripeptide (Gly-Gly-Gly) the color changed into light pink and then into pale gray. The SERS spectra of Gly amino acid and its tripeptide have similar appearance. For the normal Raman spectrum the peak at 1383 cm^{-1} shifts into peaks at 1336 cm^{-1} indicating CH_2 wagging and at 1417 cm^{-1} indicating coupling of COO- symmetric stretching with the C-C stretching vibrations [15]. In comparison with Trp and Phe amino acids the SERS signal of Gly is significantly lower. This may be explained in terms of smaller differential Raman scattering cross section for the Gly molecule, a non-aromatic amino acid, in comparison with Trp and Phe, which contain aromatic rings.

4.6 Conclusion

Experimental investigations of surface enhanced Raman scattering in silver colloid solutions have been performed for several amino acids and peptides to determine the optimum conditions for the observation of a strong Raman signal. Different types of electrolytes and mixing procedures were tested. It was found that in spite of the similar chemical structure of amino acids the conditions for which strong SERS signals are observed can be different.

For the cases of Phe and Gly amino acids no addition of any electrolyte was necessary to observe a clear signal. In contrast, the addition of NaCl and composite electrolyte led to a reduction of spectra in these amino acids. The enhancement factor we observed for Phe and Gly was $\sim 10^4$. For Trp amino acid a very high enhancement of $\sim 10^9$ was observed when a composite electrolyte was used as the electrolyte for colloid aggregation. The order of mixing of components was also found to be critically important in the case of Trp. A weak signal could also be observed for Trp without the use of

any electrolyte. Strong difference in SERS spectrum for Trp and Phe was observed though they have similar structure. The differences are mainly due to the interaction of benzene ring of Phe and the indole ring of Trp with the substrate. The binding process can be different for each analyte. This process of Trp is discussed in detail in chapter 6.

For the peptide Trp-Trp no additional electrolyte was required to obtain large signals. Tripeptide Gly-Gly-Gly also provided SERS spectrum without any electrolyte. Overall, the results indicate the possibility of collecting Raman spectra of amino acids and peptides at low concentrations with good signal to noise ratios using the SERS technique. For Trp amino acid concentration as low as $\sim 10^{-8}$ M has been detected, which is 4 orders of magnitude smaller than that reported in the literature. The impact of the type of electrolyte used for colloid aggregation and the experimental procedures for mixing of the components on the amplitude and the stability of the SERS signal have been studied.

Chapter 5

Surface Enhanced Raman Scattering Detection in Liquid Core Waveguide and in a Microfluidic Device

5.1 Introduction

Raman scattering detection in a waveguide is an important technique to increase the interaction length and sensitivity. It has been reported that by placing the sample to be detected at the center of a waveguide, the Raman scattering signals from aqueous solution can be collected with high efficiency [27–29]. In this apparatus, called a liquid core waveguide (LCW), the light emitted throughout the sample volume is guided to a common aperture and can be efficiently collected. This liquid core waveguide geometry provides longer excitation and collection lengths and requires much smaller volumes of samples compared to the case of a standard cuvette. A liquid core waveguide can be made from tubing with lower refractive index material for the wall material than that of liquid core material. Under this condition light can be guided over a significant length. A glass capillary ($n \geq 1.46$) filled with high refractive index liquids was used in some applications, but they are limited by the fact

that for total internal reflection the refractive index of the core liquids should be higher that that of the capillary wall and majority of the important solvents such as water, methanol and acetonitrile have refractive indices below that of silica glasses. Most of the wall materials have refractive indices greater than that of water and therefore are not suitable for making cladding material for aqueous solutions. Water-based waveguides have been developed with bare glass or fused silica tubes using total internal reflection at the outer (glass-air) interface. These waveguides were used in Raman spectroscopy [112, 113] and absorption applications [114]. Though these waveguides performed well they suffered from a few disadvantages. Their loss characteristics are determined by the conditions of the outer surface so they must be cleaned before use and need to be handled carefully to avoid scratching. Also such uncoated glass tubes were quite fragile. From the optical point of view as these waveguides work through the internal reflection at the outer surface, they allow the light to propagate through the tubing wall as well as the liquid core, which contributes to unwanted background in the Raman scattering measurements. A commercially available material capable of guiding light with water as the solvent is Teflon AF . Teflon AF is an amorphous copolymer of 2,2-bis(trifluoromethyl)-4, 5-difluoro-1,3-dioxole and tetrafluoroethylene [28]. Teflon AF has a low refractive index (n=1.31 for AF1600 and 1.29 for AF 2400) and therefore it supports total internal reflection for aqueous solutions (water, n=1.33). Teflon AF 2400 is transparent in the spectral range from 200 to 2000 nm and is an optically, physically and chemically stable material [115]. Teflon AF capillary has already been used to enhance the signals in Raman scattering by integration of scattered light along the length of the waveguide. The use of Teflon AF capillary tubing in Raman scattering was demonstrated by Altkorn et al. in [28] and

they showed that the Teflon AF capillary significantly enhances the Raman signal compared to the conventional sampling arrangements. Raman signal enhancement from aqueous solutions by 1 or 2 orders of magnitude, obtained with the use of liquid core optical fiber has been described in [27, 116, 117]. In this chapter we describe SERS detection we performed in a Teflon AF 2400 capillary and to our knowledge, this is first reported observation of SERS in Teflon AF 2400 [30].

Another system we used for SERS detection is a microfluidic chip. A microfluidic chip or lab on a chip is a relatively new technology in the field of bioanalysis and chemical synthesis and analysis [21, 22]. Microfluidic technology is based on analyzing small amounts of samples in channels with micrometer dimensions. This technology has several advantages such as minimum amount of sample required, low cost, short time of analysis and high resolution [118]. High specificity of SERS together with the ability of microfluidic chips to handle small sample volumes is a promising technique for sensitive detection. Microfluidic chips have been used for SERS detection by different groups [18–20]. Lee et al. have used an alligator - tooth shaped PDMS microfluidic channel and a zigzag shaped channel for mixing colloid and analyte for SERS detection [119, 120]. Individually addressable multiplexed microfluidic channels for high throughput quantitative and qualitative SERS detection has been reported by Nahla et al. [121]. Bacteria detection by SERS in a microfluidic device is described in [122]. Compared to the Raman detection in static conditions the lab on a chip detection in a flowing condition yields more reproducible results because of the availability of fresh sample and reduced photo degradation in the flow condition [123, 124]. We used a standard mi-

crofluidic chip from Micralyne [125] to detect the SERS signal and also a chip that was modified using laser micro machining to further increase the probe volume. The results obtained are presented in the following section. Most of the results were published in [30, 107].

5.2 Detection of SERS Signal in Liquid Core Waveguide

5.2.1 Light propagation in a waveguide

Propagation of light in a liquid core waveguide can be explained by total internal reflection using the ray optics approximation. A waveguide can be considered as a cylindrical core surrounded by a cladding with refractive index of cladding lower than that of core. Let n_C be the refractive index of the cladding and n_L the refractive index of core and consider the case of light traveling from a medium of high refractive index to that of low refractive index. The reflection and refraction at an interface is depicted in Fig. 5.1. If θ_1 is the angle of incidence and θ_2 is the angle of refraction, they are related to each other and to the refractive indices by Snell's law [5],

$$n_L sin\theta_1 = n_C sin\theta_2 \tag{5.1}$$

With increase in the angle of incidence (θ_1) angle of refraction(θ_2)also increases and for $\theta_2 = 90°$, the refracted ray emerges parallel to the interface between the media. This is the limiting case of refraction and the corresponding angle of incidence is called critical angle (θ_C). For angle of incidence greater than the critical angle there is no refraction and all the energy in the incident light is reflected back into the core , this phenomenon is called total internal reflection. Total internal reflection is a requirement for light propagation

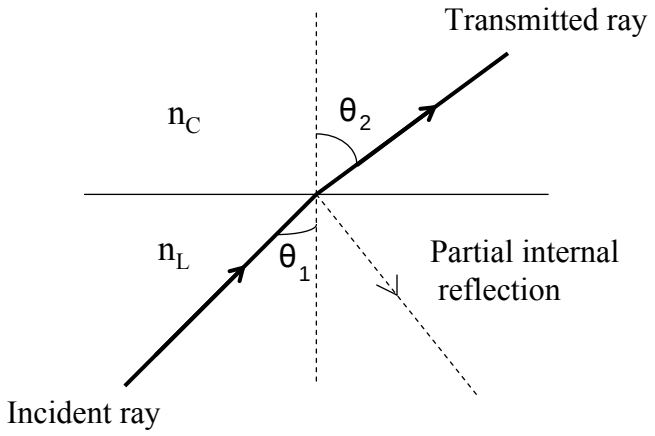

Figure 5.1: Reflection and refraction of a light ray at an interface.

inside a waveguide.

The critical angle is given by,

$$sin\theta_C = n_C/n_L \tag{5.2}$$

$$\theta_C = sin^{-1} n_C/n_L \tag{5.3}$$

In order to be propagated along the waveguide the rays need to enter the waveguide within an acceptance cone angle. The rays outside this cone angle will not be guided. The geometry for launching a ray into a waveguide is shown in Fig. 5.2 [5] and we consider that the waveguide is placed in air, a medium of refractive index n_0=1.

As shown in the figure the ray that enters the core at angle θ_a (ray A in Fig. 5.1) is incident at the core cladding interface at critical angle(θ_C) and therefore undergoes total internal reflection. Any rays entering at an angle greater than θ_a (ray B) will hit the core cladding interface at angle of incidence of less than θ_C and thus will be transmitted through the core-cladding interface

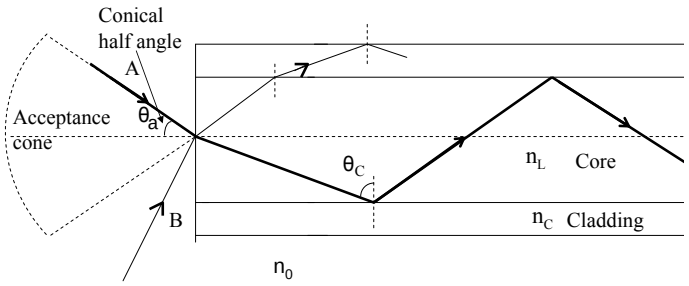

Figure 5.2: Coupling of light into a waveguide and propagation in waveguide, [5].

and therefore will not be totally internally reflected. Thus for the rays to be transmitted by total internal reflection they must be incident on the waveguide core within an acceptance cone defined by the conical half angle, θ_a and this is the maximum angle relative to the axis at which the light may enter the fiber and still be guided. This is called the acceptance angle.

The acceptance angle θ_a is given by [5]

$$\theta_a = sin^{-1}\left[\frac{\sqrt{n_L^2 - n_C^2}}{n_0}\right] \tag{5.4}$$

where n_0 is refractive index of the surrounding medium.

This relation connecting the acceptance angle and refractive indices define an important parameter of the waveguide, numerical aperture (NA), a dimensionless number which defines the range of angles a system can accept or emit light.

$$NA = n_0.sin\theta_a = \sqrt{n_L^2 - n_C^2} \tag{5.5}$$

5.2.2 Characterization of Teflon AF 2400 capillary

In our experiments we used Teflon AF 2400 capillary (n =1.29, inner diameter 112μm and outer diameter of 900μm) from Biogeneral [126]. Prior to using it

for SERS detection, we evaluated its wave-guiding performance.

In order to measure the attenuation in capillary vs length, the Teflon AF 2400 capillary was filled with ethanol(n= 1.36) and laser light was allowed to pass through the capillary. A diode pumped second harmonic solid-state laser laser source(Nd:YVO_4) at wavelength of 532 nm with a beam diameter of 2 mm was used. A lens of focal length 5 cm and 2.5 cm diameter was used to focus the light into the end of the capillary and the power was measured before entering the capillary and after coming out from the capillary using photo diodes. An entrance window consisting of a glass slide of thickness 0.1mm was used. We did not use an exit window but the fiber was placed close to the photo diode. The power of the laser light was measured for different lengths of capillary 6cm, 10.5 cm and 48 cm. A graph plotted of the optical transmission(ratio of light transmitted through the end of waveguide to the light entering into it) versus the capillary length is shown in Fig. 5.3. From the measurement it was determined that the loss coefficient was 0.47 $\pm$0.13 m^{-1} for the capillary.

To find the bending losses, laser light from He-Ne laser (632nm) was allowed to pass through the capillary filled with ethanol. A lens of focal length 2cm was used to focus the light into the capillary and the power was measured before entering the capillary and after coming out from the capillary using photo diodes. Teflon AF capillary of length 48 cm was used. A loop of radius of curvature of 2.5 cm was made in the capillary and the output signal was measured. The measurements were repeated for more number of loops and also for a straight capillary without any loop. A graph plotted of the optical transmission(ratio of light transmitted to the end of waveguide to the light entering into it) versus the number of loops is shown in Fig. 5.4. An exponential fit to the attenuation coefficient per turn gives a value of 0.09 $\pm$ 0.01 per

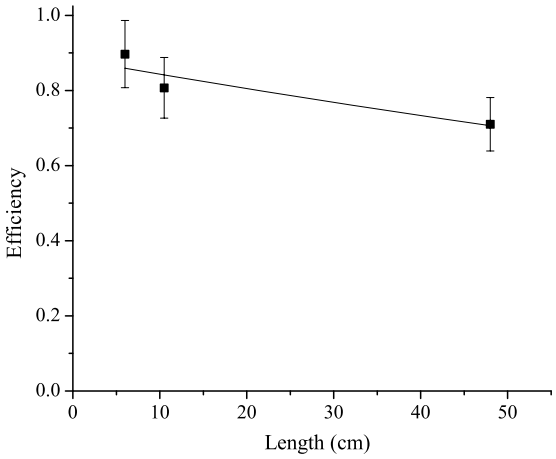

Figure 5.3: Measured transmission as a function of length for AF 2400 capillary tubing filled with ethanol. The solid line is an exponential fit indicating an e-folding absorption coefficient of 0.47 cm^{-1}

.

turn.

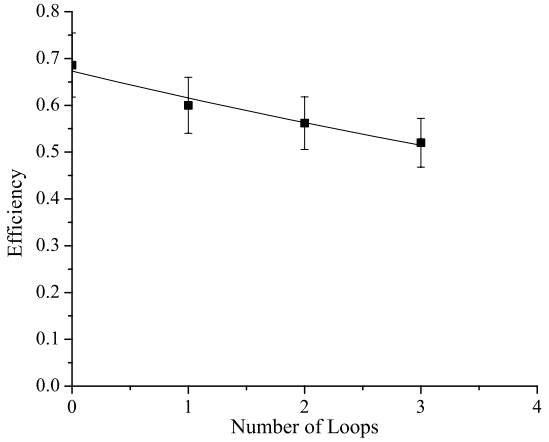

Figure 5.4: Measured capillary transmission versus number of loops. The solid line is an exponential fit with a loss coefficient of 0.09±0.01 per turn.

The attenuation coefficient estimated for the straight waveguide from Fig. 5.3 is (1/t1) = 0.47±0.13 m^{-1}. This value is in good agreement with the

measurements performed by Altkorn et al. [28]. Where an attenuation loss of 0.8 dB/m to 1.7dB/m was reported for ethanol in Teflon AF capillary. As the transmission losses are low we do not have to take the attenuation into account for short capillaries of the order of 20 cms which we used for the measurements. The bending losses per loop calculated from Fig. 5.4 is 1-$e^{-1/t1}$ = 0.09±0.01 per turn. The performance of the capillary also depends on the acceptance cone angle and the coupling efficiency. The light collecting efficiency estimations are given in section 5.2.4

5.2.3 Detection of Raman and SERS signals in LCW

The same experimental set up described in chapter 3 (Fig.3.1) was used for measurements with liquid core waveguide using the same 8 mm collection and 8 cm imaging lens. Light was coupled into and collected from the waveguide axially both at the input end. A special mount was designed to hold the liquid core waveguide (LCW) at the input end. The mount had a V groove in which the capillary was mounted. The input end was perpendicularly cleaved and tightly positioned against a thin microscopic cover glass slide of thickness 0.1mm. The capillary was filled through the far end using a syringe. By applying pressure the capillary was slowly filled until a small drop of liquid appeared at the input end as the liquid slowly leaked out between the end of the capillary and the glass slide. In order to have reliable measurements a small drop of liquid was maintained at the input end to avoid the formation of an air bubble. The layout of the LCW SERS detection system is shown in Fig. 5.5.

Before performing SERS measurements Raman signals of ethanol(n=1.36) and hexane (n=1.37) were measured in the capillary. The dependence of Ra-

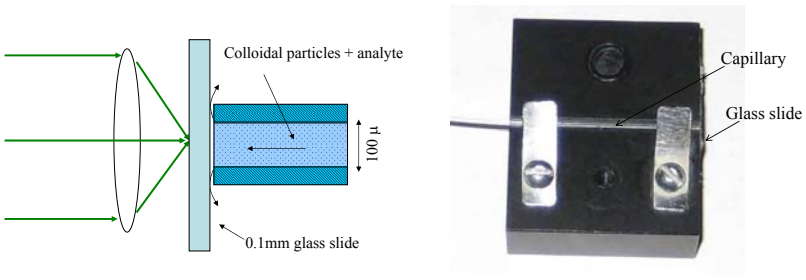

(a) (b)

Figure 5.5: (a)Layout used for SERS detection from liquid core waveguide and (b) a picture of the liquid core waveguide on the mount.

man signal from ethanol on the length of the capillary is shown in Fig. 5.6. Raman signals were measured using capillaries of different lengths 6cm, 15cm and 48 cm and the graph is plotted of the strength of Raman signal peak at 889 cm^{-1} versus length of the capillary.

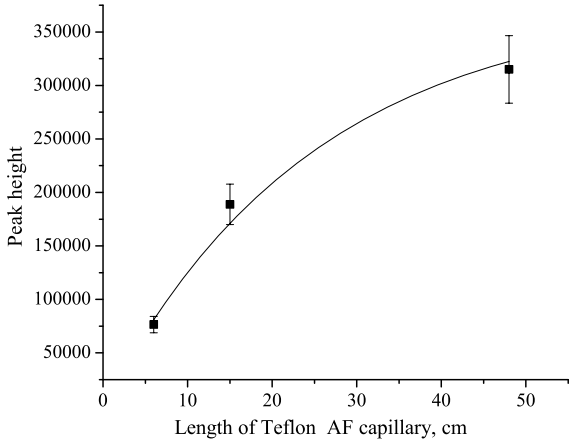

Figure 5.6: Peak Raman signal measured from Ethanol in a Teflon AF capillary for different capillary lengths. An integration time of 1 seconds was used for the measurements and a monochromator slit width of 200 μm used. The solid curve shows the least squares fit of Eq.5.6.

As one can see the peak height increases with capillary length and approaches a saturation value. Assuming an increasing cumulative Raman signal

versus length and taking into account the attenuation coefficient determined from Fig. 5.3 the expected dependence of the intensity of Raman signal versus capillary length is [127]

$$I_{LCW} = CI_0\frac{1}{2\alpha}(1 - e^{-2\alpha L}) \tag{5.6}$$

Where C is a constant, I_0 is the incident laser intensity coupled into the waveguide, α is the loss coefficient of the waveguide and L is the length of the fiber filled with liquid. Fitting the experimental data using the above model gives the value of loss coefficient α equals to 2.0$\pm$0.5 m^{-1}. This is higher than the loss coefficient calculated for light transmission directly through the capillary, which was 0.47 $\pm$0.13 m^{-1}. One of the reasons for this discrepancy in loss coefficient measurements can be from using different pieces of fibers for the measurements. As mentioned by Altkorn et al. [28], the loss characteristics vary between different sections of the fiber. Increased losses can be from scattering from imperfections in the fiber and there can be local regions with high losses. Another source of error can be from bending as during the Raman measurements the fiber was not kept straight because of the restrictions of the experimental set up. Therefore the additional losses can be from that. From fitting parameters, the asymptotic value obtained for the curve is $\sim$ 350000 which is close to the value of peak height $\sim$ 320000 we obtained with 48cm fiber, so the length of capillary is close to the optimum length which can be used for observing maximum Raman signal.

Fig. 5.7 shows the Raman signal from ethanol measured in a cuvette and in a Teflon AF capillary of length 15 cm for 1s integration time and 200μm slit width on the spectrometer. The Raman signal observed in the capillary is $\sim$50 times enhanced compared to that observed in the cuvette. The small

peak observed around 1000 cm^{-1} in Fig. 5.7(a) is the peak from the wall of polystyrene cuvette used for the measurements. A spectrum measured from deionized water in polystyrene cuvette is shown in the inset of Fig. 5.7(a) to show that this peak comes from the cuvette.

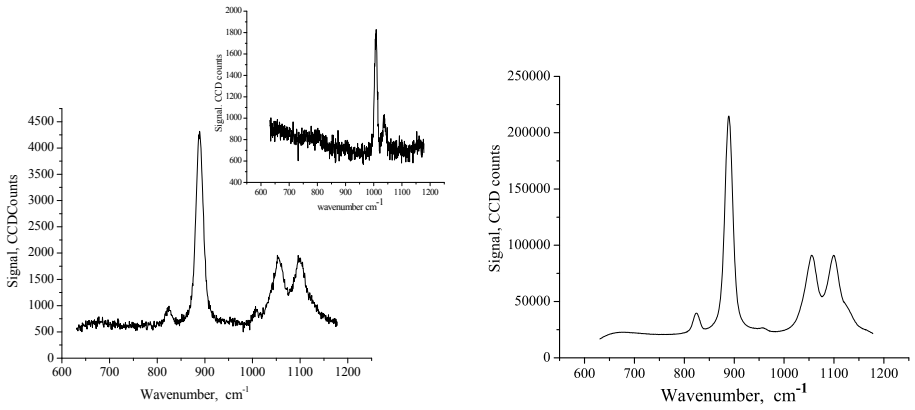

(a) (b)

Figure 5.7: Raman signal measured from Ethanol in (a)cuvette and (b)Teflon AF capillary. The inset Fig in (a) shows the peak observed from the polystyrene cuvette filled with deionized water.

The Raman signal of hexane measured in a cuvette and in a capillary of 10.5cm in length for an integration time of 0.5 seconds is given in Fig. 5.8 in this case an enhancement of ~ 30 was obtained.

SERS spectra were measured for acridine orange (AO) and tryptophan and comparisons of spectra in the cuvette and capillary were made. First the Raman spectrum of the waveguide tubing alone and pure water alone was also measured. To measure the spectrum from the waveguide tubing, the waveguide was moved so that the incident light was focused onto the wall of the waveguide and the resultant spectrum is shown in Fig. 5.9. The spectrum from capillary tubing filled with water does not show any distinct features that may mask the spectrum of the sample in the waveguide.

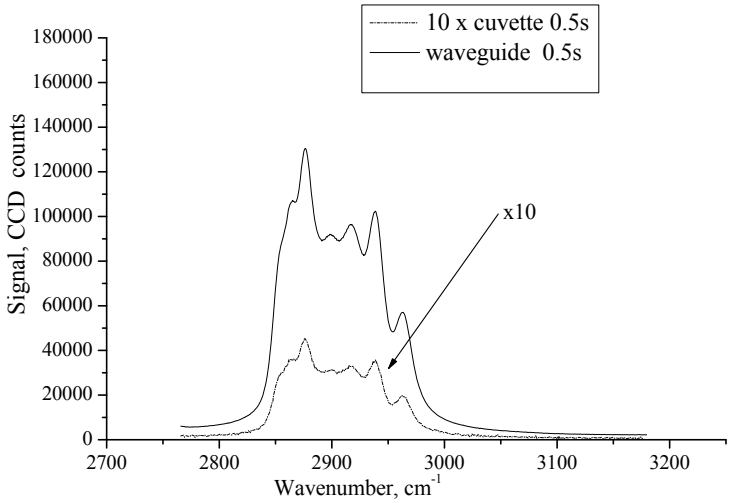

Figure 5.8: Raman signal measured from hexane in a cuvette and in a Teflon AF capillary.

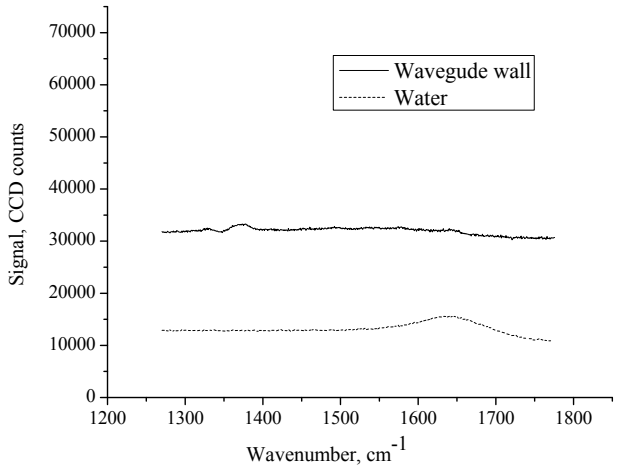

Figure 5.9: Raman signal measured from waveguide wall alone and the capillary filled with pure water for an integration time of 5 seconds.

A sample solution for acridine orange (AO) measurement was prepared by adding an aqueous solution of AO into 10 ml of silver colloid prepared by the method described in chapter 3 followed by NaCl(10^{-1} M) giving a final concentration of 4.4×10^{-8} M AO in the final solution. An integration time of

5 seconds was used for the measurements. The spectra measured in a cuvette and in the Teflon AF capillary are given in Fig. 5.10. The same sample solution was used for both the measurements. A signal enhancement of ~ 7 times was measured for the the capillary versus direct cuvette measurements.

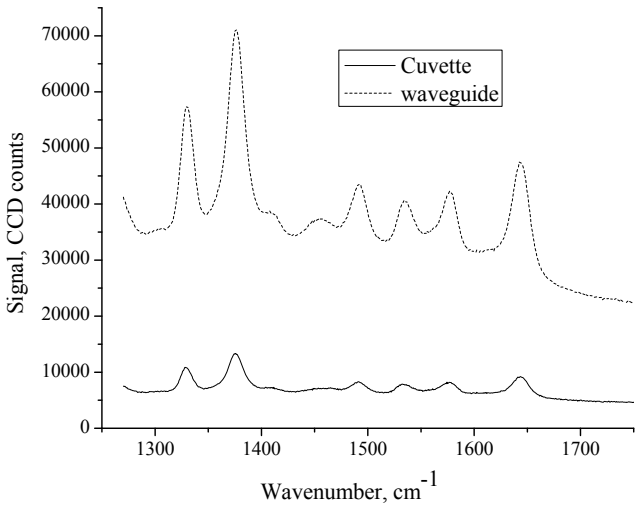

Figure 5.10: SERS signal measured from acridine orange in a cuvette and in a Teflon AF capillary .

The SERS spectra of amino acid Trp obtained in a cuvette and a capillary are compared in Fig. 5.11. The solution for the SERS measurement was prepared by adding 1 ml of 2×10^{-3} M Trp into 10 ml of concentrated colloid followed by 2 ml of 10^{-1} M NaCl giving a final concentration of 1.6×10^{-4} M Trp in solution. The spectrum from both cuvette and Teflon AF capillary were measured when there was a stable signal from the prepared solution a few hours following mixing. We found that the maximum signal was observed when there was flow in the capillary and when the flow was stopped the signal degraded quickly with time. This decrease can be due to photodegradation; degradation of molecules caused by the absorption of light. With LCW geometry the enhancement obtained for a capillary of length 20 cm was about a factor of 10

compared to that from a cuvette.

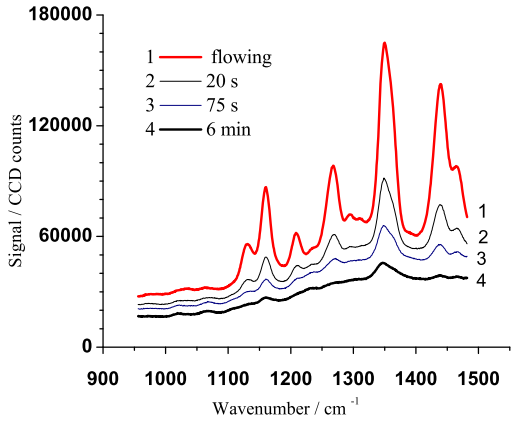

(a)

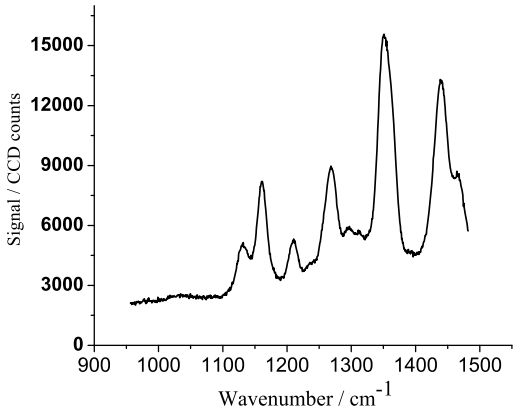

(b)

Figure 5.11: (a) SERS spectra of Trp (1.6×10^{-4} M) in a Teflon capillary at different times after stopping the flow (b) corresponding spectrum in a cuvette.

5.2.4 Light collection efficiency estimations

The experimental setup used has an 8mm collecting lens (L1) and an 8cm imaging lens (L2) as shown in Fig. 5.12, so the magnification of the light collecting system onto the spectrometer entrance slit was 10 times. Light collecting efficiency can be estimated as follows. The backward Raman scattered

light emitted from the capillary is re imaged onto a spot on the monochromator entrance slit. The diameter of the image spot is equal to the inner diameter of the capillary multiplied by the magnification of the lens collecting system. D1 is the inner diameter of Teflon AF capillary and D2 is the slit size. The numerical aperture(NA) for aqueous solution (n=1.33) in Teflon AF 2400 capillary (n=1.29) is 0.32 from Eq. 5.5 and the corresponding solid angle is 0.31 sr. The monochromator has an entrance NA of 0.1 and the slit width used was 150 μm. The inner diameter of the Teflon AF capillary is magnified 10 times by the lens system, so for a 112μm diameter capillary the beam diameter on the slit is $\sim$1.12mm. The area of the beam falling on the monochromator is 0.98 mm^2 (S1= πr^2 =π(0.56)^2) and the area of the slit is 0.17 mm^2(S2= 0.15x1.12), so we are collecting only 0.17 (S2/S1) of the light emitted from the capillary end.

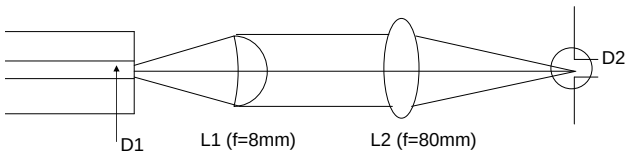

Figure 5.12: Detection lens system.

The effective scattering length of Teflon AF capillary for measurement of Trp spectrum shown in Fig. 5.11 is 20cm and in the cuvette the experimentally measured scattering length over which the backscattered Raman signal is collected was 0.4mm as defined in chapter 3 (see section 3.4). If one compares the scattering lengths then $\sim$500 times enhancement might be expected in the capillary compared to that in the cuvette. However to make a correct comparison the light collection efficiency should also be taken into account. For cuvette measurements the numerical aperture (sin 45) is 0.7 and the solid

angle collection angle is 1.9 sr. The solid angle of light collected from the cuvette is 6.1 times larger than that of the capillary and only 0.17 of this light is transmitted through the entrance slit for the Teflon AF capillary measurement, so a factor of 36 times reduction is expected for the capillary geometry in comparison to that in the cuvette. Thus instead of 500 times enhancement we should expect $500/36 = 13.9$ times enhancement in SERS signal. We observed 10 times enhancement of SERS signal from Trp in the capillary compared to that in cuvette which is close to this estimated value.

For the case of Raman signal from ethanol we observed 50 times enhancement in the capillary compared to that from the cuvette. Ethanol has a higher refractive index (n=1.36) compared to the aqueous solution. The numerical aperture for ethanol in the capillary 0.43 and the corresponding collection solid angle is 0.63 sr, which is two times higher than the numerical aperture of aqueous solution in capillary. The 5 times smaller enhancement of Raman signal from Trp in silver colloid solution in capillary compared to the Raman signal enhancement of ethanol in capillary is due to this difference of a factor of two in collection solid angle and also due to the additional scattering and absorption losses caused by the silver colloid solution itself. The aggregated silver colloid has noticeable absorption near ~ 532 nm.

In the present measurement additional losses arise due to Fresnel reflection losses when coupling light into the capillary. It is expected that the collection efficiency can be increased by optimizing the detection system, that is by matching the numerical apertures of the Teflon capillary and the collecting lens and by matching the capillary output beam to the entrance slit of the monochromator so that all the emitted light passes through the entrance slit. In this case the enhancement factor should approach a factor of 50 times as

discussed above.

The utilization of LCWs as biological and chemical sensors have been reported in several papers [29, 116, 128]. Raman signal enhancement from aqueous solutions by 1 or 2 orders of magnitude have been obtained using Teflon AF waveguides as described in [27, 116, 117] . A hollow core photonic crystal fiber for enhancing Raman signals from ZnO nanoparticles in solution has been reported by Irizar et al. [129]. To the best of our knowledge the use of Teflon AF capillary for surface enhance Raman scattering detection and the comparison of SERS detection in a cuvette geometry and in a Teflon AF capillary has not been reported to date. The enhanced Raman signal observed in SERS is further increased by the use of Teflon AF capillary. SERS in optical waveguides has been reported by several groups. Measor et al. [130] has reported the detection of SERS on an optofluidic chip. Where they used interconnected solid and liquid core antiresonant reflecting optical waveguides (ARROWs) for detection of Rh 6G molecules and a detection sensitivity of a minimum concentration of 30 nM was found. Improvement of the SERS signal using a hollow core micro structured optical fiber was reported by Cox et al. [131].A modified hollow core photonic crystal fiber for SERS detection of rhodamine 6G, human insulin and tryptophan in the concentration range 10^{-4} - 10^{-5} M has been reported by Zhang et al. [132]. The solution used here for observation of SERS signal of Trp in the Teflon AF capillary was prepared using NaCl electrolyte. With optimization of electrolyte, for example by using the composite electrolyte mentioned in chapter 7, we achieved large SERS enhancement factors of up to 10^8. An additional enhancement of 10 times can be obtained with the help of a liquid core waveguide technique as demonstrated

above. With a fully optimized optical detection system we expect that we can further increase the detection limit by another factor of the order of 5 times. Thus by using an optimum electrolyte and using a Teflon AF capillary with an optimized detection system we expect that we can further increase the detection limit by a factor of 50 times. These results are thus promising for the use of SERS in LCW devices for performing very high sensitivity detection of organic molecules.

5.3 SERS Detection in a Microfluidic Chip

The application of SERS to detect organic molecules in microfluidic systems was also studied. To perform the these measurements, a microfluidic chip from Micralyne [125] was used. The chip has an 80 mm long 50μm $\times$ 20μm channel between two 1.05 mm thick glass slides . The channel is etched into one of the glass slides. The details of the chip are shown in Fig. 5.13

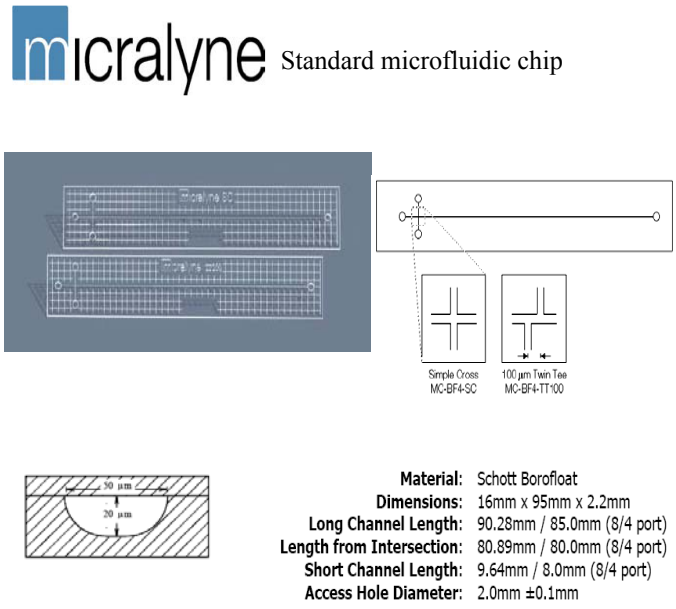

Figure 5.13: Microfluidic chip.

The same experimental setup as described in chapter 3 was used for microfluidic chip measurements and the scattered light was collected in a back scattered direction transverse to the channel. A picture of the microfluidic chip setup is shown in Fig. 5.14

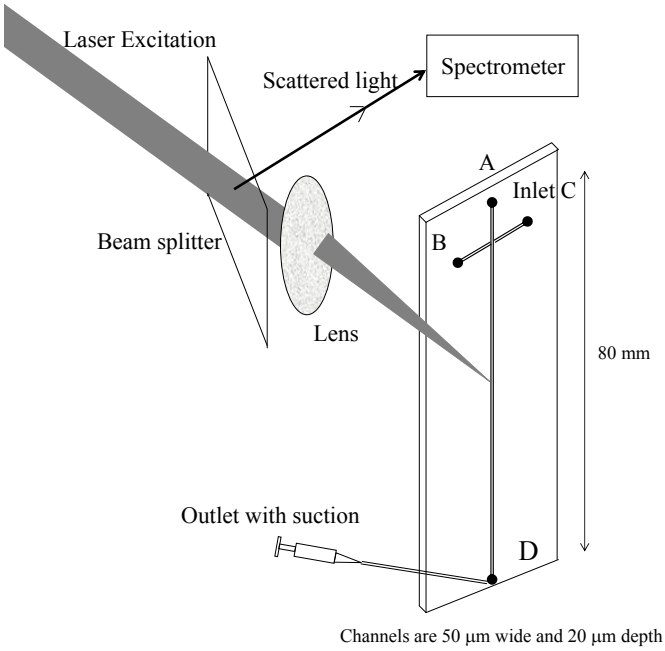

Figure 5.14: Schematic of microfluidic chip detection system.

The SERS signal of Trp was measured in both a cuvette and in the microfluidic chip for comparison. The sample solution was prepared by adding 1 ml of 2×10^{-3} M solution of Trp into diluted colloid (4ml of silver colloid + 80ml of deionized water), giving a final concentration of 2.3×10^{-5} M with no additional electrolyte. The SERS signals measured in the microfluidic chip geometry was compared with that from a cuvette as shown in Fig. 5.15. An integration time of 5s seconds was used for the sample in cuvette and 50 seconds integration time for the sample in the microchannel. The signal from the microfluidic chip was significantly weaker than that from the cuvette which

can largely be attributed to the difference in the probed scattering length. In the case of the cuvette the experimentally measured scattering length over which the backscattered Raman signal collected was $\sim$400μm versus a 20 μm probe depth for the microfluidic channel. The measured ratio of measured signal intensities was 30 times as compared to the ratio of interaction lengths of 20. .

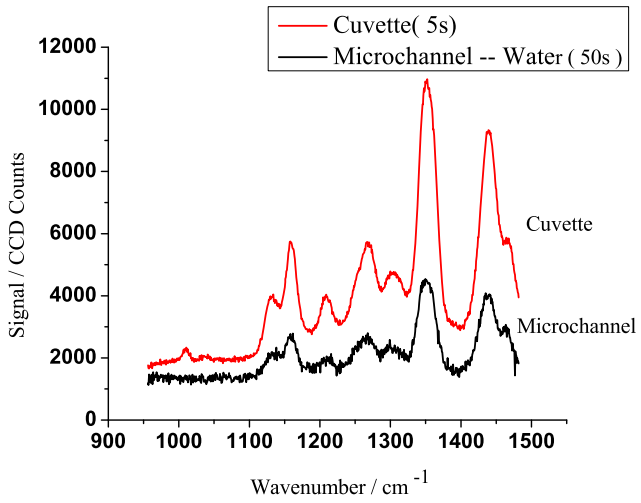

Figure 5.15: SERS spectra of Trp (2.3 $\times 10^{-5}$ M) in a microfluidic channel and in a cuvette.

In order to increase the interaction volume in the microfluidic system, laser micro machining has been carried out to modify a standard microfluidic chip from Micralyne. To increase the scattering length of the transverse probe beam we made a 1 mm well in the standard microfluidic chip. For micro machining a Q-switched Nd:YAG laser (Big Sky) operating at the wavelength of 266 nm was used. The laser provided 5 ns pulses with energy of 3mJ at 20 Hz repetition rate. Laser light was focused onto the chip and the micro machining was monitored through the other side of the chip using a CCD viewing camera. The drilling process took $\sim$ 2minutes to complete and the completion could

be seen by the appearance of a hole on the channel wall. After that we took a few more shots to clean the channel from debris. The resulting hole had a tapered shape with a surface entrance hole with a diameter of $\sim 150\mu$m and hole diameter of $\sim 50\mu$m at the bottom where it met the microfluidic channel. The details of the microfluidic chip layout and a photograph of the laser machined well are shown in the Fig. 5.16.

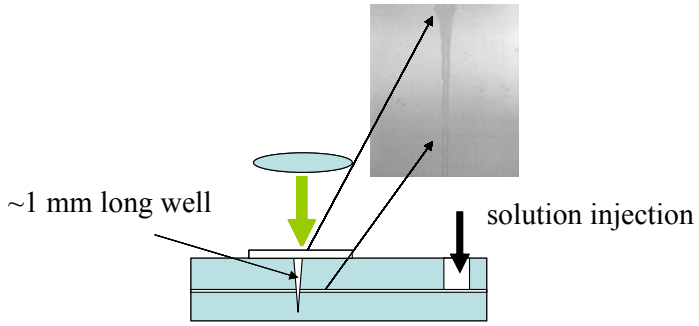

Figure 5.16: Layout for laser micro machining of an enhanced interaction length probe hole in the microfluidic chip and photograph of the hole produced.

In the modified microfluidic chip the signal was collected by focusing the light into the resultant well, covered by a 0.2 mm thick glass cover slip. The SERS signal observed for Trp in a modified microfluidic chip is shown in Fig. 5.17 along with that measurement in a cuvette and a standard microfluidic chip. The same sample solution was used in all the measurements. The sample solution for the SERS measurement was prepared using the composite electrolyte mentioned in chapter 4. Stock solution of Trp was added to silver colloid followed by composite electrolyte giving a final concentration of 2.3×10^{-6} M Trp. The signal was measured for an integration time of 5 seconds in the cuvette and in the microfluidic chip. An increase of the signal by a factor of almost 2 times was observed from the measurement in a standard microfluidic chip. This increase is much smaller than the ratio of probe chan-

nel depth to original channel depth. However, this can be explained in terms of the small numerical aperture of the channel and scattering from the walls interfering with the collection of the light into the F/1 collection cone. In this case the probe was focused approximately at the depth of the original channel. In addition, the fluid which enters the long probe channel may also stagnate undergoing photo bleaching and interacting with the rough walls causing a decrease in detectability of the Trp molecules. Such photo degradation of the solution during the actual irradiation has previously been reported [133].

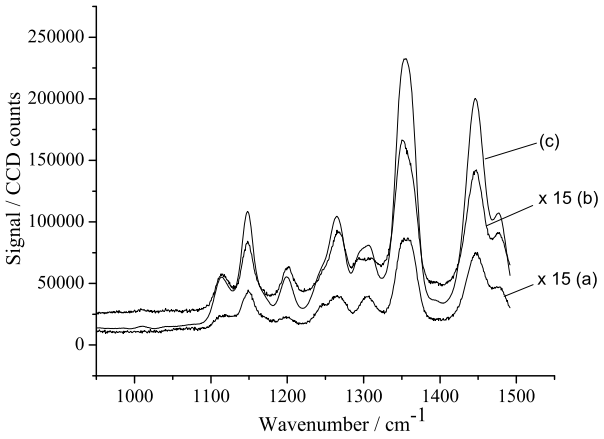

Figure 5.17: (a) Spectrum from Trp in a microfluidic chip (50μm width and 20μm depth) (b) SERS signal from Trp in a modified microfluidic chip (c) SERS signal from Trp in a cuvette (scattering length $\sim$ 400μm).

Further work is needed to improve the probe channel,geometry and flow of analyte through the channel. In our studies we used a commercially available standard microfluidic chip for SERS detection and detected a final concentration 2.3×10^{-6} M of Trp in the microfluidic channel. Assuming a detection limit of 1×10^{-6} M using the 80 mm long 50 μm $\times$ 20 μm channel the amount of sample required is 80 fmol. If we assume that only 10mm of the channel needs to be used for detector system, the amount of sample that would be

required is $\sim$ 10 f mol. As discussed in chapter 6 and 7 we have detected good quality SERS signal from Trp at concentrations 10^{-7} M and lower, which is lower than that previously reported in the literature [1, 25]. Assuming a 10^{-7} M detection limit , the amount of sample required will be as low as 1 fmol. We can further increase the detection limit by increasing the integration time and the monochromator slit width. Park et al. [18] detected SERS signals from the mixture of two different dye -labeled (TAMRA and cy3) sex determining Y genes, SRY and SPGY1 adsorbed on alligator teeth shaped microfluidic channel under flowing conditions. The major SERS peaks in this case were observable down to the concentration of 10^{-11} M. The micro channel they used (300μm $\times$ 100μm) had larger dimensions than that we used in our studies. A SERS detection limit of 10 pM was achieved for adenine molecules by Wang et al. [134], they used an opto-fluidic device that has a pinched and step micro channel- nanochannel junction that can trap and assemble nanaoparticle and target molecules into optically enhances SERS active clusters by using capillary forces. Essentially this technique is equivalent to preconcentration technique as the concentration of nanoparticles/analyte molecules in the measuring spot is much higher than the initial concentration of 10^{-11} M. Only a limited amount of work has been reported on the implementation of SERS in microfluidic system. The short interaction length of microfluidic channel typically gives a smaller signal. Our results shows that when we have high SERS enhancement even standard microfluidic chips can be used for SERS detection and we expect that we can modify the chip and improve the detection. An optimum system would be a waveguide incorporated into the microfluidic system.

5.4 Conclusion

With the high enhancement factor observed for Trp amino acid and resultant low detection limit we have demonstrated we could measure signals in a standard microfluidic channel at low concentrations. However, in the standard microfluidic channels, the SERS signals observed are reduced relative to those in large open probe volumes due to the much smaller transverse probe length across the channel used here. Special designs for extending the light collecting geometry are needed to optimize the use of the SERS technique in the microfluidic channels. Laser micro machining was employed in order to fabricate an extended interaction volume in the microfluidic geometry. However this was not optimized and further work is required to optimize the resultant probe geometries to allow for large effective numerical aperture probing and optimum flow through the measurement sample. Once optimized, it is expected that similar sensitivities can be obtained in microfluidic systems as with the open geometry cuvette measurements and these should be in the fmol range as required to analyze the contents of single cells extracted into such microfluidic channels. Liquid core waveguides provide the possibility of an additional signal enhancement up to 50 times giving the possibility to achieve detection limit for Trp as low as $\sim 10^{-10}$ M. In principle short waveguide channels on the order of centimeters in length could be incorporated into microfluidic systems allowing such high sensitivities for lab on a chip analysis. The results obtained will be useful in the further development and optimization of microfluidic chip devices utilizing SERS.

Chapter 6

High sensitivity Detection of Tryptophan Amino Acid

6.1 Introduction

This chapter describes a detailed study of low concentration detection of the amino acid tryptophan (Trp). L-Trp, the left handed form of Trp was used for the measurements. SERS studies of different amino acids; tryptophan, phenylalanine, tyrosine, alanine, lysine etc have been reported in the literature [12–17]. In the vast majority of papers concentrations of amino acids under study lie above 10^{-5} M. Recently surface enhanced Raman scattering of Trp in silver colloidal solution has been reported by Aliaga et al. [25]. They observed SERS spectra from Trp molecules in the concentration range of 10^{-4} to 10^{-5} M. The spectra exhibited certain spectral characteristics, which can be attributed to different configurations of the adsorbed molecule on the metal surface. Also the authors observed variations of SERS spectra with time and reproducible data could be obtained only after 12 hours of incubation period. It is believed that in most cases Trp molecules would attach to the silver surface through carboxylic and amino groups while the indole ring does not interact with the surface [1, 25, 26]. Many of the applications demand reproducible and

sensitive spectra together with smaller incubation time and fast observation of the signal. In this chapter we report a detailed study of SERS effect in L-Trp in the concentration range 1.4×10^{-8} to 5×10^{-4} M. The lowest concentration of Trp studied is 3 orders of magnitude smaller than the previously reported [1, 25, 26]. We found that we could obtain good signals even at very low concentrations and that the SERS spectrum undergoes noticeable changes with the increase of concentration above $\sim 10^{-5}$ M. The maximum enhancement of Raman signal observed in experiments is about 10^8 which is several orders of magnitude stronger than recently reported [1]. The recorded spectra are very stable in time and highly reproducible. The key results obtained are presented in detail in the following sections and many of these results have been published in reference [135].

6.2 Sample Preparation

The samples used for the detection of SERS spectra of Trp molecules in silver colloidal solution were prepared using the following procedure . We added the required amount of stock solution of tryptophan to 10 ml of freshly prepared silver colloid, followed by addition of 30 ml of DI water and 20.5 ml of the composite electrolyte (a mixture of 20 ml of 5×10^{-3} M of sodium bicarbonate and 0.5ml of 10^{-3} M of sodium chloride).The silver colloid was prepared by the method described in chapter 3. The colloid was used just after preparation. We added deionized water to dilute the colloid as it was found during the experiments that the SERS signal strength is affected by the concentration of the colloid solution. Sodium bicarbonate(NaHCO3 ,Fisher,$\geq$98%), sodium chloride (NaCl, Fisher,$\geq$98%) and amino acid tryptophan (Trp, Sigma Aldrich, reagent grade $\geq$98%) were used as received without further purification. 18

MΩ deionised water was used for preparing the solution. The sodium bicarboante solution was aerated for several hours before use, using a porous carbonaceous stone aerator, which leads to significantly stronger SERS signals. Stock solutions of Trp at concentrations 2×10^{-5} M, 2×10^{-4} M, 2×10^{-3} M, and 2×10^{-2} M, were prepared using deionised water.The pH of the final solutions was in the range 8.8 ± 0.5. The SERS spectra started to appear approximately 2 minutes after mixing, reaching the maximum intensity at about 15 minutes.

6.3 Orientation of Trp on Colloidal Silver

The position and relative intensities of the peaks in the SERS spectrum of Trp depend on several factors such as the type of metal nano particles, the pH of the solution, colloid aggregation, and, primarily, on the way the molecules bind to the nano particle surface. Because of these factors, the Trp SERS spectra reported in the literature have different appearances. Based on the position of the peaks and their relative intensities it is possible to estimate how the molecules are attached to the nano particle surface. For most of the observations reported in the literature, it is believed that Trp molecules are attached to the surface through carboxylate and amino groups [1,25,26]. However, the binding should depend on the preparation and surface conditions of the nano particles and the combination of electrolytes used to promote attachment of the molecules to the surface. In the current experiment we observed two slightly different spectra of Trp, one for low concentrations below $\sim 10^{-5}$ M and one for high concentrations above $\sim 10^{-4}$ M. As will be explained later, we believe this indicates a different orientation of the binding of the molecules on the surface.

The SERS spectra of Trp at low and high concentrations as well as the normal Raman spectrum of Trp in water solution (0.03 M) are shown in Fig. 6.1. At high concentration of Trp ($> 10^{-4}$ M) the SERS spectral pattern looks similar to that of the normal Raman spectrum in water. As one can see from the figure, the intensity of the SERS signal from the colloid with low concentration of Trp shows a few differences in spectral features and is much stronger than that from the higher concentration solution. This can be attributed to the differences in the binding of the molecules to the nano particles and also perhaps to changes in the aggregation of the colloidal particles for the different concentrations of Trp, which is another important factor in strong signal enhancement.

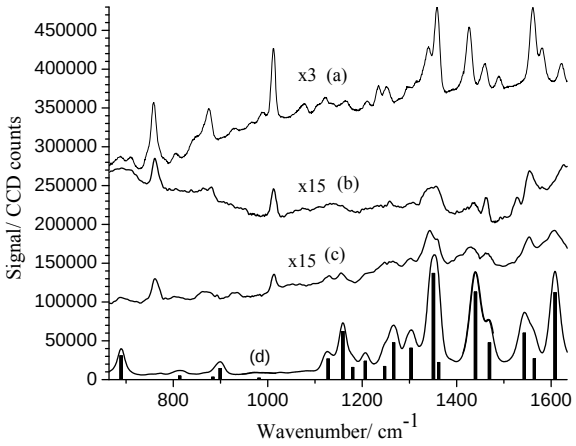

Figure 6.1: Raman and SERS spectra of L-Tryptophan.(a) solid powder; (b) 0.03 M aqueous solution, 100 s acquisition time;(c) silver colloid, concentration of Trp 5×10^{-4} M, 50s acquisition time;(d) silver colloid, concentration of Trp 4.2×10^{-7} M, 5s acquisition time. Curves b and c are smoothed using a 5 point FFT filter. All spectra are shown as acquired without background correction. Vertical lines represent position and height of the individual peaks obtained using a multi peak fitting procedure of the spectral curve d.

While in the spectral range above 1100 cm^{-1} all three curves have similar structures with very well defined peaks, below this region they have substantial differences. The most important of these differences are the absence of strong peaks near 760 cm^{-1} and 1000 cm^{-1} in the case of low concentration (4.2×10^{-7} M), which are usually assigned to the ring breathing modes, and the appearance of a strong peak at 690 cm^{-1} for the lower concentration range. We also did not observe a peak near 1400 cm^{-1}, which is often observed in SERS spectra of amino acids and is assigned to the stretching COO mode [1, 12]. It is interesting that in Ref. [136] the authors observed the appearance of a new band in the SERS spectra of adenine near 690 cm^{-1}, which they assigned to the out-of-plane deformation (torsion and wagging) of the adenine heterocyclic ring system [136]. Taking into account the general consideration that vibration bands with the polarizability oriented parallel to the surface of the nano particle are not active in the SERS spectra (ref. [137]) and using band assignments from ref. [1] and ref. [138] one may speculate that in the current experimental conditions for low concentrations, the Trp molecules are adsorbed to a large extent with the orientation of indole ring flat to the nano particle surface. In Table.6.1 we provide peak positions for the Trp SERS spectra observed in our studies in comparison with some of the previously published studies.

To calculate the enhancement factor we used the band at 1350 cm^{-1} vs the valley around 1400 cm^{-1} as it is the strongest band in both the normal Raman and SERS spectra. The corresponding peak height for 4.2×10^{-7} M Trp in colloid solution is about 140000 counts, whereas the peak height for 0.03 M Trp in water solution is 2200. Taking into account the differences in the integration time (5 s and 100 s) and concentrations, the ratio of the amplitude

Band, cm^{-1}	Intensity(wavenumber)[1]		
	Current Paper Trp Concentration $<\sim 10^{-5}$ M	Kim [12]	Chuang [1]
689	S	NO	NO
758	NO	VS	VS, θR), θ(r)
770	W	NO	NO
813	W	M(802)	S (806), γCH_2, $\nu CCOO_-$
883	W	NO	M (876), αH(R), αH(r)
899	M	NO	S(903), νCCOO (Ref. [137])
929	NO	S	S (927), $\nu CCOO_-$, γNH^{3+}, γCH_2
981	W	NO	W (974), δH(R)
1011	NO	VS	VS (1013), θ(R), θ(r)
1128	M	NO	NO
1159	S	S	NO
1180	W(shoulder)	NO	NO
1207	M	NO	S (1213), ν(r), $\nu CCOO_-$
1247	W (shoulder)	W	NO
1266	S	NO	S(1253),γH(R),γH(r),βCH
1303	S	S	S (1306), βH(C), ωCH2
1351	VS	S(1357)	S (1348), β CH, β H(CH2)
1362	M(shoulder)	NO	VS (1362), ωCH2, βCH
1396	NO	VS	VS (1405), ν_S CO_{2-}
1440	VS	W	S(1442), ν(r), ν(R)
1469	S	NO	S (1463), αCH2
1543	S	S (1546)	S (1549), ν(r), ν(R)
1565	M	M(1558)	NO
1608	VS	W	S (1605) V(R), V(r)
1700 to 3000	NO or W		

Table 6.1: Identification of lines observed for SERS spectra of Trp at concentrations below 10^{-6} M. [1] Assignments from Ref. [1] unless indicated otherwise. Signal strengths: (VS) very strong, (S) strong, (W) weak, (M) moderate, and (NO) not observed. (θ) Ring breathing, (ν) stretching; (β) bending (ω: wagging, γ: rocking, δ:twisting);(s) symmetric; (R) benzene ring, and (r) pyrrole ring.

of the peaks gives a value of the enhancement factor as 0.9×10^8, which is four orders of magnitude higher than previously reported [1].

6.4 Influence of the Morphology of Colloidal Particle Aggregates on SERS Spectra of Tryphtophan

Transmission electron microscope (TEM) images of silver colloid with low and high concentrations of tryptophan are shown in Fig. 6.2. Though as in all TEM measurements sample preparation included sample drying, which can impact the final morphology of the samples, the TEM pictures are still useful to indicate morphological differences between the two sample conditions.

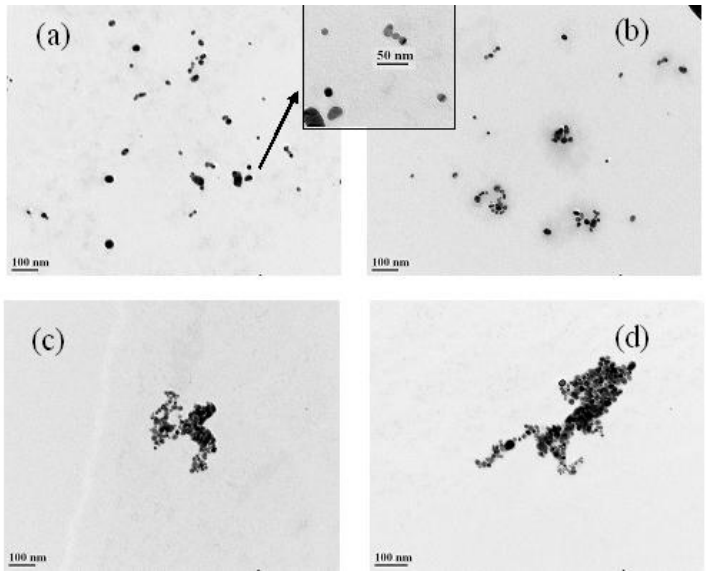

Figure 6.2: TEM pictures of silver colloid taken at two concentrations of Trp:(a) and (b) 4.2×10^{-7} M, and (c) and (d) 5×10^{-4} M.

To prepare samples for TEM, a drop of the sample solution was placed on the grid and excess solution was taken out using a filter paper and after then the sample on grid was air dried. In the first case, at low concentration, there are many small aggregates containing fewer than 20 particles with a

large number of dimers, trimers, and isolated particles. Many of them consist of loosely connected particles with gaps of a few nano meters between them. It is well known that such aggregates provide the highest electromagnetic enhancement, especially when molecules are trapped in the junction between nano particles [139,140]. At higher concentration, aggregates are much bigger, containing more than 100 particles that seem to be quite densely packed. Such large clusters of aggregates provide much reduced EM enhancement compared to dimers and trimers. These morphological differences can partly explain the observed difference in the Raman signal enhancement for high and low concentrations of tryptophan. Also, from the symmetry point of view, one may suggest that for the molecules having a large flat fragment (such as the indole ring in the Trp molecule) and that are trapped in the junction between nano particles, the preferable binding configuration would be a configuration with that flat fragment parallel to the surface of the nano particle. A 2D electromagnetic model described by Brown et al. [139] on enhancement around two silver nano particles shows that there is strong dependence of the enhancement on the separation between particles. The smaller the distance between the nano particles the larger the observed enhancement. The difference in predicted Raman enhancement for two nano particles 1 nm apart and 25nm apart can be as much as six orders of magnitude. The calculated maximum enhancement for two nano particles with 1 nm separation is approximately $\sim 10^9$ and they state that this value agrees within an order of magnitude with that has been observed experimentally. The authors also state that clusters of more than two particles modeled did not produce significantly large enhancements. This result suggests that the hot spots has more to do with extremely close location of two nano particles of optimum geometry rather than clusters

of large number of particles. This is similar to what we have observed experimentally in our studies. Hao et al. also described that the spacing of nano particles has a crucial role and SERS enhancement factor of $\sim 10^{10}$ has calculated for two silver nano particles with 2nm separation [52]. A recent study on relationship between the degree of aggregation and SERS enhancement by Sun el al state that there is a strong correlation between aggregate size and SERS intensity. They report that for certain excitation wavelengths the optimum size of aggregate for observing greater SERS enhancement is 116.2 nm [141] compared to other smaller and larger aggregates.

6.5 Concentration Dependence of SERS Signal

To study the concentration dependence of the SERS signal we simultaneously prepared seven solutions with final concentrations of tryptophan of 1.4×10^{-8} M, 4.2×10^{-8} M, 1.4×10^{-7} M, 4.2×10^{-7} M, 1.4×10^{-6} M, 1.4×10^{-5} M, and 1.4×10^{-4} M. The SERS spectrum from each of these solutions was measured over approximately a 2 hour period of time. After mixing, the solutions underwent some color changes due to nano particle aggregation. After approximately 10 minutes, the colors of the solutions were more or less stable and were yellow-orange for low concentrations and green-blue for high concentrations ($>4\times10^{-7}$ M). In Fig. 6.3 the spectra taken approximately 15 min after mixing are shown on a log scale for better comparison. One can see that the shape of the spectral curves stays almost unchanged over the whole range of concentrations except for the highest one. It is worth noting that the recorded spectra are also free of the broad background commonly seen in the SERS spectra of Trp published in the literature.

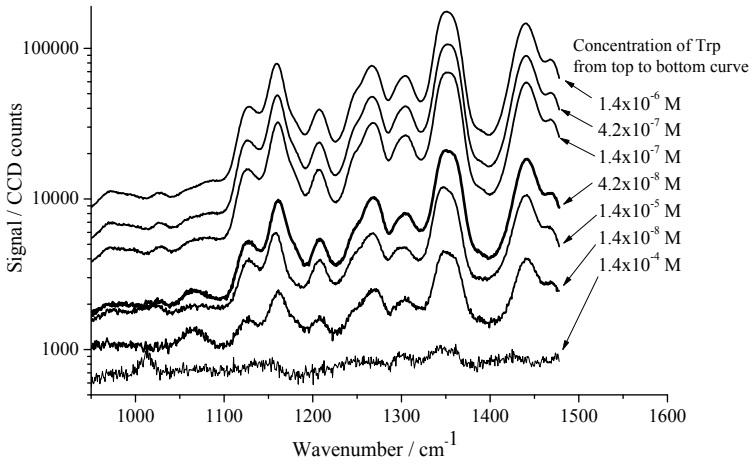

Figure 6.3: SERS spectra of Trp at different concentrations at 15 min after mixing.

The variation of the intensity of the highest peak at 1350 cm^{-1} versus concentration is shown in Fig. 6.4 (curve a). In the same figure the corresponding signal per molecule (obtained by dividing the peak height by the molar concentration and multiplying by 10^{-11}), which essentially represents the Raman scattering cross-section, is also shown (curve b). As one can see, up to a concentration of 10^{-6} M the signal per molecule stays approximately constant and then it drops significantly by 10^5 times as the concentration is increased. Such decrease in the Raman scattering cross-section at high concentration can be caused by two factors. First,the surface of the nano particle can adsorb only a limited number of molecules. Assuming that the silver colloid contains monodispersed nano particles with a size of 10 nm [1], one can estimate that 1.4×10^{-6} M concentration corresponds to approximately 520 molecules per particle, which would be approximately the number of molecules required to fully coat the surface of the nano particle. Above this concentration not all the molecules contribute to the SERS signal. Secondly, at concentrations higher than $\sim 2 \times 10^{-6}$ M the decrease could also be caused by a change in the binding

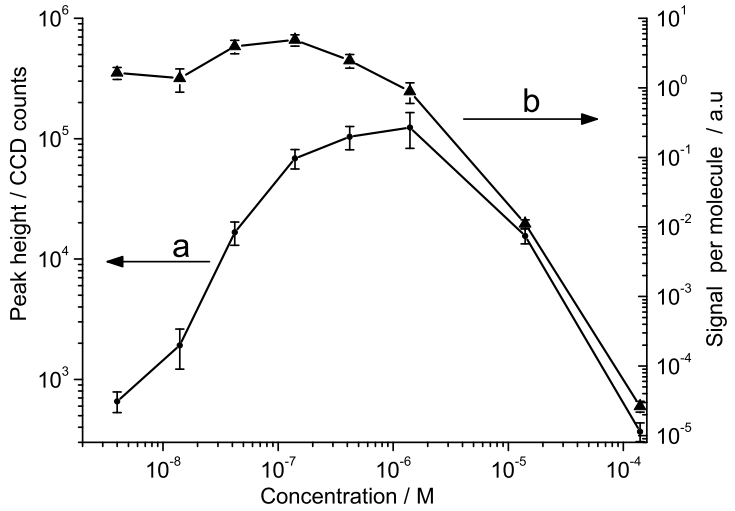

Figure 6.4: (a) The magnitude of SERS peak at ∼1350 cm^{-1} (relative to the valley at 1400 cm^{-1}); The data is a result of the averaging over three separate experimental measurements performed over a few months; (b) The corresponding signal strength per molecule versus Trp concentration.

geometry. The latter reason becomes even more evident when we examine the absolute amplitude of the signal (curve a in Fig. 4). It appears that even if the molecules coat all of the nano particle surfaces, the total emission drops with concentration,indicating that the binding geometry is changing with increased concentration leading to reduced SERS enhancement. The qualitative changes of the SERS spectra with concentration also support this conclusion. For a given concentration of Trp we observed very good batch-to-batch reproducibility of the SERS spectra. A standard deviation in spectral peak height of 46% was found from one measurement to another and a reduced mean error bar of 20% in the absolute intensity of the SERS spectral peaks could be obtained when 6 repeat measurements of one sample were averaged. These variations did not influence the relative intensities and position of the peaks.

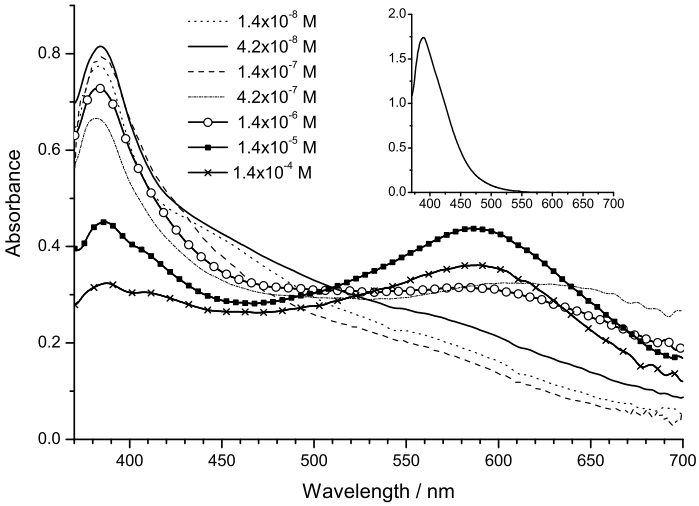

Figure 6.5: Absorbance spectra of silver colloids with different concentration of tryptophan taken 15 minutes after mixing. In the insert the absorbance of the original silver colloid before addition of the electrolyte and tryptophan is shown.

Optical absorbance spectra of the samples taken approximately 15 minutes after preparation are shown in Fig. 6.5. It can be seen that with the increase of tryptophan concentration the shape of the absorption curves changes from single peak (typical for surface plasmon resonance absorption of spherical particles) to double peak. Such double-peak structure is typical for small agglomerates, isolated elongated particles, and doublets [6]. As the concentration of tryptophan is the only difference between the samples, we can conclude that tryptophan molecules directly participate in the colloid aggregation and strongly interact with the silver nano particles. Thus, we can speculate that the strong enhancement observed in our experiment could be due to the localization of the Trp molecules in the gap between the nano particles, where the electromagnetic enhancement reaches its maximum value.

6.6 Time Dependence of SERS Signal

For most practical applications of SERS spectroscopy targeting detection of molecules at trace concentration levels, it is desirable to have a spectrum that does not change with time. In many cases, especially when metal colloidal solutions are used, the SERS spectra change in time not only in intensity but also in shape. Sometimes stable spectra can be observed only after a long incubation time [25]. This makes it difficult to apply SERS spectroscopy to quantitative measurements. In our experiments we observed very high stability of the measured spectra.

Fig. 6.6 illustrates the typical temporal behavior of the SERS signal for the 4.2×10^{-7} M concentration solution. Similar behavior was observed for the other concentrations studied. As one can see from the figure, the spectrum starts to appear at 2 minutes after mixing and reaches maximum intensity 15 minutes after mixing. During the first 15minutes the signal grows and approaches the peak value at a rate given by an exponential time constant on the order of 2.7 minutes with a delayed onset of approximately 1.5 minutes. Later it very slowly decreases over the course of several hours. An exponential fit for the increase and decrease of signal is also shown in Fig. 6.6. It should be noted that the shape of the spectral pattern does not change with time. This is contrary to the data reported in Ref. [25]. Such high stability of the SERS spectra can be explained by the fact that the tryptophan molecules are attached to the surface of the nano particles in only one certain orientation, which does not change with time. The other evidence for this hypothesis is the low background observed for the spectral curves. It would be expected that differences in the binding orientation would cause changes in relative in-

tensities and positions of the peaks, leading to broadening and an increase in the baseline for the spectral curves.

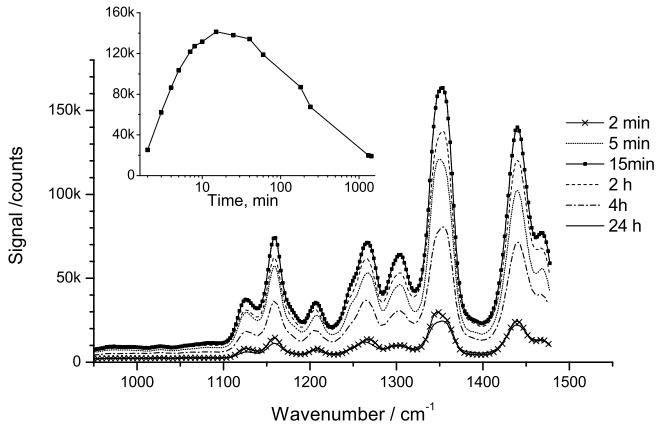

(a)

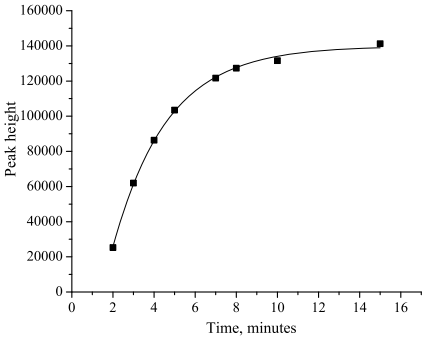

(b)

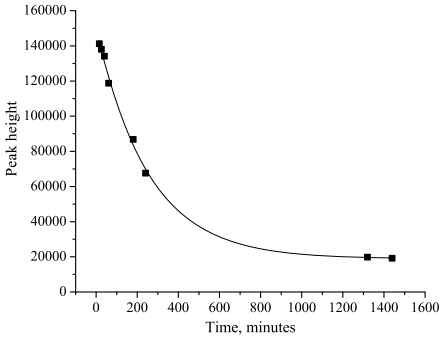

(c)

Figure 6.6: (a)SERS spectra of Trp (4.2×10^{-7} M) in silver colloid solution at different times after mixing. Inset figure is the time dependence of the peak height (peak at $\approx$1350 cm^{-1} minus the valley at 1400 cm^{-1}). Exponential fits to the early and late time signals showing (a) increase of signal with time constant 2.7 minutes (b) decay of signal with time constant 4.25 hours.

The time evolution of the optical absorbance spectra for 4.2×10^{-7} M concentration of Trp is shown in Fig. 6.7. One can see that the optical

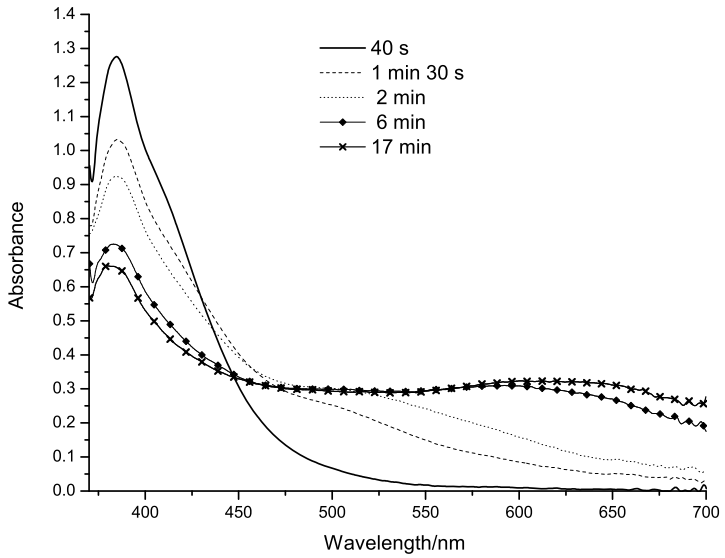

Figure 6.7: The time evolution of the absorbance spectra of silver colloid with 4.2×10^{-7} M of Tryptophan.

absorbance spectrum starts to evolve from a single-peak curve to a double-peak curve immediately after sample mixing, reaching a well-defined double-peak curve after approximately 6 minutes. The time scale of these changes is close to the time scale of the increase in the SERS signal. Qualitatively the temporal evolution of the absorbance spectra observed in our experiments is very similar to the evolution of the absorbance spectra of the system of two silver nano particles as the particles move towards each other [6]. In that paper the authors calculated the absorption spectra of a pair of nano particles and also for fractal aggregates. The evolution of absorption spectra as a function of interparticle distance they calculated for the case of two nano particles is given in Fig. 6.8. As the particles start to interact a shoulder appears at the absorption peak. As the particles move closer towards each other the shoulder moves to the longer wavelength side and eventually transforms to a separate peak around 500-700nm. In the experiment one has a mixture of

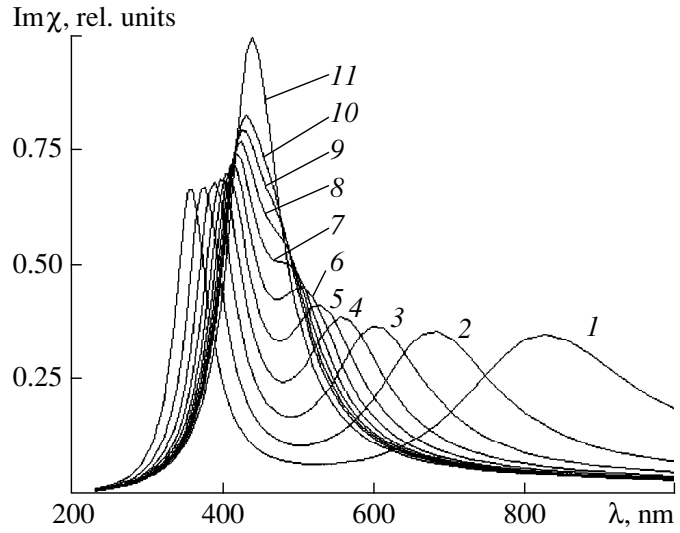

Figure 6.8: Absorption spectra of the pairs of monoresonance particles during their dipole-dipole interactions as a function of distance R_{ij} between the pairs: R_{ij} (1) 10, (2) 11, (3) 12,(4) 13, (5) 14, (6) 15, (7) 16, (8) 17, (9) 18, and (10) 19 nm. Curve 11 corresponds to the initial spectrum of single noninteracting particles.Reproduced from [6] (Reproduced by permission of Springer).

single particles and dimers with different separation of particles thus this peak not so pronounced. A further discussion of aggregation kinetics is given in chapter 8.

6.7 Conclusion

In conclusion, a highly sensitive technique for observing SERS spectra from tryptophan in borohydride silver colloidal solution has been developed. High-quality SERS spectra have been obtained in the concentration range 10^{-8} to 5×10^{-4} M. Below 10^{-4} M the shape of the spectral curves does not change with the concentration of Trp and the incubation time, indicating stable and reproducible binding geometry of the molecules to the nano particles. We believe that the very high SERS signal from Trp molecules we observed is attributed

to the optimization of colloid preparation method and electrolytic buffer. This leads to enhanced binding of Trp molecules observed in our experimental conditions. The very low detection limit together with the high stability of the spectra makes the procedure very useful for analytical applications. The high enhancement of the Raman signal from tryptophan observed in the experiments (about eight orders of magnitude) is explained in part by the particular binding geometry of Trp molecules to the silver nano particle surface under the given experimental conditions. We suggest that for the low concentrations studied in the present experiment the Trp molecules bind to the nano particle surface with the indole ring parallel to the surface.This geometry appears to be different from the geometry commonly reported in the literature.

Chapter 7

Electrolytes

The electrolyte plays an important role in surface enhanced Raman scattering studies. The use of different electrolytes for obtaining Raman enhancement has been widely reported in the literature [142–145]. The addition of electrolytes not only changes the pH of the solution but also can have a large impact on SERS sensitivity. According to Gronchala et al. [146] the possible explanations for enhancement due to anion activation might be increased charge transfer, an increase in electromagnetic enhancement caused by aggregation of colloidal particles, the reorientation of adsorbed molecule and increased adsorption caused by the co-adsorption with anions. In order to get high enhancement of Raman signal, it is important to tune the surface charge of the colloid solution. The effects of electrolytes and pH on SERS spectrum has been studied in [147]. Seong et al. reported that the presence of halide ions is a prerequisite for the observation of SERS signal [148]. The effect of anions, Cl^-, $SO_4{}^{2-}$, $NO_3{}^-$ on the SERS spectrum of acridine derivative lucigenin has been studied by Juan et al. [110]. They reported that the adsorption of lucigenin is different depending on the type of anions present and the adsorption is weak in the presence of sulphate and nitrate compared to the case with chloride ions. Co-adsorption of electrolyte and protein has observed in

the case of protein lysosyme. Zhen et al. reported the co-adsorption of NO_3^- with lysosyme and the presence of bands from electrolytes in the SERS spectra, the adsorption of NO_3^- can be controlled by using different experimental conditions [149]. The commonly used electrolytes in SERS are those containing chloride or halide ions like sodium chloride and potassium chloride [145]. Chloride activation of Raman signals for pyridine is reported by Otto el al and Wetzel et al. [142,143]. Use of KCl electrolyte for enhancing signals from Rh6G molecules with silver colloid prepared by Lee and Meisel method is reported by Hildebrandt and Schrader [150]. KNO_3 and NaCl aggregating agent for citrate colloid is reported in [144]. The effect of pH and adsorption mechanism of biological molecules on silver colloids has been widely studied [151] for silver sols prepared by hydroxylamine hydrochloride. A study on the effect of different anions on the stability of silver colloid and on SERS enhancement factors of different organic dyes has been performed by Schneider et al. [152], they reported that each dye experiences SERS enhancement only with certain anions.

During the course of this thesis we tested and used different electrolytes. This chapter describes a comparative study of various electrolytes we used in our experiments. We tested electrolytes for amino acids Trp, Phe ,Gly and the dyes acridine orange (AO), rhodamine 6G (Rh6G) and rhodamine B (RhB). It is observed that the conditions for obtaining SERS spectra for different analytes are different for each electrolyte and different mixing procedures are required to optimize the signals. We studied a number of electrolytes in order to get a high enhancement of Raman signal from Trp. Though we tested the electrolytes for other amino acids and dyes as well, our main focus was to develop an electrolyte which works well for Trp. After trying differ-

ent electrolytes for Trp and other amino acids and dyes, we developed a new electrolyte, which is a mixture of $NaHCO_3$, Na_2CO_3, NaCl and Na_2SO_4, this composite electrolyte provides high enhancement of Raman signal with reproducible and stable spectrum. We obtained this electrolyte after trying different combination of its components in different concentrations and amounts. In the following sections we present the details of experiments for observation of SERS signal from different analytes and the enhancement factors obtained for a number of electrolytes screened. In certain cases the kinetics of SERS signal observed was also studied in more detail. We used sodium chloride (NaCl), sodium bicarbonate ($NaHCO_3$) and two composite electrolytes as background electrolytes for SERS experiments. During our experiments we did not observe a large variation of pH. The pH values of the final solutions with all electrolytes used were in the range 8.8 ± 0.5. A comparison of the enhancement factors for certain analytes have been made. It is known that SERS enhancement is very sensitive to experimental conditions such as mixing procedure, incubation time and the type of electrolyte used for colloid aggregation. This becomes especially important for microfluidic devices because of the limited analyte-colloid interaction time and also due to the limited time that the analyte can be present in the probe volume. Thus, for practical applications it is very important to optimize the conditions to get strong and reproducible SERS signal.

7.1 Sodium Chloride

A solution of sodium chloride with a concentration in the range of 0.1-0.01 M is the most common electrolyte used to make silver colloid SERS active [109,110,142,153,154]. We used NaCl to observe SERS spectrum from different

analytes such as amino acids; tryptophan, phenylalanine , glycine and dyes; acridine orange(AO) rhodamine 6G(Rh6G).

7.1.1 Tryptophan

In oder to obtain SERS spectra from Trp using NaCl electrolyte, a sample solution was prepared by adding 1 ml of 2×10^{-3} M Trp into 10ml of concentrated silver colloid followed by 2ml of 10^{-1} M NaCl, giving a final concentration of 1.5×10^{-4} M Trp and 1.5×10^{-2} M NaCl in solution. The SERS signal started appearing a few seconds ($\sim$ 45 seconds) after preparation of the solution. The SERS spectrum observed at 30 minutes after the preparation of sample solution is shown in Fig. 7.1.

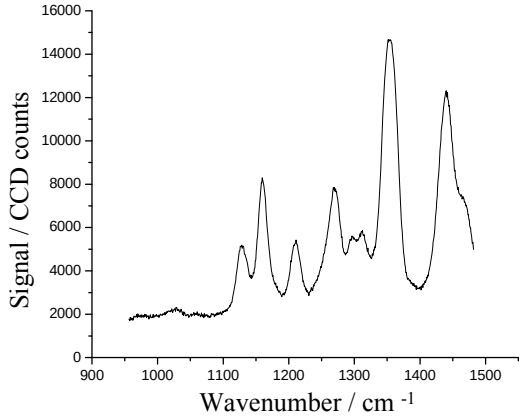

Figure 7.1: SERS signal of Trp (1.5×10^{-4} M) with NaCl electrolyte (1.5×10^{-2} M) at $\sim$ 30 minutes after preparation of the sample solution.

A concentration dependence study of Trp SERS spectrum with NaCl electrolyte has also been performed. Five sample solutions were prepared by adding proper amount of water solution of Trp into 10 ml of silver colloid followed by 2 ml 10^{-1} M NaCl. The final concentration of NaCl was 1.7×10^{-2} M for the first three samples. The last two samples with higher concentration

of Trp had slightly lower concentration of NaCl 1.6×10^{-2} M and 1.5×10^{-2} M for the 2nd highest and highest concentration samples respectively due to the effective dilution of the sample by the amount of Trp added. The final concentrations of Trp in solution were 3.3×10^{-6} M, 1.0×10^{-5} M, 3.3×10^{-5} M, 8.3×10^{-5} M, 2.5×10^{-4} M. SERS signal started appearing a few seconds after preparation of the sample solutions, then the signal intensity increased with time and a stable signal was observed. This signal intensity did not change more than 15% during the next 24 hours. The solutions were dark yellow in color when prepared and changed into light yellow at around 5 minutes and remained that color for the order of a day. The SERS spectra observed 2 hours and 40 minutes after preparation of the sample solution is shown in Fig. 7.2.

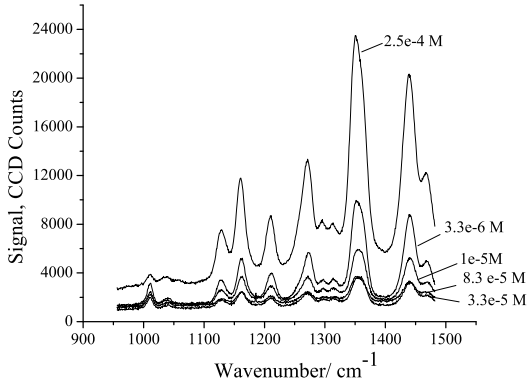

Figure 7.2: SERS signal from Trp using NaCl(1.7×10^{-2} M) electrolyte for different concentrations of Trp.

7.1.2 Phenylalanine

We could not observe SERS spectrum from amino acid phenylalanine using NaCl electrolyte for the concentrations we studied and for the sample preparation methods used. Sample solutions for SERS measurements were prepared by adding Phe into 10 ml of silver colloid followed by 2 ml of 0.1M NaCl, with

final concentration of Phe in the solution between 2×10^{-6} to 1.5×10^{-4} M. The sample solution was yellow in color similar to that of the original colloid and remained in that color without showing any aggregation.

7.1.3 Glycine

NaCl electrolyte was not tested for observation of Raman enhancement for Gly amino acid in our experiments. We did observe SERS signal from Gly without the addition of any electrolyte as mentioned in chapter 4. In the case of tripeptide of glycine, Gly-Gly-Gly , a sample solution was prepared by adding 1ml of 2×10^{-3} M Gly-Gly-Gly into 10ml of silver colloid followed by the addition of 2 ml of 0.1M NaCl. The final concentration of peptide in solution was 1.5×10^{-4} M. The solution changed its color from yellow to green in 5 minutes, but no spectrum observed. The solution was monitored for SERS signal for 1 hour after the preparation of solution. Also no spectrum was observed when the order of mixing was changed by adding NaCl into colloid before the addition of tripeptide for a final concentration of 8.9×10^{-5} M peptide in solution.

7.1.4 Acridine orange

Acridine orange(AO) is a fluorescent dye, widely used in cell analysis [155], and whose derivatives also exhibit strong biological activity (antimitotic, mutagenic etc) [156]. We have found that in AO enhancement of Raman scattering and kinetics of SERS signal are strongly dependent on the time when sodium chloride is added. The Raman spectra of acridine orange, dependences of Raman peak height (difference between maximum at 1375 cm $^{-1}$ and minimum at 1347 cm $^{-1}$) and the absorbance of the colloid versus time are shown in Fig. 7.3. These data correspond to the case when 0.024 ml of AO (10^{-5} M)

was added to 10 ml of silver colloid 1 min after colloid formation followed immediately by the addition of 2ml of 0.1M NaCl. As shown in the figure, the amplitude of Raman signal was relatively low and it rapidly decreased to zero during the first two minutes. We did not observe any Raman signal even after colloid aggregation, which is revealed in change of the colloid absorption spectrum (see Fig. 7.3(c)). This aggregation could also be seen by the change of the solution color from yellow to green. After about 40 minutes the solution started to change its color again from green to pale yellow, and after 2 hours it was almost colorless. The next day a small amount of light gray precipitation could be seen on the bottom of the cuvette. It should be noted that the background signal is much smaller than fluorescence from AO in the absence of the colloid (see Fig. 7.3(a)). This fluorescence spectra is observed in the same spectral region as the SERS. Thus we can conclude that AO is mainly absorbed on the silver nanoparticles and does not exist in free form in the solution during these experiments. So the lack of Raman signal cannot be explained in terms of lack of binding of AO with nanoparticles.

A Completely different kinetics of the SERS signal was observed when sodium chloride was added to the already aggregated colloid. Data shown in Fig. 7.4 corresponds to the case when 0.024 ml of AO (10^{-5} M) and then 2 ml of NaCl (0.1 M) were added to 10 ml of colloid solution after about 40 min of colloid formation (at that time, the colloid had a green-gray color which is an evidence of aggregation). As shown in the figures the signal increased during the first 10 minutes and then slowly decreased. The maximum peak height was 5 times higher than that in the previous case. It should be noted that we did not observe any extra aggregation upon addition of sodium chloride. Instead of this, 2 minutes after the addition of sodium chloride the colloid

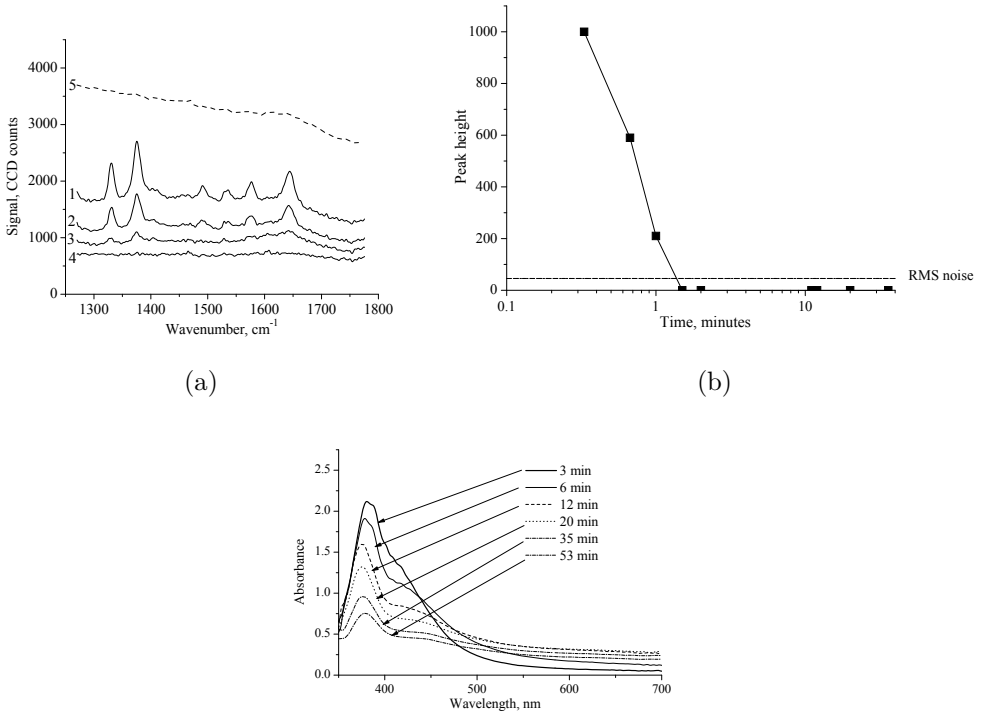

Figure 7.3: Behavior of AO SERS spectra and silver aggregation with sodium chloride electrolyte, when AO is added just before sodium chloride. (a) solid lines 1-4 are Raman spectra of AO ($2\times\ 10^{-8}$ M) in silver colloid taken after 20s, 40s, 1 min and 36 min after addition of AO, respectively; the dashed line is a spectrum of AO (same concentration) in water which is primarily fluorescence. (b) time dependence of Raman peak height (1375 cm $^{-1}$) with background subtraction and (c) absorbance spectra of final solution at different times.

solution started to become lighter.

We have performed a concentration dependence study of acridine orange by adding colloid into a solution containing different concentrations of acridine orange. We prepared 6 sample solutions by adding 1 drop (12 micro liter), 3 drops, 10 drops, 30 drops, 1.2 ml and 3.6 ml of 10 $^{-6}$ M acridine orange into a solution of 5 ml of deionized water and 3 ml of NaCl (0.1M). To each of these solutions 2 ml of aggregated silver colloid was added. The final concentrations

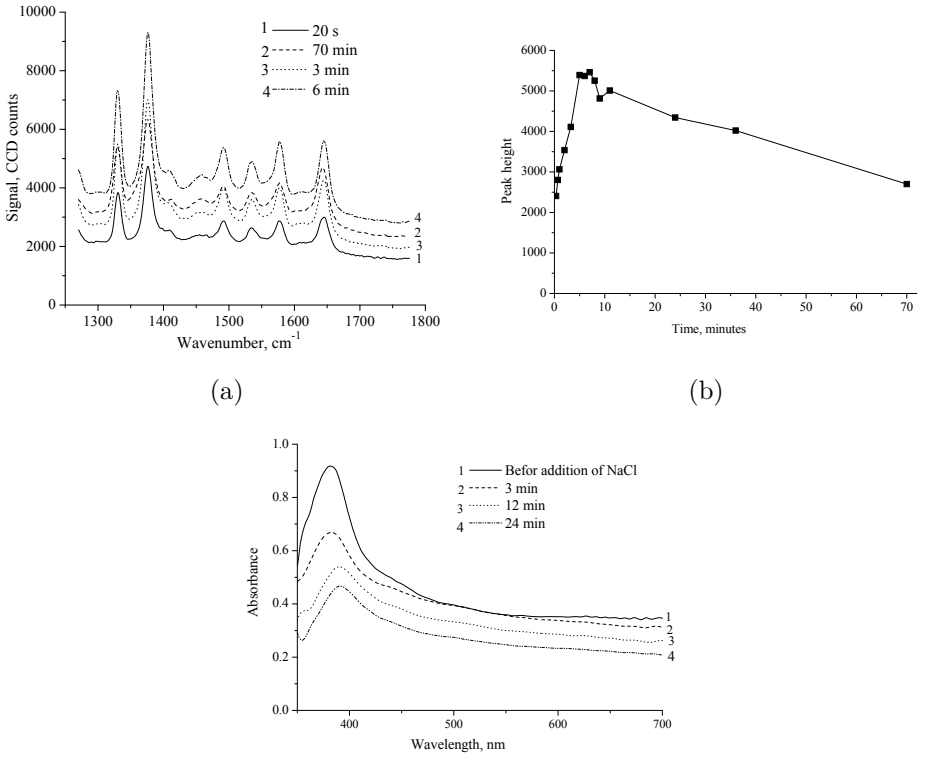

Figure 7.4: Behavior of SERS spectra and silver aggregation with sodium chloride electrolyte when NaCl and AO were added 40 min after colloid generation. The final concentrations were 2×10^{-8} M for the AO and 2.6×10^{-2} M for the NaCl. (a) Raman spectrum at different times, (b) time dependence of Raman peak height and (c) absorbance spectrum of silver colloid at different times after addition of NaCl.

of AO in the solutions were 1.2×10^{-9} M, 3.6×10^{-9} M, 1.2×10^{-8} M, 3.5×10^{-8} M, 1.1×10^{-7} M and 2.8×10^{-7} M respectively. The peak height versus the concentration of AO is shown in Fig. 7.5. As shown in Fig. 7.5 the peak height increases linearly with the concentration in the range from 3.6×10^{-9} M to 4×10^{-8} M and then it saturates at higher concentrations.

From the time and concentration dependence studies of SERS signal of AO in silver colloid, it is shown that the surface enhancement of Raman scattering has strong and nontrivial time dependence. For AO, non aggregated colloid

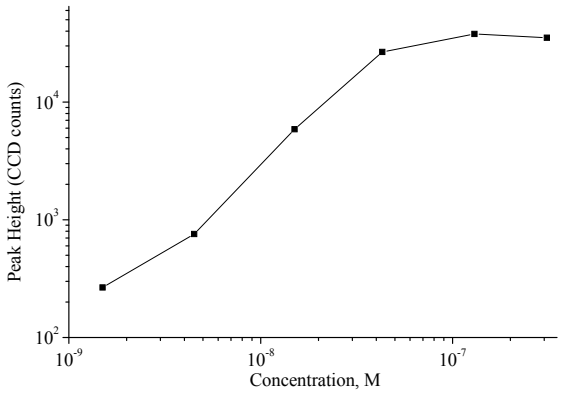

Figure 7.5: Concentration dependence of SERS signal from acridine orange with NaCl electrolyte.

gives small signal and fast decrease of signal with time. Slow aggregation using NaCl gives moderate signal and fast increase of signal with time. Zimmermann et al. studied SERRS spectra of acridine orange and its binding to DNA strands [157]. They recorded spectra of AO to a concentration of 10^{-8} M. In their study they used KI and HNO_3 solution to suppress the fluorescence of AO. SERS of AO on micro surface has been studied in [158]. We could obtain good quality SERS spectra for concentration as low as $\sim 10^{-9}$ M. The spectra of acridine orange we observed are in very good agreement with the spectra reported in literature [157,158]. We also studied a Kinetics of AO SERS signal for the first time.

7.1.5 Rhodamine 6G

Rhodamine is a fluorescent dye, used in fluorescence microscopy, flow cytometry and fluorescence correlation spectroscopy. Rhodamine 6G is also used as laser dye, or gain medium in dye lasers. The sample solution for SERS measurement was prepared by adding Rh6G into 10 ml of aggregated silver colloid (40 minutes after preparation) of colloid followed by 2 ml of 0.1M NaCl giving

a final concentration 9.3×10^{-8} M Rh6G and 1.7×10^{-2} M NaCl in solution. The spectra observed and the variation of intensity with time are shown in Fig. 7.6. The solution was milky gray in color when prepared and remained grayish yellow color during the observation period. No SERS spectrum was observed for the same procedure when Rh6G was added to the fresh colloid without any time delay.

Cl^- activation of colloid has been reported in the SERS study Rh6G molecules, it was observed that SERS enhancement factor varies strongly depending on the concentration of Cl^- ions [140, 145, 159]. NaCl, KCl and HCl activation of substrates have been reported in the SERS study of Rh6G [145,150,160]. The SERS spectrum we observed for Rh6G is in agreement with literature reported spectra [140,159]. For a final concentration of 9.3×10^{-8} M Rh6G with 1.7×10^{-2} M of NaCl we observed a fluorescence background as shown in Fig. 7.6, similar to the spectrum reported in [161]. Cyrankiewicz et al. reported that Rh 6G gave the largest SERS enhancement 40 min after introducing analyte into colloid suspension [145]. In our experiments we added analyte into colloid 40 minutes after preparation of the colloid. Though the procedure was not exactly the same, a delay in time was required in our case too. In [160] SERS spectrum of single Rh6G molecule was reported. In that study they incubated 2 nM R6G in colloidal silver containing 10mM NaCl for 2 hours and the SERS spectrum was measured with an integration time of 60 seconds. We used an integration time of 5 seconds for our SERS measurements. A time dependence of SERS signal reported for Rh 6G with KCl electrolyte is different from what we observed using NaCl electrolyte [145]. In our studies we have maximum signal in the beginning and then the signal intensity decreased with time, but an increase in signal intensity with time was

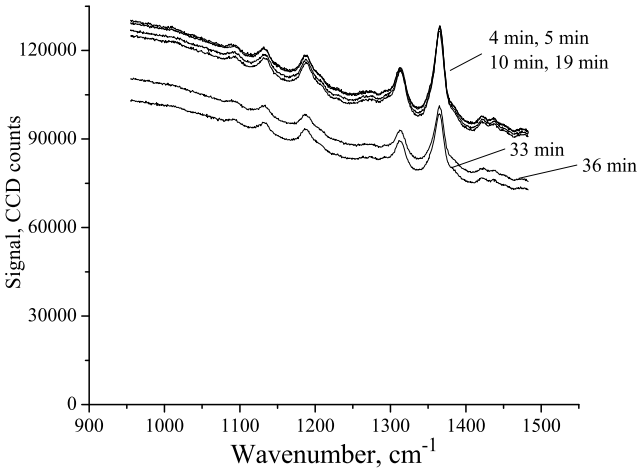

(a)

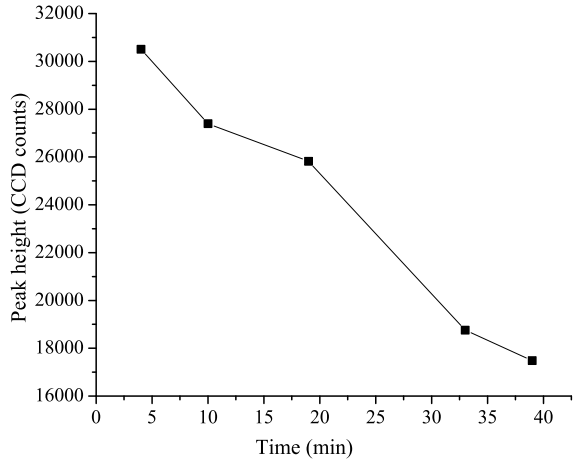

(b)

Figure 7.6: (a) SERS signal from Rhodamine 6G using NaCl electrolyte for 9.3×10^{-8} M Rh6G and 1.7×10^{-2} M NaCl when added 40 min after colloid preparation (b) variation of peak height at 1365 cm^{-1} with time.

reported with KCl electrolyte in [145].

In summary the enhancement factor we obtained for Trp with NaCl electrolyte for a final concentration of 10^{-4} M Trp in solution is $\sim 10^4$, which is in agreement with the enhancement factor reported in literature for similar

concentrations of Trp [1]. A study of Cl^{-1} activation of SERS for acridine in silver sol was reported in [162], where they studied the dependence of SERS signal on the pH of the solution. As discussed above halide ion activation was reported to be an important factor in observing SERS spectrum from Rh6G [145]. As we can see the NaCl electrolyte allows one to obtain the SERS spectra from different analytes. But as shown in later sections, NaCl gives smaller enhancement factors for some compounds compared to optimized electrolytes.

7.2 Composite Electrolyte I (CE I)

During screening of electrolytes we found that a bottled drinking water from Nestle, (Nestle purelife) gave a surprisingly high enhancement of Raman signal. We performed SERS studies with this electrolyte, which has the following ions according to manufacturer specification HCO_3^-, Ca^{2+}, Cl^-, SO_4^{2-}, Mg^{2+}, Na^+ (45, 19, 8, 7, 4, 2 ppm). We call this a composite electrolyte I (CE I) and this background electrolyte resulted in the highest enhancement of Raman signal compared to the other commonly used electrolytes for the amino acid Trp studied here. A chemical analysis of a sample of this solution gave HCO_3^- (63.8ppm), Ca^{2+} (14.7ppm), Cl^- (15.1ppm), SO_4^{2-} (2.04ppm), CO_3^{2-} (38.3ppm), Mg^{2+} (4.11ppm) , Na^+ (3.67ppm) and K^+ (1.12ppm). The SERS studies performed using this electrolyte for different analyte samples are given below.

7.2.1 Tryptophan

The solution for SERS measurements was prepared by adding Trp into silver colloid followed by deionized water and composite electrolyte I. An example

of the SERS spectrum of Trp in silver colloid is shown in Fig. 7.7. The final concentration of Trp in solution was 4.2×10^{-8} M. A much higher enhancement of the Raman signal was observed compared to that obtained with NaCl as background electrolyte (Fig. 7.1). This is one of the electrolytes we tested which gave high enhancement of Raman signal with stable and reproducible SERS spectra. Based on the peak to background height at $\sim$ 1350 cm^{-1} from aqueous solution and at $\sim$1345 cm^{-1} from the SERS one can estimate the enhancement of Raman scattering as high as$\sim10^9$, which is several orders of magnitude higher than previously reported for Trp in silver colloids [1]. The time dependence study of SERS signal using this electrolyte and a concentration dependence study were performed as explained in chapter 4 and shown in Fig. 7.8.

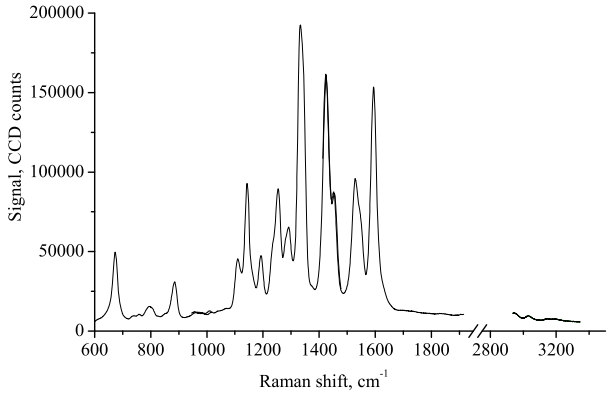

Figure 7.7: SERS spectra from Trp (4.2×10^{-8} M) in the silver colloid with composite electrolyte.The spectrum was taken 10 minutes after addition of Trp to the colloidal solution.

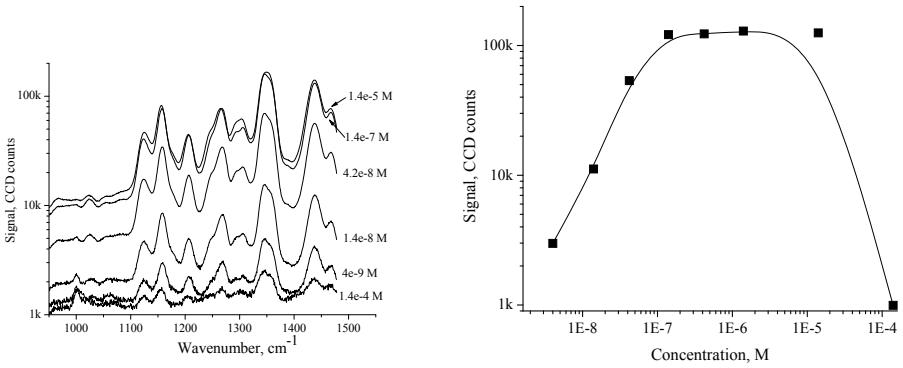

(a) (b)

Figure 7.8: (a) SERS spectra of Trp with composite electrolytes at different concentrations at 10 min after mixing (b) Concentration dependence of the magnitude of SERS peak at ∼1345 cm^{-1} of Trp.

7.2.2 Phenylalanine

We used the composite electrolyte I for SERS study of Phe amino acid using same method for sample preparation as that we used for Trp. The solution was prepared by adding Phe into 10 ml of silver colloid followed by 30 ml deionized water and 20 ml of nestle water, giving a final concentration of 2.3×10^{-6} M. The solution was yellow in color when prepared and changed into pink color in 3 minutes after preparation and became light brown around 1 hour but no SERS spectrum was observed from the solution. The lack of spectrum may be due to the reason that Phe molecules do not bind to the colloidal particles on substrate with CE1. The interaction of analyte molecule with the substrate is necessary for the SERS enhancement. This may be a possible reason for not observing spectrum from Phe though we observed SERS signal from Trp with CE1 which has similar chemical structure to that of Phe.

7.2.3 Acridine orange

Raman spectra of acridine orange in silver colloid when a composite electrolyte was used as an activator is shown in Fig. 7.9. In this experiment 14 ml of CE I was added to 10 ml of a freshly synthesized colloid. Immediately after addition of the electrolyte the colloid changed its color to red then green and gray. This process, which lasted not more than three seconds, indicates very fast and strong aggregation (this is confirmed by the absorbance spectrum in Fig. 7.9(d) for which the single nanoparticle plasmon resonance maximum is very undistinguishable). Right after that 0.05 mL of 10^{-5} M AO was added to the colloid (final concentration of AO was 2×10^{-8} M). As shown in the figure the intensity of scattering light was much higher than for the case of pure sodium chloride (Fig. 7.3 and 7.4) and it changed non-monotonically with time. Another noticeable feature of the SERS spectrum in this case is a deformation of the spectrum with time for relative amplitude of the peaks, in particular, at 1650 cm^{-1} and 1400 cm^{-1}. Also additional peaks appear at 1612 and 1560cm^{-1}. This can be caused by a changing of the geometry of the colloid-analyte binding and could be evidence of very strong interaction between the AO molecules and colloidal particles.

A different time dependence of Raman signal was observed when the analyte was added after some time of colloid aggregation. Data shown in Fig. 7.10 corresponds to the case when AO was added 10 minutes after addition of the electrolyte. In this case the intensity of Raman signal increased in the beginning and then slowly decreased. The relative peak intensities did not change with time and the peak at 1400 cm^{-1} has almost vanished. The absolute value of SERS intensity was approximately two times smaller than that observed in the case when the dye was added just after the electrolyte.

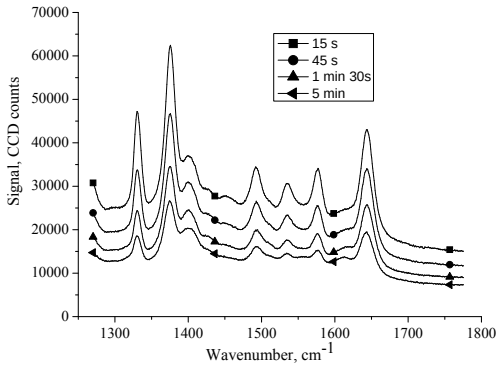

(a)

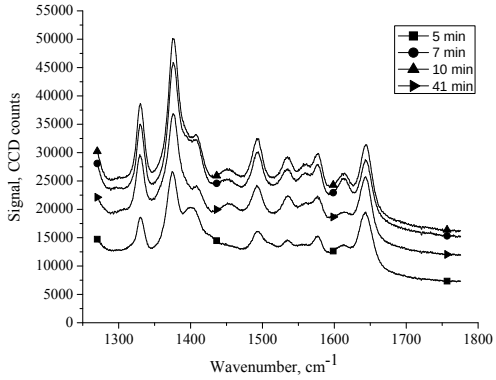

(b)

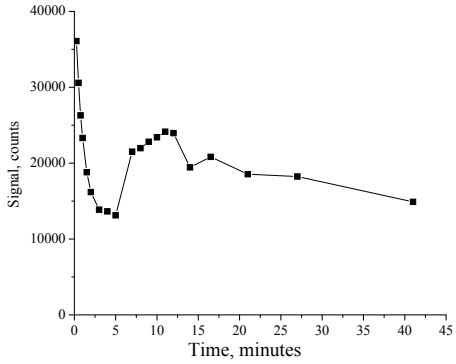

(c)

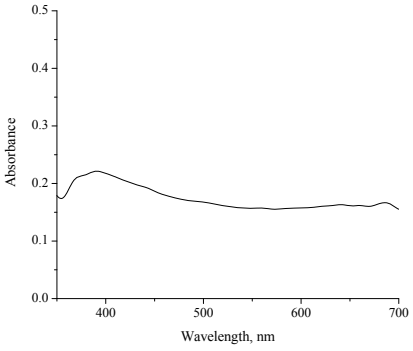

(d)

Figure 7.9: Behavior of SERS spectra of AO when a composite electrolyte I is used for aggregation. AO is added just after aggregation. The final concentration was 2×10^{-8} M for the AO. (a) and (b) Raman spectrum at various times; (c) dependence of the peak height (1375 cm^{-1}) with time; and (d) absorbance spectrum of the colloid 12 min after addition of the electrolyte.

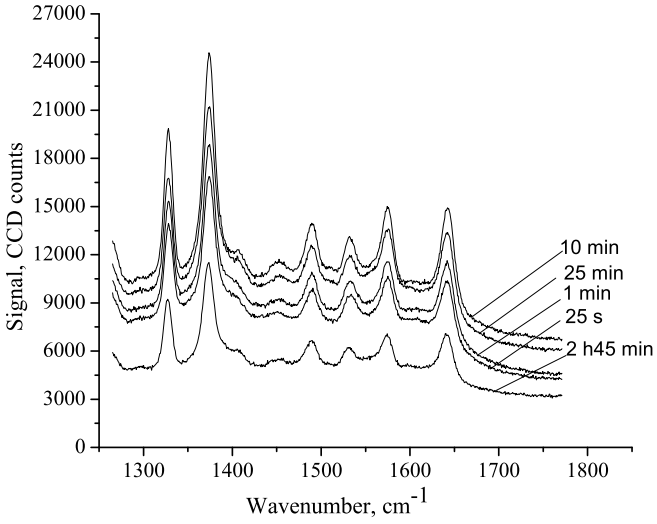

(a)

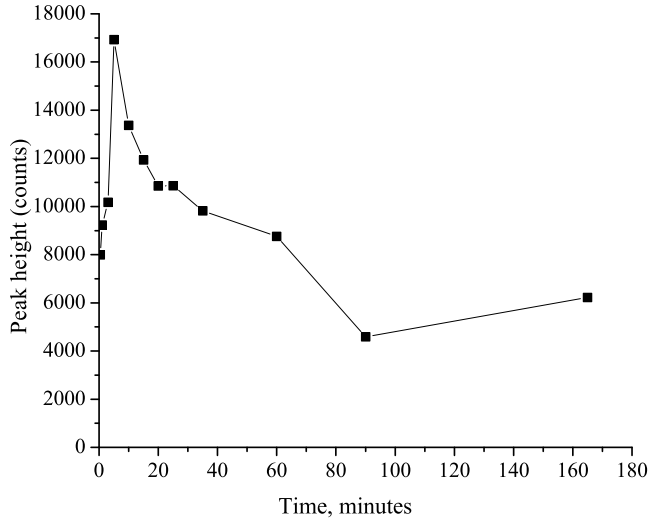

(b)

Figure 7.10: Behaviour of SERS spectra when composite electrolyte I is used for aggregation. AO was added 10 min after aggregation. The final concentration was $2\times\ 10^{-8}$ M for the AO.(a) SERS spectrum at different moments of time, (b) time dependence of peak height at 1375 cm^{-1}.

As shown in Fig. 7.9 fast aggregation with composite electrolyte gives high signal and fast decrease. The highest enhancement is observed at the first stage of fast aggregation initiated by the complex electrolyte containing HCO_3^-, Cl-, SO_4^{2-} anions. In this case maximum enhancement is observed over a short period of time within 1-3 min after the start of the aggregation process. In the case when the addition of dye is delayed with respect to the the start of colloid aggregation (10-40 min) the signal was several times smaller. From the time and concentration dependence studies of SERS signal from acridine orange (AO) optimum conditions have been determined. It has been found that at optimum conditions AO can be easily detected at concentrations 10^{-8} M and even lower. In general AO exhibits reproducible SERS spectra similar to that reported in the literature for AO and other acridine derivatives [157, 158, 162]. In some of the reported studies the electrolytes used were similar to composite electrolyte [162], where they used KCl for colloid activation and H_2SO_4 and NaOH for adjusting the pH. No reported kinetics study of the SERS signal of AO was found in the literature.

7.2.4 Rhodamine B

SERS measurements from Rhodamine B were performed by adding 10 ml of CE I into 10 ml of silver colloid followed by RhB. The final concentration of RhB in solution was $9\times\ 10^{-9}$ M. After adding the composite electrolyte the solution became green in color and then changed into transparent gray. The spectrum measured from the solution is given in Fig. 7.11.

The SERS spectum of RhB we measured is in agreement with the spectra reported in literature [163, 164]. In the spectrum reported for RhB by Fang et al. [163], an incubation period of 1 hour was used and the spectrum has a big

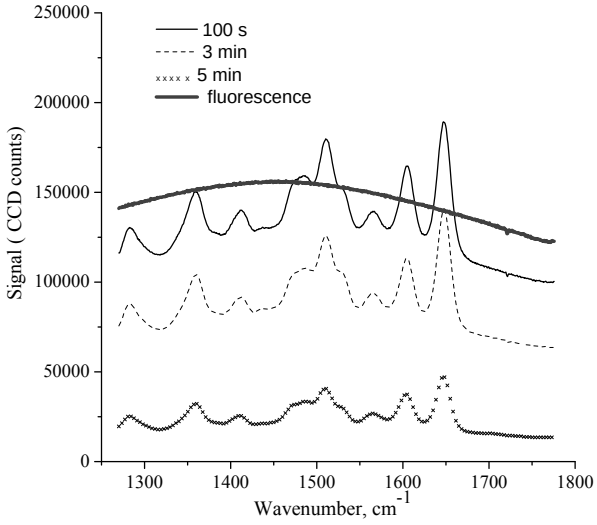

(a)

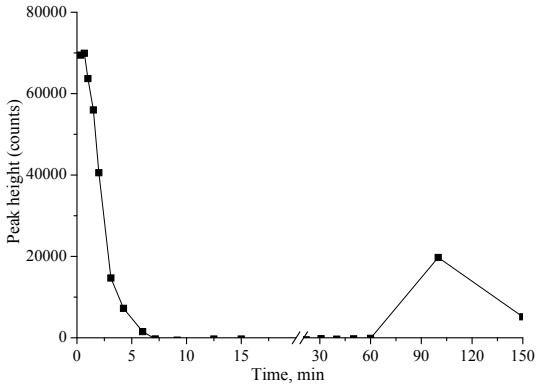

(b)

Figure 7.11: Behavior of SERS spectrum of Rhodamine B (9×10^{-9} M) in silver colloid with CE I activation. (a)Thin curves are SERS spectra at different moment of time after addition of the dye, thick curve is a fluorescence signal of Rhodamine B in water (9×10^{-9} M) taken under the same experimental conditions as SERS spectra; (b) Time dependence of the peak height at 1650 cm^{-1}.

fluorescence background [163].

In summary, as described above the composite electrolyte I (Nestle water) gives high enhancement of Raman signals for certain samples. It works with most of the molecules we tested and gave significantly bigger Raman signal.

For example for Trp amino acid CE I gave $\sim$ 300 times enhancement compared to that obtained with NaCl electrolyte. Though it works well and gives reproducible results, we could not rely on this electrolyte as it is a commercial bottled drinking water which may not always be available. Also its components could change in the future. Therefore we tried to produce an electrolyte which works the same as the composite electrolyte and which gives SERS enhancement of the same order as that of Nestle water. The details of the electrolyte developed are described in the following sections.

7.3 Sodium Bicarbonate

CE I gave stable and reproducible SERS signal with high enhancement and the main component of CE I was the bicarbonate (HCO_3^-) ions. Thus, we tried sodium bicarbonate ($NaHCO_3$) electrolyte in our experiments. We conducted some experiments using $NaHCO_3$ for amino acid Trp, as given in chapter 4. In the case when 5×10^{-3} M solution of sodium bicarbonate was used instead of the composite electrolyte the results did not show high reproducibility. The shapes of the spectral curves were the same as for the case of the composite electrolyte I. Old solutions of $NaHCO_3$ gave higher enhancement of Raman spectrum from Trp, but different results were obtained for new solution. As $NaHCO_3$ electrolyte worked in some cases but did not give reproducible spectra we decided to check if there is any effect of dissolved gases on the observation of SERS signal. To check this we prepared a fresh solution of $NaHCO_3$ and aerated it using an aquarium aeration stone named Topfin, a porous stone. The aeration stone was powered by an air pump (Elite799) [165]. The stone was connected to the air pump through an airline tubing as shown in Fig. 7.12. After aeration for a day the $NaHCO_3$ electrolyte gave spectra for amino acid

Trp with reproducible results and we suspected that there was some oxygen saturation effect or aging effect of $NaHCO_3$ which affected the SERS signal.

Figure 7.12: Aerating $NaHCO_3$ solution using air pump and airstone. A picture of airstone is given in the inset.

We aerated 5×10^{-3} M solution of $NaHCO_3$ for a day and then used it for SERS measurements from Trp giving a reproducible SERS signal. Sample solution was prepared by adding Trp into 10 ml of silver colloid followed by 40 ml of deionized water and 10 ml of $NaHCO_3$. The final concentration of Trp in solution was 2.3×10^{-6} M. The yellow color solution changed into pink in 1 minute after preparation and remained that color for an observation period of 1 h. The spectrum observed from Trp using aerated $NaHCO_3$ is shown in Fig. 7.13.

A concentration dependence study of SERS signal has been performed by preparing six solutions of Trp with aerated $NaHCO_3$ as mentioned above with final concentrations of Trp 1.4×10^{-8} M, 4.2×10^{-8} M, 1.4×10^{-7} M, 4.2×10^{-7} M, 1.4×10^{-6} M and 1.4×10^{-5} M. The SERS signal observed with different

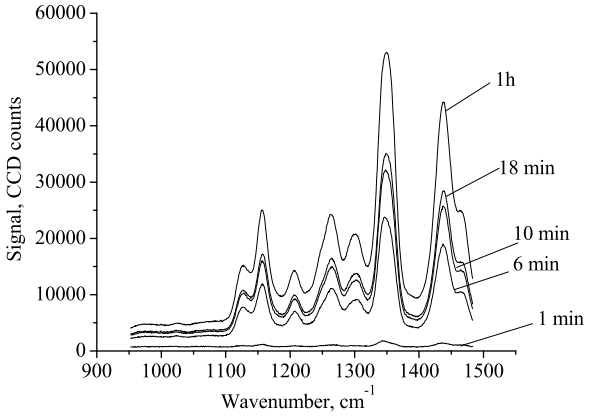

Figure 7.13: SERS spectrum from Trp using aerated $NaHCO_3$.

concentrations and the dependence of peak height on concentration are given in Fig. 7.14.

The signals observed using aerated $NaHCO_3$ were still less reproducible, and were less intense than that observed with composite electrolyte I. We tried to increase the Raman enhancement by adding Cl^- ions with the addition of NaCl also to the aerated $NaHCO_3$. We tested by adding different amounts of 10^{-3} M NaCl into the solution such as 10 ml, 2ml, 1 ml and 0.5ml and we found that when we used the combination of 20ml aerated $NaHCO_3$ and 0.5ml 10^{-3} M NaCl, we obtained high enhancement of Raman signal and reproducible SERS measurements. Thus, we used this electrolyte for a detailed study of Trp amino acid for high sensitivity of detection. The results obtained are presented in chapter 6.

But we also aerated the $NaHCO_3$ solution using a pipette made of polyethylene, and then used it for SERS measurement from Trp in the same manner as above. However, we could not observe any SERS signal. It was clear that it was something from the aeration stone material itself that actually

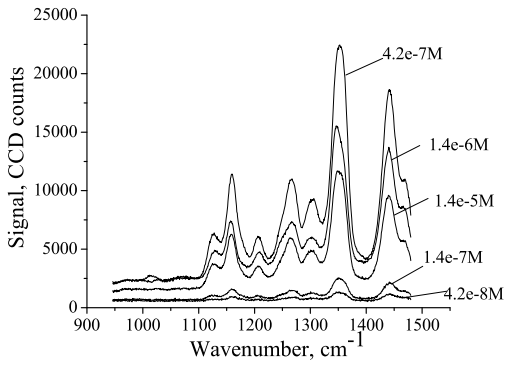

(a)

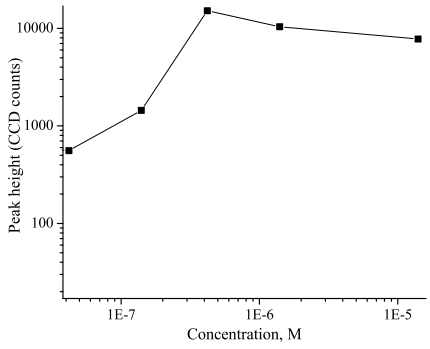

(b)

Figure 7.14: Concentration dependence of SERS signal of Trp using $NaHCO_3$ aerated for a day, take at a time of 1 hour after mixing.

contributed to the enhancement. Later, a chemical analysis of the aerated $NaHCO_3$ gave Ca^{2+} (1.4ppm), Na^+ (105ppm), HCO_3^- (372ppm) and CO_3^{2-} (223ppm). $NaHCO_3$ without aeration gave Na^+ (133ppm), HCO_3^- (401ppm) and CO_3^{2-} (241ppm) and Cl^- (1ppm). From the analysis of the airstone material it was concluded that the aeration stone was made up of some carbonates and during aeration,the porous material of the aeration stone was adding minor chemicals to the solution. This led to the conclusion that minor chemical constituents introduced from the aeration stone can have a significant influence on the SERS spectra. This led to the development of a new

electrolyte which was similar to that of of (CE I) and aerated $NaHCO_3$ plus NaCl as discussed in the next section.

7.4 Composite Electrolyte II(CE II)

7.4.1 Trp

The electrolyte containing aerated $NaHCO_3$ plus NaCl and bottled drinking water gave high Raman signal enhancement with reproducible spectrum. Therefore we attempted to reproduce those electrolytes using a fixed chemical composition so that we can get rid of the aeration process or the use of a commercially available drinking water as an electrolyte. With the assumption that the ability of an electrolyte to enhance the SERS signal depends mainly on the anion composition we attempted to emulate anion composition of the electrolyte using $NaHCO_3$, Na_2CO_3, NaCl and Na_2SO_4 as components. We did not achieve a strong enhancement comparable with the Nestle water(CE I). After varying the amount of some of the components we found that the electrolyte with the following composition provides the enhancement similar to that of (CE I). This is termed as composite electrolyte II (CE II). The composite electrolyte was a mixture of $NaHCO_3$ (5×10^{-3} M), Na_2CO_3 (10^{-4} M) , NaCl (10^{-3} M) and Na_2SO_4 (10^{-1} M). The solution for surface enhanced Raman measurements were prepared by adding Trp into 10 ml silver colloid followed by 30 ml of deionized water and 17.5 ml of composite electrolyte. The electrolyte was taken from the solution prepared by mixing 100 ml of 5×10^{-3} M $NaHCO_3$, 20ml of 10^{-4} M Na_2CO_3, 5 ml of 10^{-3} M NaCl and 50 ml of 10^{-1} M Na_2SO_4. The final concentrations of ions in CE II from chemical analysis are Ca^{2+} (2), Na^+ (1467ppm), $HCO_3{}^-$ (193ppm) and $CO_3{}^{2-}$ (116ppm) and Cl^- (1 ppm) and $SO_4{}^{2-}$ (988ppm).

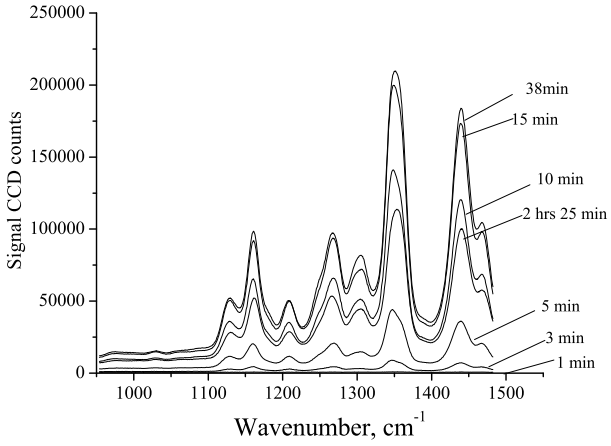

(a)

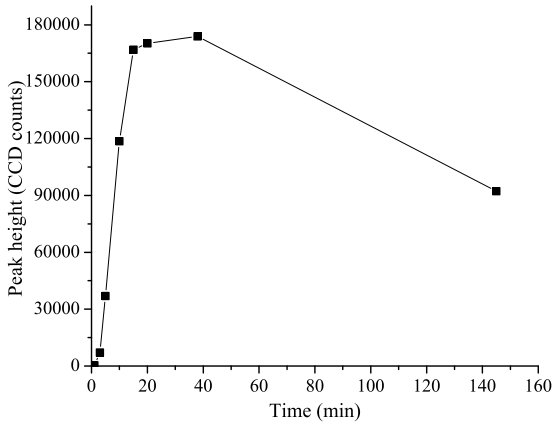

(b)

Figure 7.15: SERS signal from Trp amino acid using composite electrolyteII for a concentration of 4.4×10^{-7} M Trp: (a) spectra at various times and (b) peak height of 1345 cm^{-1} line above background.

The SERS spectrum obtained for a concentration of 4.4×10^{-7} M Trp in solution and time dependence of the signal is shown in Fig. 7.15. We repeated the SERS measurements for 4.4×10^{-7} M Trp a number of times to check the reproducibility of the signal. The results obtained from six measurements with error bars indicating the standard deviation spread in measurement is shown

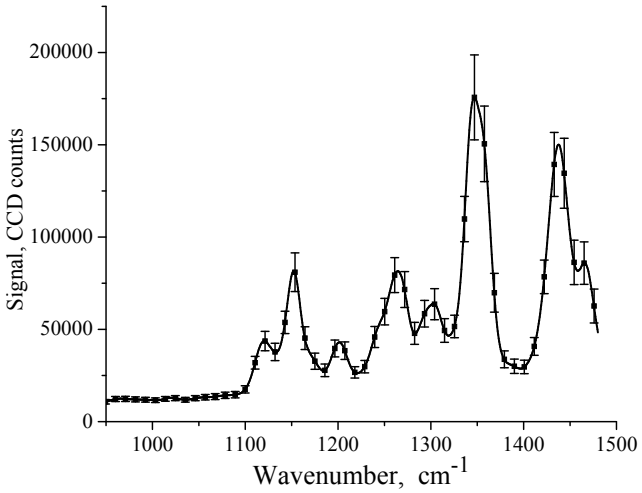

Figure 7.16: The average Trp SERS signal with standard deviations indicated by error bars using CE II background electrolyte from six separate measurements.

in Fig. 7.16.

7.4.2 Acridine orange

The solution for SERS measurement was prepared by adding 30 ml of deionized water and 17.5 composite electrolyte II into 10 ml of silver colloid followed by AO. The final concentration of AO in the solution was 2.4×10^{-8} M. The prepared solution was yellow in color and the spectrum started appearing from 1 minute after preparation. In about 6 minutes the solution became brown in color and then became pale yellow around 1 hour 30 minutes after preparation of the solution. The SERS spectrum measured during the observation period increased monotonically in time during this period as shown in Fig. 7.17. The peak signal levels are similar to those obtained with CE I but the time behavior and evolution of the detailed spectral features are different.

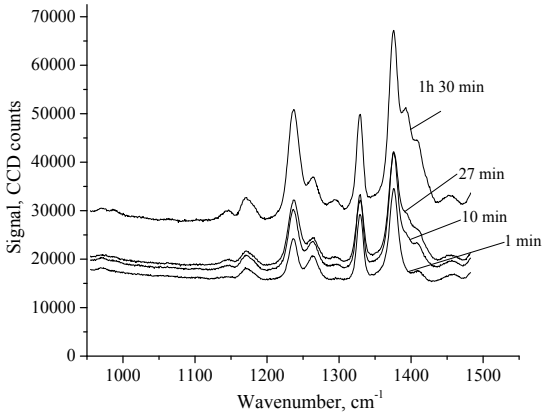

Figure 7.17: SERS measurement from acridine orange using composite electrolyte II.

7.4.3 Rhodamine 6G

SERS spectrum from Rh6G was obtained from a sample solution prepared by adding 10 ml composite electrolyte II to 10 ml of silver colloid followed by Rh6G, giving a final concentration of 5.6×10^{-8} M Rh 6G in solution. The yellow color colloid changed into a gray colored solution after the addition of composite electrolyte and became pale gray in about 20 minutes. The spectra observed at various times after preparation are given in Fig. 7.18. The spectra started to appear before 1 minute after preparation of the solution and disappeared after around 6 minutes .

7.5 Discussion

In this section we present a comparison of SERS enhancement we observed using different electrolytes. Results were obtained using NaCl, the commonly used electrolyte, bottled drinking water (CE I) which gave a high enhancement of Raman signal for Trp amino acid and the composite electrolyte (CE II) that we developed are compared in the following sections. The results presented

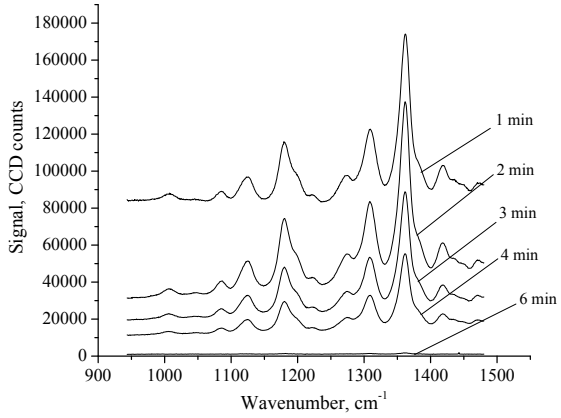

Figure 7.18: SERS measurement from Rh 6G using composite electrolyte II.

in the previous sections for different analyte molecules and electrolytes are compared and summarized here.

7.5.1 Amino acids

We studied Trp amino acid for a a wide concentration range. The SERS behavior and enhancement factor depend on the concentration of the analyte. We did a comparison of enhancement factors for three concentration regions: low concentration ($\sim 4\times10^{-7}$), intermediate concentration ($\sim 10^{-6}$) and high concentration ($\sim 10^{-4}$). A comparison is made based on the peak height of the signal observed around $\sim$ 1350 cm $^{-1}$ vs the nearest peak minimum at 1395 cm $^{-1}$. Each experiment was repeated three or more times. The results obtained for Trp using background electrolytes CE I, CE II , Aerated $NaHCO_3$ + NaCl, and NaCl are presented in Table.7.1.

As shown in Table.7.1 for low concentration of Trp, CE I and CE II gives 450 to 500 times more enhancement than that with sodium chloride. The aerated $NaHCO_3$ plus NaCl mixture gives an enhancement 400 times higher than NaCl alone. For intermediate concentration of Trp in solution, compos-

ite electrolyte II gives $\sim$ 10 times enhancement compared to that with NaCl. Aerated $NaHCO_3$ plus NaCl mixture and CE I give 15 and 20 times enhancement compared to NaCl. For high concentration of Trp, NaCl gives stronger signals than the other electrolytes. A comparison of peak heights from SERS spectra from different electrolytes for Trp for low concentration measurements is shown in Fig. 7.19.

Peak Height				
Electrolytes $\rightarrow$	NaCl	Aerated $NaHCO_3$+ NaCl	CE I	CE II
Trp Concentration $\sim 4\times10^{-7}M$	300 $\pm$ 100	120000 $\pm$ 55000	140000 $\pm$ 30000	150000 $\pm$ 50000
$\sim 10^{-6}M$	8000	116000 $\pm$ 26000	160000 $\pm$ 44000	75000
$\sim 1\times10^{-4}M$	3000 $\pm$ 900	700 $\pm$ 300	2000 $\pm$ 400	900

Table 7.1: Comparison of Peak heights in CCD counts of Trp SERS spectrum observed using different electrolytes; NaCl, Aerated $NaHCO_3$ + NaCl, CE I and CE II at optimum measurement times of $\sim$ 15 minutes. Integration time used was 5 seconds. Error bar shows the estimated standard deviation of peak height. The measurements are taken at 15 minutes after mixing of solutions, when we have maximum signal. For NaCl at high concentration, at a time of around 40 minutes we observed 4-5 times higher signal compared to that at 15 minutes.

At high concentrations ($>10^{-4}$ M) of Trp studied the SERS spectra observed were different from that observed at low concentrations. The difference in spectral features at high and low concentrations of Trp were observed with all the electrolytes studied. High concentration spectra observed with different electrolytes have similar spectral features. One of the important difference from low concentration spectra is the appearance of a strong peak near 1000 cm^{-1} corresponds to benzene ring breathing. This feature became more prominent in the high concentration spectra observed with NaCl electrolyte. The

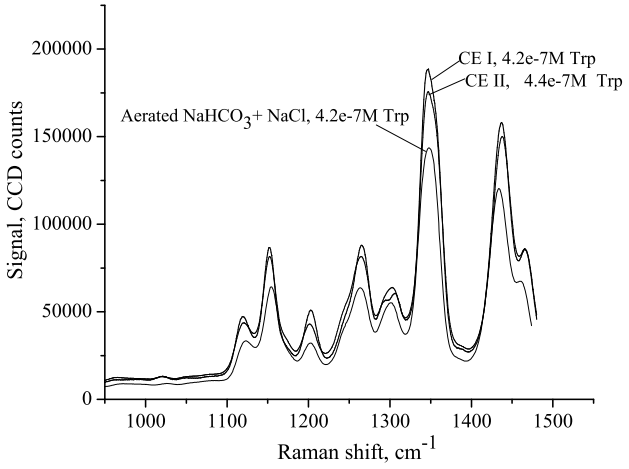

(a)

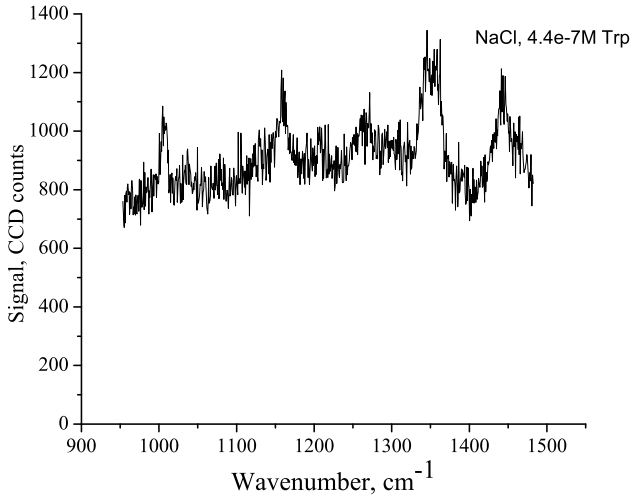

(b)

Figure 7.19: Comparison of peak heights (a) SERS spectrum obtained from Trp with CE1, CE2 and aerated $NaHCO_3$ + NaCl (b) spectrum with Trp (4.4×10^{-7} M) obtained with NaCl.

peak around 1350 cm^{-1} does not change at high and low concentrations. This difference may be due to the orientation of the binding of molecules on the nanoparticle surface. A detailed discussion of spectral features and binding

Electrolytes	CEII	CEI	NaCl
Concentration	2.4×10^{-8} M	2×10^{-8} M	2×10^{-8} M
Peak height	36000	32000	10000

Table 7.2: Comparison of peak heights in CCD counts from acridine orange with different electrolytes; CEII, CEI and NaCl at optimum measurement times of 1 hour 30 minutes , 15 seconds and 6minutes after mixing of the solution respectively. At these times we observed maximum signal. In the case of NaCl, NaCl and AO were added to the colloid 40 min after colloid generation.

geometry is provided in chapter 6 section 6.3. The spectra observed at high concentrations of Trp are in good agreement with that reported in literature [1]. The composite electrolyte developed, CE II did not work well for the other amino acids studied; Phe and Gly.

7.5.2 Dyes

For acridine orange a peak height of $\sim$ 36000 was observed with CE II for 2.4×10^{-8} M AO in solution. For 2×10^{-8} M AO in solution a peak height of $\sim$ 32000 observed with CE I and peak height $\sim$ 7000 observed with NaCl electrolyte. The comparison is shown in Table.7.2. The use of CE II reduced the waiting period in the sample preparation compared to that with NaCl and gave 3-4 times higher signal levels.

SERS spectra were observed from Rh6G using NaCl and composite electrolyte II as explained above in sections 7.1.5 and 7.4.3. The peak height observed for the peak at $\sim$ 1360 cm^{-1} versus the minimum at $\sim$ 1335 cm^{-1} for 9.3×10^{-8} M Rh6G in solution with sodium chloride electrolyte was $\sim$ 33000. However a 40 minute waiting period before adding Rh 6G into colloid was required for observation of spectrum. Spectrum observed for 6.4×10^{-8} M Rh6G in solution using CE II gave a peak height of $\sim$ 83000 for the same peak and there was no waiting time required before adding Rh6G into colloid. So

the composite electrolyte II provides better enhancement than the NaCl and no waiting period required for the sample preparation.

7.6 Conclusion

SERS spectra of important organic molecules; dyes and amino acids for biological applications have been studied using different electrolytes for colloid activation. It has found that SERS signal from these substances strongly depends on the colloid preparation and colloid/analyte mixing protocol. For several amino acids and dyes optimized conditions (mixing order, type of activating electrolyte and incubation time) have been found to give greatly enhanced signal levels . Diluted colloid is preferable to use for detection of SERS signal from some amino acids as SERS signal appears faster and has higher magnitude. In our experimental observations we found that the commonly used electrolyte NaCl is not as good as enhanced electrolyte mixtures. Also long incubation times for observation of SERS signal is required in some cases. For Trp amino acid, NaCl electrolyte provided significantly smaller enhancement for very low concentrations of Trp than mixtures of electrolytes. At high concentrations it gave similar or better enhancement than mixtures of electrolytes. The spectrum observed using this electrolyte is stable and reproducible and thus should be useful as an analytical tool for high sensitivity detection of Trp and other organic molecules in solution.

Chapter 8

Aggregation Dynamics

The aggregation of colloidal particles plays an important role in surface enhanced Raman scattering. It has been reported that aggregation of colloidal solutions is required to obtain high enhancement factor [144,145] and the largest enhancement occurs at the junction between two particles [139]. Therefore, the way colloidal particles aggregate and form clusters is very important in order to understand their use as SERS substrates. In our SERS experiments with Trp in silver colloid we observed a high enhancement of Raman signal up to 10^8. The TEM image of silver colloid with low concentration of Trp ($4.2\times\ 10^{-7}$ M) where we observed high enhancement of SERS signal ($\sim 10^8$) is shown in Fig.8.1 and the absorption spectra of same solution is shown in Fig. 8.2. The TEM pictures and the absorption spectra confirm the presence of aggregated silver particles in solution. As shown in the figure the absorption spectrum starts to evolve from a single peak to a double peak after sample mixing and after around 6 minutes it developed into a well defined double peak. The appearance of double peak in the absorption spectrum represents aggregated particles in solution [6]. We observed high enhancement of Raman signals when we have more number of small aggregates like dimers and trimers in solution. Thus the evolution and dynamics of the colloidal solution

are very important in the development of the enhanced SERS signal. In order to understand the temporal evolution of the SERS enhancement the dynamics of the colloidal solution have been modeled numerically as described in the following sections.

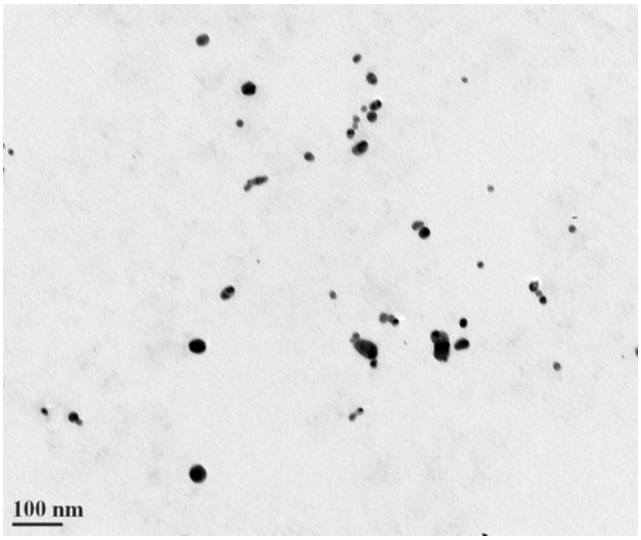

Figure 8.1: TEM image of silver colloid with with low concentration of Trp ($4.2\times\ 10^{-7}$ M).

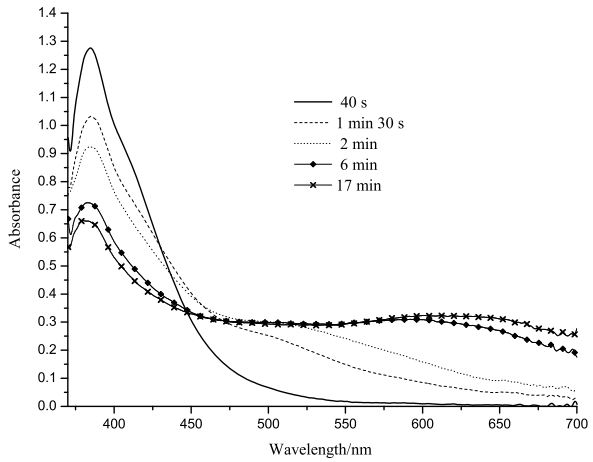

Figure 8.2: The time evolution of the absorbance spectra of silver colloid with ($4.2\times\ 10^{-7}$ M)Tryptophan

8.1 Colloid Aggregation and DLVO Theory

Brownian motion plays an important role in understanding the molecular and particle interactions in the colloidal domain. Brownian motion keeps the particles suspended in the solvent, also it contributes to the diffusion of colloidal particles through the solution. Due to Brownian motion the colloidal particles collide with each other and these collisions may result in aggregation of particles. The metal colloidal particles in solution develop a net surface charge depending on the details of the solution electrolyte. The surface charge affects the distribution of neighboring ions and this results in an increased concentration of oppositely charged ions close to the surface and formation of an electric double layer(EDL) in the particle-liquid interface. An imaginary surface separating the layer of liquid bound to the solid surface and rest of the liquid is called the slipping plane and the electrical potential at this plane is called the zeta potential(ζ) [166]. The zeta potential provides information about the charge carried by the nanoparticles and its ability to interact with other particles and therefore the colloidal stability is dependent on this potential [166]. The steady state of the colloidal solution is actually a metastable state, occurring due to a fine balance between the electrostatic repulsion, van der Waals attraction and hydrodynamic forces arising due to the movement in fluid.

The interaction between colloidal particles can be described by DLVO (Derjaguin, Landau, Verwey and Overbeek) theory [167, 168], a theory developed to solve the electrostatic problem of electrolyte with charged boundaries. According to the theory, colloidal stability is described by the potential energy of particles, which has a positive interaction potential due to Coulomb repulsion,

in many cases the Coulomb interaction is affected by the presence of other ions in the solution and its strength is reduced, therefore it is called a screened Coulomb potential (linear approximation of the screened Coulomb repulsion potential) of charged particles $V_{Coul}(r)$. In addition there is a negative interaction potential for the van der Waals attraction $V_{vdW}(r)$. Hydrodynamic interaction, the interaction in colloids due to the flows of moving particles in solution is usually ignored in DLVO theory. In general Coulomb repulsion and van der Waal attraction together with some approximations constitute the DLVO theory of colloidal stability. Some of the approximations in DLVO potential are not always valid, still the DLVO theory provides a general approach which agrees with observations in many cases and has been used in the past to describe colloid dynamics and aggregation effects.

The DLVO interaction potential $U_{DLVO}(r)$ (normalized to the thermal energy K_BT) for two identical spheres is given by [43]

$$\frac{U_{DLVO}(r)}{K_BT} = \frac{V_{vdW}(r)}{K_BT} + \frac{V_{Coul}(r)}{K_BT} \tag{8.1}$$

Where $V_{vdW}(r)$ is the van der Waals interaction and $V_{Coul}(r)$ is the screened pairwise Coulomb interaction. The van der Waals contribution can be given as:

$$V_{vdW}(r) = -\frac{A_{HC}}{6}\left[\frac{2a^2}{r^2-4a^2} + \frac{2a^2}{r^2} + ln(1-\frac{4a^2}{r^2})\right] \tag{8.2}$$

Where A_{HC} is the Hamaker constant, which depends on the material of the objects under consideration, and on the medium in which they are immersed in, a is the particle radius and r is the center to center separation of the particles. Coulomb interaction is taken via the screened electrostatic interaction between two objects with effective charge Ze /1+ka.

$$V_{Coul}(r) = \frac{1}{4\pi\epsilon}\left[\frac{Zee^{ka}}{1+ka}\right]^2 \frac{e^{-kr}}{r} \tag{8.3}$$

Z is the charge of the particles. k^{-1} is the Debye- Huckel screening length of the electrolyte, which can be calculated from the concentrations (n_j) and charges (Z_j)of the involved ions.

$$k^2 = \frac{e^2}{\epsilon K_B T}\sum_{j=1}^{N} n_j {Z_j}^2 \tag{8.4}$$

At the shortest distances the van der Waals attraction dominates and the DLVO potential diverges to - infinity, this corresponds to the minimum of interaction potential and causes irreversible aggregation. At intermediate distances, the Coulomb repulsion is stronger and creates a potential barrier, which prevents aggregation and the colloidal solution remains in a metastable state if this barrier can not be overcome. For a barrier height above $\sim$ 15- 20 K_BT a solution is usually considered to be metastable [43]. The barrier height can be changed by changing the ionic content of the solution. When the maximum Coulomb potential barrier is less than or equal to zero, there is no potential barrier for collisions and the aggregation process is mainly driven by Brownian motion. In some cases the overall potential also has a secondary minimum at larger distances, this shallow potential hump can be responsible for reversible binding of colloidal particles called flocculation , a less evident effect for metallic colloids with regards to SERS. Thus the DLVO theory provides a useful description of colloidal stability and aggregation.

The first step of aggregation is the formation of dimers from two single colloidal particles, with a rate constant 'k_r' which depends on the potential barrier and viscosity. In the initial stage dimer - dimer collision and dimer- sin-

gle particle collision, that is the formation of higher aggregates are neglected. In this case if C_s is singe particle concentration, and C_p is dimer concentration ,

$$\frac{dC_s}{dt} = -k_r C_s^2,$$

$$\frac{dC_p}{dt} = \frac{k_r}{2} C_s^2,$$

$$C_s + 2C_p = C_s^{(0)},$$

The solution to this set of equations for the time dependent concentration of dimer C_p is given by [169]

$$C_p = \frac{C_s^{(0)}}{2} \left(\frac{C_s^{(0)} k_r t}{1 + C_s^{(0)} k_r t} \right) \tag{8.5}$$

where $C_s{}^{(0)}$ is the initial single colloidal particle concentration. if, $\tau = 1/C_s{}^{(0)}k_r$, is the time constant,

Then Eq.(8.5) becomes,

$$C_p = \frac{C_s^{(0)}}{2} \left(\frac{t/\tau}{1 + t/\tau} \right) \tag{8.6}$$

For later stages of aggregation we need to consider all the interactions and the formation of higher aggregates, when the probability of two particles to aggregate does not depend on the type of particles, that is when the rate constants are independent of the particle size we have a set of differential equations which leads to the solution [43].

$$C_n(t) = C_0 \left[\frac{t}{\tau} \right]^{n-1} \left[1 + \frac{t}{\tau} \right]^{-(n+1)} \tag{8.7}$$

Where n=1 for single particles, n= 2 for dimers, n =3 trimers etc. and $\tau = 2/\mathrm{k}_r C_0$

Eq.(8.7) is true for the case when the probability of two colloids to aggregate does not depend on the type of the particles, that is when the probability of two single particles to interact and form a dimer is same as that of the probability of two dimers to form a tetramer or a trimer and a dimer to form a bigger aggregate. We can not directly apply this analytical solution to our results, because in our case the probability depends on the particle type due to the increase of potential barrier as the particles combine.

The interaction potential is additive that is the interaction of a colloid with a dimer is the sum of the interactions between the colloid and each of the two colloids forming dimer. So if there is no potential barrier, the potential remains attractive for larger structures and the aggregation leads to complete coagulation. A positive potential barrier of a few $\mathrm{K}_B\mathrm{T}$ will not stop the aggregation, but just makes the aggregation slower. When the potential barrier V_{max} is between 0 and 15 $\mathrm{K}_B\mathrm{T}$, that is the range,which can be achieved by the screening of Coulomb potential by the addition of electrolyte, the aggregation process is different. As the repulsive electrical interaction potential for a colloid and a dimmer is larger than that for a pair interaction of two monomers, for a barrier height of few $\mathrm{K}_B\mathrm{T}$'s it might be possible to form a cluster of two particles, but forming large clusters will be less and less probable. Thus under certain conditions the aggregation of colloid can be limited to the formation of small aggregates with 2, 3 or 4 particles(dimers, trimers or tetramers). This self limiting aggregation, where the colloid is partially aggregated with small clusters is an interesting aspect of SERS and the dynamics of formation can be calculated in a simple Monte Carlo simulation, as described by Meyer et

al. [169].

8.2 Monte Carlo Simulation

In order to understand the kinetics of colloidal aggregation and to check the validity of our experimental observations, silver colloid aggregation has been modeled with the help of a simplified two dimensional Monte Carlo simulation as in Meyer et al. [169]. In the simulation, initially we consider a number of particles, randomly distributed over a finite Cartesian lattice. We used 50 particles randomly distributed over a square lattice of size 2500 × 2500, with lattice cell size = 20 nm. The number of particles and the lattice size we have chosen corresponds to a concentration of 1×10^{12} cm^{-3} silver particle in solution. A schematic potential shown in Fig.8.3 has been chosen to model the Coulomb potential hump in the DLVO potential, similar to the schematic potential described in [169] . The potential is selected such that two colloidal particles separated by a distance smaller than 1.5 lattice units(d_l) are trapped in a very deep potential well ($V_{min}/K_BT < -40$). This includes the four nearest neighbors and the four next nearest neighbors in a square lattice that are separated from the reference site by $\sqrt{2}d_l<1.5\ d_l$. The model potential then has a shallow positive hump (V_{max}/K_BT) and then drops to zero for particles separated by more than 3.5 d_l. The potentials from neighboring particles are added linearly.

To model the particle motion and aggregation, for each Monte Carlo iteration we choose a random particle and calculate its potential energy, U_{ref} then move the particle to a random neighboring position on the lattice . After moving the particle we calculate its new potential energy, U. If $U_{ref} \geq U$, the move is accepted or else the move is accepted with a probability $P= e^{-(U_{ref}-U)/K_BT}$

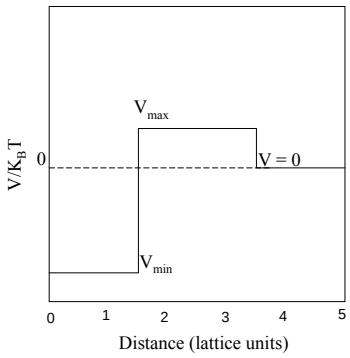

Figure 8.3: Schematic potential

given by Boltzmann factor at temperature T. These simulations were programmed in Matlab and the program listing is given in Appendix B. The simulation has been carried out for various potential barrier heights. Periodic boundary conditions were used in the simulation we performed.

In one of the test runs we simulated with the same conditions as in [169] with 500 particles in a 200×200 lattice with potential barrier of $10K_BT$ with closed boundary conditions, the results obtained are shown in Fig. 8.4. The results are in good agreement with the results presented in [169] with similar number of single particles and dimers after 10^6 iterations.

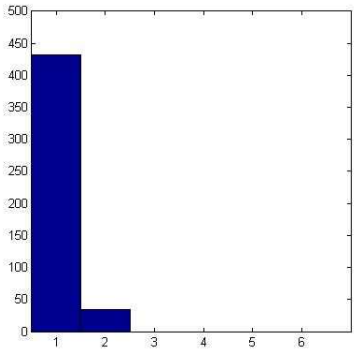

Figure 8.4: Histograms showing number of particles forming clusters of size 1,2,3 etc after 10^6 iterations for $V_{max}/K_BT = 10$ (square lattice 200×200, 500 particles, closed boundaries).

The use of closed boundary conditions used in that paper is not very well justified. Usually periodic boundary conditions are used to simulate the aggregation in free volume. As reported in [170] when the observation region is a small representative cut out from a larger region, periodic conditions should be used, where the particle that moves out of the observation region at one side reappears at the opposite side. Closed boundary conditions are used when the observation region is delimited by fixed walls and in this case the particles are not supposed to leave the system [170]. Simulations with a similar potential using periodic boundaries showed significant difference in the results with much higher aggregation rate and a number of agglomerates of bigger size. It shows that closed boundary conditions may slow down the aggregation process by slowing down the motion of particles at the boundaries. This becomes more evident for lower potential barriers. Higher discrepancy in results obtained for periodic boundary and closed boundary condition simulations for lower potential barriers. The results obtained for the same simulation shown in Fig. 8.4 but for periodic boundary conditions is given in Fig. 8.5

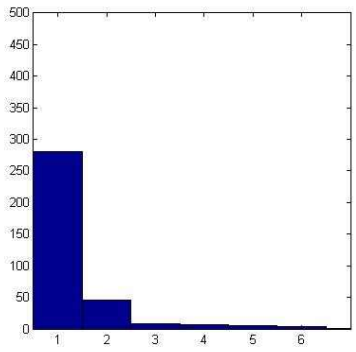

Figure 8.5: Histograms showing number of particles forming clusters of size 1,2,3 etc after 10^6 iterations $V_{max}/K_BT = 10$(square lattice 200×200, 500 particles, periodic boundaries).

To choose the range of the potential values the following assumptions were

used. When there is no potential barrier the aggregation of particles is controlled by diffusion. The diffusion controlled binary association rate constant of two similar particles is equal to the collision rate constant and is given by [171]

$$k_r = \frac{4K_BT}{3\eta} \tag{8.8}$$

Where $K_B = 1.38\text{x}10^{-23}$ J K^{-1} is the Boltzmann's constant, Temperature T = 295 K, $\eta = 8.9\times10^{-4}$Pa s, is the viscosity of water at room temperature.

The value of k_r is calculated as $0.6\times10^{-17}m^3$ / particle/ second.

The corresponding time constant, $\tau = 1/C_s{}^{(0)}k_r$, where $C_s{}^{(0)}$ is the concentration of colloidal particles.

When there is a potential barrier U, the probability of particles to aggregate depends on the potential barrier and in that case the rate constant becomes,

$$k_p = k_r e^{-U/K_BT} \tag{8.9}$$

The correponding time constant for dimer formation is

$$\tau_p = \frac{1}{C_s^{(0)} k_r e^{-U/K_BT}} \tag{8.10}$$

During our SERS experiments we observed a build up time of signal of several minutes (few hundred seconds). If we assume that the SERS signal build up is due to colloid aggregation, the time constant observed in experiments should be in agreement with the colloid aggregation time. For potential barriers of U/ K_BT = 4, 5, 6 and $C_s{}^{(0)} = 2\times10^{-17}$ m^{-3}, the corresponding time constants τ_p are 45 seconds, 123 seconds and 322 seconds respectively. These values of potentials also correspond to the potential values reported in [169, 172], where a metastable state, which has self limiting aggregation

with small clusters is reported for potential barrier heights between 0 and 15 K_BT.

The results for different potential barrier heights V_{max}/K_BT =2, 3, 5 and 6, for 3×10^8 iterations and $V_{max}/K_BT = 7$ for 4×10^8 iterations for 50 particles in 2500x 2500 lattice are given in Fig. 8.6. The dynamics of aggregation of particles with different potentials are depicted in these plots. The number of particles forming clusters with size one (single particle), two (dimer), three (trimer) and four (tetramer) particles are shown versus the number of Monte Carlo steps. For V_{max}/K_BT =2, for the lowest barrier considered here, after 3×10^8 iterations, dimers are the dominating cluster types with some trimers and tetramers formation. When the barrier height increases dominating particles are single particles for $V_{max}/K_BT > 5$ with small number of dimers and very few number of big clusters like trimers and tetramers after 3×10^8 iterations. It is clear from Fig. 8.6 that the rate of formation of dimers depends on the height of the potential barrier.

In order to calculate the time interval per step corresponding to one iteration, we can use the relationship between diffusion time and random walk times.

In diffusion the mean square displacement in two dimension after time t is given by [173].

$$<S^2> = 4Dt \tag{8.11}$$

and for diffusion in three dimensions,

$$<S^2> = 6Dt \tag{8.12}$$

where D is the diffusion coefficient, which can be calculated from the equa-

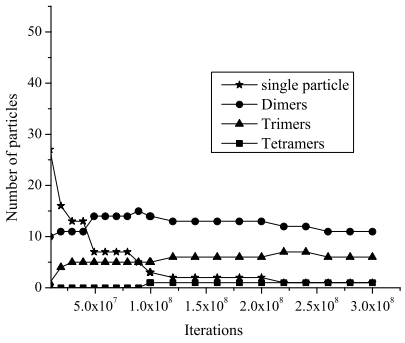

(a) V_{max}/K_BT =2

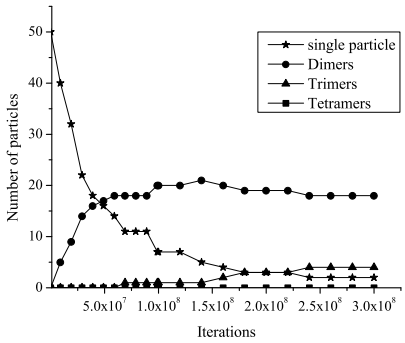

(b) V_{max}/K_BT =3

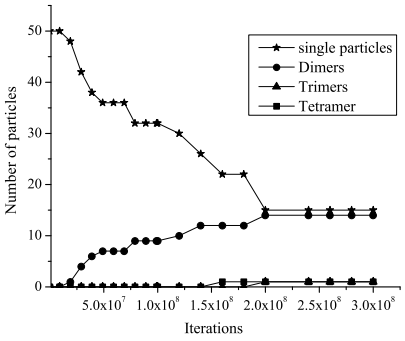

(c) V_{max}/K_BT =5

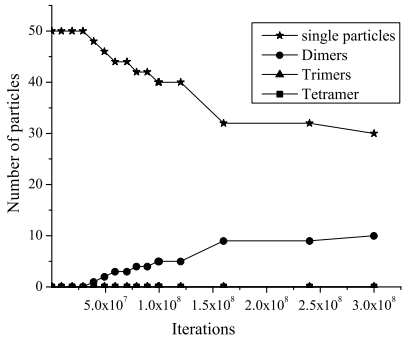

(d) V_{max}/K_BT =6

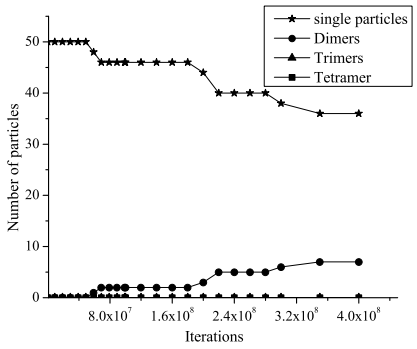

(e) V_{max}/K_BT =7

Figure 8.6: Cluster formation in Monte Carlo simulation for different barrier heights (a) V_{max}/K_BT =2 ,(b) V_{max}/K_BT =3, (c) V_{max}/K_BT =5, (d) V_{max}/K_BT =6, (e) V_{max}/K_BT =7, (f)V_{max}/K_BT =5 for 500 particles.

tion [171],

$$D = \frac{K_B T}{6\pi\eta R} \tag{8.13}$$

Where $K_B = 1.38\text{x}10^{-23}$ J K^{-1} is the Boltzmann's constant, Temperature T = 295 K, $\eta = 8.9\times10^{-4}$Pa s, is the viscosity of water at room temperature and R is the particle radius, for 20nm size silver particle D = $2.43\times10^{-11}$$m^2$ /s.

From the other hand in random walk of particles, the average square of net displacement is given by [174]

$$<S^2> = <N>d^2 \tag{8.14}$$

When N is number of steps and d = 20nm is step size (cell size)

Comparing the above equations, we get

$$4Dt = Nd^2 \tag{8.15}$$

and thus time interval corresponding to one iteration is equal to

$$t = \frac{d^2}{4D} \tag{8.16}$$

In the simulation we consider the motion of one particle at a time, whereas in reality all the particles undergo random iterations simultaneously, so the time interval for one iteration of the system corresponds to the iteration of 50 particles, therefore in our case, the time step is 50 times smaller than that calculated using Eq.(8.16). Using diffusion coefficient D = 2.43×10^{-11} m^2/s from Eq.(8.13) for 20nm particles and for the 20 nm step size(d) we calculated t = 0.082 microseconds per iteration. As one iteration corresponds to 0.082 microseconds 3×10^8 iterations correspond to $\sim$25 seconds.

The formation of dimers as a function of time for different values of the potential barrier are shown in the figures 8.7, 8.8 , 8.9 and 8.10. A least square fit to the equation (8.5) in the form

$$C_p = \frac{C_0}{2}\left(\frac{C_0 A t}{1 + C_0 A t}\right) \tag{8.17}$$

to the various plots results in values of A = 0.0095 ± .0.0007, 0.0015 ± 0.00006, 0.0006 ± 0.00003, 0.0002± 0.00001 for V_{max}/K_BT = 3,5,6 and 7 respectively. From the curves plotted the time constant has been calculated for different potential barriers , for V_{max}/K_BT = 3,5,6 and 7 the time constants are 2.1, 13.5, 35.1 and 89.4 seconds respectively. The results indicate qualitative agreement with experimental times of 10's of seconds to minutes and plateau in region of dimer formation.

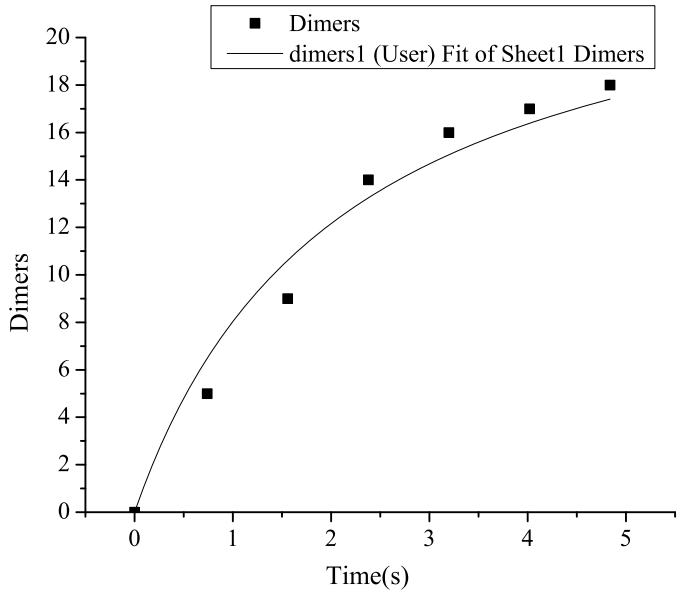

Figure 8.7: Growth rate of dimers for V_{max}/K_BT = 3. The line shows least squares fit of Eq: 8.17 to the data giving a value of A= 0.0095 ± .0.0007.

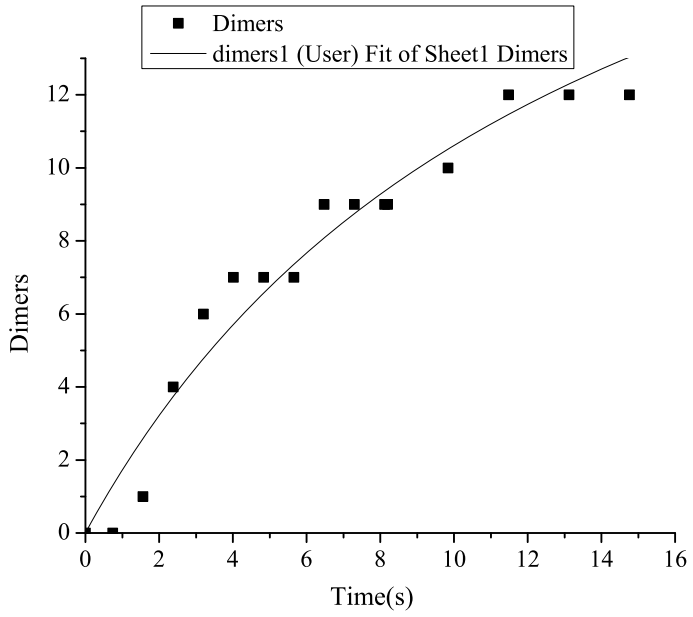

Figure 8.8: Growth rate of dimers for $V_{max}/K_BT = 5$. The line shows least squares fit of Eq:8.17 to the data giving a value of A= 0.0015 ± .0.00006.

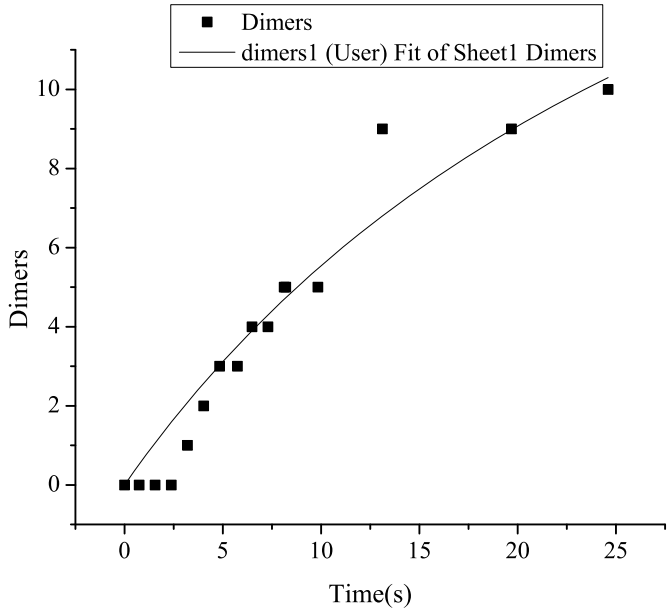

Figure 8.9: Growth rate of dimers for $V_{max}/K_BT = 6$. The line shows least squares fit of Eq:8.17 to the data giving a value of A= 0.0006 ± 0.00003.

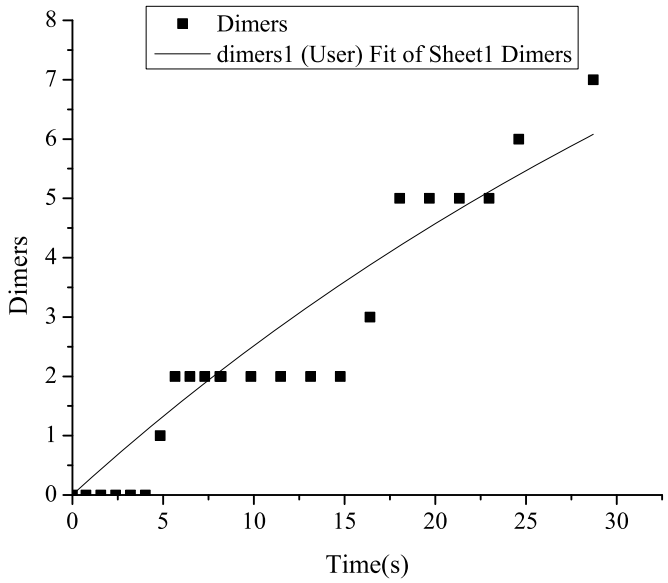

Figure 8.10: Growth rate of dimers for $V_{max}/K_BT = 7$. The line shows least squares fit of Eq:8.17 to the data giving a value of A= 0.0002± 0.00001 .

8.3 Discussion

Monte Carlo simulation results show that the self limiting aggregation can lead to relatively small aggregates given an appropriate potential barrier. From the simulation plots, it is clear that the time constant for dimer formation is sensitive to the potential barrier. The experimental observations also confirm this as there is a strong dependence of the SERS signal on the electrolyte concentration which would agree with a potential which depends on the concentration of the electrolyte. We also observe that our sample solution for the SERS measurement has small aggregates of colloidal particles when high enhancement is observed and that the SERS active solution was stable for more than a day with detectable SERS spectrum. The colloid concentration in our sample solution is 6 times more diluted than that used in the simulation which would indicate that the time scales observed in the simulations should be reduced by

a factor of 6 times. For the potential barrier of $6K_BT$ ($V_{max}/K_BT = 6$), the time scale of formation of dimer is approximately 35s for the concentration used in the simulation. So for our sample solution the time constant would be 3.5 minutes, which agrees with the value of time constant of 2.7 minutes which we obtained for the growth of SERS signal in our experiments as given in chapter 6. Thus the sample solution we used appears to be consistent with a potential barrier close to 6 K_BT for a 2D DLVO model of aggregation. The TEM image also confirms the presence of small aggregates with a high number of dimers, trimers and isolated particles when we have high enhancement of SERS signal. Thus, the self limiting aggregation suggested for the Lee Meisel preparation of colloid solution [43] is also observed in the case of borohydride reduced silver colloid, which we used here for the SERS studies.

8.4 Conclusion

In this chapter we used 2D numerical simulations to study the colloid agglomeration process using a simplified potential model and random walk algorithm as described in [169]. The assumption of an additive potential proposed in the same reference [169] was also used. Though the model used in the simulations is very simplified it is able to predict the key features of the experimental observations showing the presence of small aggregates for an extended period of time and also gives the aggregation time constants within reasonable agreement with the experimentally observed values of the SERS signal build up time.

Chapter 9

Summary and Future Work

9.1 Summary of Thesis Results

This thesis investigated different aspects of surface enhanced Raman scattering technique in order to obtain reproducible high sensitive detection of amino acids with a focus on tryptophan in particular. In the process various aspects of SERS using silver colloid nanoparticles were studied such as impact of experimental conditions, sample preparation procedure and role of background electrolytes on the SERS signal. SERS studies of a few different amino acids, peptides and dyes in silver colloid have been carried out during the course of this thesis. SERS studies were also performed in different detection geometries such as liquid core waveguides and in microfluidic channels in order to increase the sensitivity and prepare for future investigation into lab on a chip systems.

The capability to detect low concentrations is an important aspect of SERS. With the high sensitivity detection system developed we could detect SERS spectra from the amino acid tryptophan at concentrations as low as $\sim 10^{-8}$ M. The SERS enhancement obtained for this amino acid is of the order of $\sim 10^{9}$. We performed a detailed study of SERS effect of Trp amino acid for a broad

range of concentrations and with different background electrolytes. The lowest concentration of Trp detected is 3 to 4 orders of magnitudes smaller than the tryptophan detection previously reported in literature. For this amino acid high quality SERS spectra have been obtained in the concentration range 10^{-8} to 5×10^{-4} M. During this study it was discovered that the enhancement of Raman signal dramatically depends on the concentration of Trp. These changes in enhancement are accompanied by the changes in the shape of the spectral curves. Some of the strong peaks such as indole ring breathing mode around $\sim$ 1000 cm^{-1} disappeared at low concentration whereas new peaks appeared compared to the spectra of high concentration of Trp ($> 10^{-4}$ M). This transformation of the SERS spectra of Trp has not been reported in the literature. We observed that below 10^{-4}M of Trp the shape of the spectral curves does not change with the concentration of Trp and the incubation time, indicating stable and reproducible binding geometry of the molecules to the nanoparticles. The high Raman signal enhancement observed for Trp can be explained in part by the particular binding geometry of Trp molecules to the silver nanoparticle surface under the experimental conditions developed. In particular, it is suggested that the largest enhancements obtained derive from the preferential binding of the Trp molecules in between nanoparticles in dimer and trimer configurations. We have observed that Trp directly takes part in the aggregation process and plays an important role in binding and thus ends up in the correct spot for the maximum enhancement. The observation of saturation in observed signal levels would be consistent with the filling of such sites by the Trp molecules. At the same time, under the same experimental conditions the peak signal strength obtained from different measurements were reproducible with a standard deviation of the order of 50%.

The enhancement factor we observed for the amino acids Phe and Gly was $\sim 10^4$. For these amino acids SERS enhancement was observed without any additional electrolyte. In contrast, the addition of NaCl and composite electrolyte led to a reduction of spectra in these amino acids. It was found that in spite of the similar chemical structure of Phe and Trp amino acids the conditions for which strong SERS signals observed can be different due to the different binding process of each analyte to the substrate. For the peptide Trp-Trp no additional electrolyte was required to obtain large signals. Tripeptide Gly-Gly-Gly also provided SERS spectrum without any electrolyte. Overall, the results indicate the possibility of collecting Raman spectra of amino acids and peptides at low concentrations with good signal to noise ratios using the SERS technique. However it is expected that optimization of electrolytes could improve the signal enhancements of these other species further.

Liquid core waveguides provide the possibility of an additional signal enhancement. We have demonstrated enhancement of up to 50 times giving the possibility to achieve a detection limit for Trp as low as $\sim 10^{-10}$ M. To the best of our knowledge this is the first reported SERS detection in a Teflon AF capillary waveguide. In principle short waveguide channels on the order of centimeters in length could be incorporated into microfluidic systems allowing such high sensitivities for lab on a chip analysis. We have also demonstrated the SERS spectra measurement in a standard microfluidic channel at low concentrations. However, in the standard microfluidic channels, the SERS signals observed are reduced relative to those in large open probe volumes due to the much smaller transverse probe length across the channel used here. Laser

micro machining was employed in order to fabricate an extended interaction volume in the microfluidic geometry. However this was not optimized and further work is required to optimize the resultant probe geometries to allow for large effective numerical aperture probing. Once optimized, it is expected that similar sensitivities can be obtained in microfluidic systems as with the open geometry cuvette measurements and these should be in the fmol range as required to analyze the contents of single cells extracted into such microfluidic channels.

Throughout the study it was found that the background electrolyte is an important factor in SERS measurements as it can change the aggregation and binding. In most cases, addition of electrolyte is necessary to observe an enhanced SERS signal. Along with the commonly used electrolyte NaCl, we also developed some composite electrolytes which led to high enhancement of Raman signals reported. The spectra observed using this electrolyte were stable and reproducible and thus should be useful as an analytical tool for high sensitivity detection of Trp and other organic molecules in solution.

In order to better understand the time evolution of the spectra, a numerical simulation has also been performed of the aggregation process in silver colloid which could qualitatively explain the experimental results observed.

9.2 Future Work

The work presented here is the first step towards ultra sensitive detection of amino acids and proteins. In the present work we have been able to optimize conditions for one amino acid tryptophan. Many issues remain which would

require more investigation.

Further improvement of the composite electrolyte is an interesting aspect. The composite electrolyte developed in the current work showed good SERS spectra enhancement for the amino acid Trp and dyes rhodamine 6G and acridine orange. But for the other amino acids studied Phe and Gly this electrolyte did not give SERS enhancement and different electrolytes electrolyte solutions would be required to give enhanced binding and SERS signal for these molecules.

A related aspect would be to study and compare the binding geometry and orientation of phenylalanine and tryptophan in silver colloid in order to understand the difference in observation of SERS signal from these amino acids with similar chemical structure.

A significant enhancement of detection could potentially be obtained by the incorporation of the LCW technique into a microfluidic chip using the unique total internal reflection properties of Teflon AF capillaries with short lengths of a few cm. In principle this could lead to extremely low levels of detection potentially allowing analysis of the contents of single cells. Thus a study of increased probe volumes in microfluidic systems including the possibility of incorporating a LCW as part of the system would be very interesting.

The SERS enhancement depends critically on the optimum binding of the species to the nanoparticles and optimum binding of the nanoparticles. A better fundamental understanding of the binding and aggregation process is

required in order to fully optimize the SERS enhancement. We have taken only a first step in this detection with the aggregation kinetics model presented here.

9.3 Conclusion

In summary, this thesis has significantly improved the lower concentration detection limit of Trp amino acid by developing new composite electrolytes and analysis procedures. The composite electrolyte developed provides higher and reproducible SERS enhancement for some of the analytes studied compared to the commonly used electrolytes. The detection of SERS in a Teflon AF capillary has also been investigated for the first time during the course of this thesis, which further increases the Raman enhancement.

The results presented in this thesis are an important step towards the future application of SERS in microfluidic lab on chip systems for the detection of biomolecules. The high sensitivities and reproducibilities obtained here together with the further improvements expected from future work should enable SERS to be used for the analysis of the bio molecular content of single cells in such systems.

Appendix A

Mie Resonance of Silver and Gold

Plasmon resonances are the core of electromagnetic enhancement that makes SERS possible. The most used materials for SERS and plasmonics are silver (Ag) and gold (Au). These metals are important because of their unique optical properties. Metals have complex dielectric constant ϵ (ω). The real part of dielectric constant, Re(ϵ) changes from small positive values in the ultra violet region to negative values in the visible and very negative values in the infra red. The imaginary part Im(ϵ) has a small value for silver and a larger value for gold. This is one of the important characteristics of metal that makes possible the interesting optical effects.

Plots showing optical constants n and kappa, which are the real and imaginary parts of the refractive index, and the real and imaginary part of dielectric constants are given in Fig. A.1. The optical constant for Ag and Au were taken from the measurements carried out by Johnson and Christy [175], these measurements were based on reflection and transmission measurements on carefully prepared surfaces to avoid contributions from scattering.

The absorption cross - section of a spherical particle which has dimensions

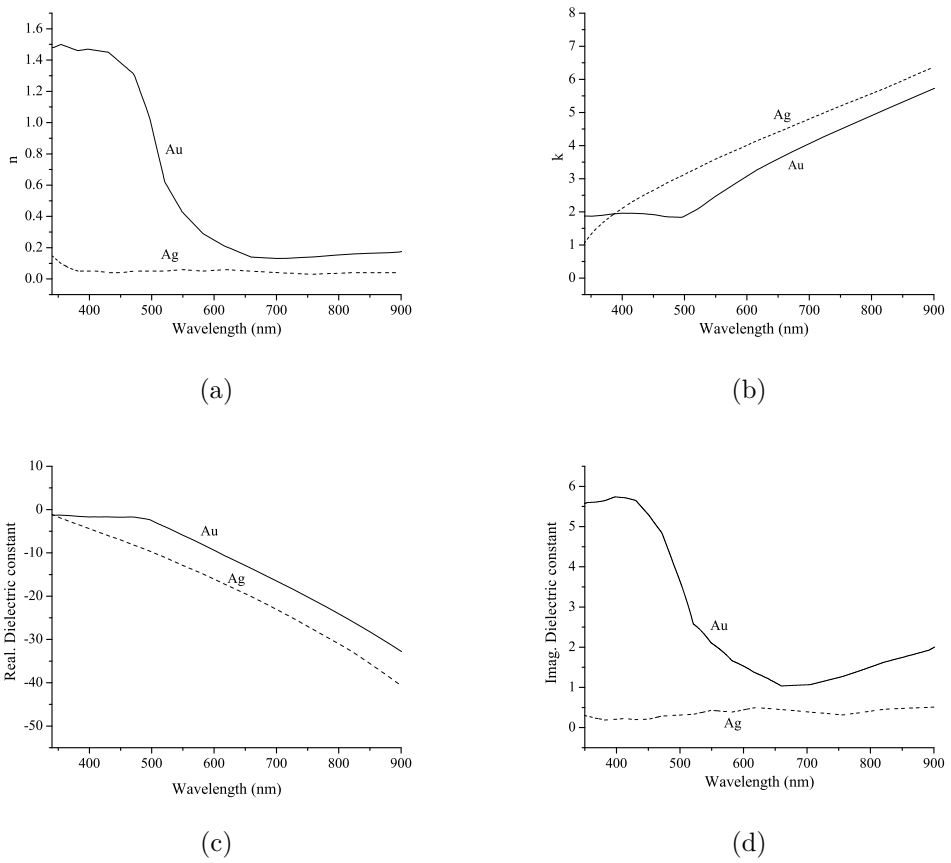

Figure A.1: Plots (a) and (b): optical constants of silver and gold as a function of wavelength. Plots (c) and (d): real and imaginary part of dielectric constant of silver and and gold as a function of wavelength.

much smaller than the wavelength of light is given by [176],

$$\sigma_{abs} = \frac{k}{\epsilon_0} Im[\alpha(\omega)] \tag{A.1}$$

where k, is the wave vector in the surrounding medium and $\alpha(\omega)$ is the polarizability and $\epsilon_0 = 8.85\times\ 10^{-12}$ F/m is the permittivity of vacuum. The polarizability is given by

$$\alpha(\omega) = 4\pi\epsilon_0 a^3 \frac{\epsilon_1(\omega) - \epsilon_2}{\epsilon_1(\omega) + 2\epsilon_2} \tag{A.2}$$

where ϵ_1 is the dielectric constant of the metal , ϵ_2 is that of the medium and a is the particle radius.

The frequencies at which Re(ϵ_1) = -2 ϵ_2, the absorption cross- section becomes very high. This is an example of localized surface plasmon resonance. The optical resonance conditions in small metallic objects are strongly dependent on its geometry.

The absorption cross - section as a function of wavelength for a spherical silver and gold particle of 20 nm diameter in different media; vacuum (n=1), water (n=1.33) and glass (n=1.5) are plotted as shown in Fig.A.2.

The resonance for silver particle is in the ultraviolet-visible spectral range, while for gold the resonance occurs around 500 nm. The resonant condition is determined primarily by the real part of ϵ_1. The width of resonance is determined by the imaginary part of dielectric constant. The imaginary part is related to the absorption of the material. The larger the imaginary part the more lossy the resonance is. Strong damping leads to a decrease in the Q of the resonance which gives a broader and lower absorption peak. Since the imaginary part of the dielectric constant is fairly small for silver it has a stronger and narrower resonance than for gold. The resonance condition for Ag is satisfied at frequency where the imaginary part of dielectric constant for silver is smaller compared to that of gold. Gold has a comparatively higher imaginary part of dielectric constant and therefore the resonance in gold is more lossy and broader.

The resonance in absorption also leads to enhancement in the surface electric field. These in turn lead to the electromagnetic enhancement observed in SERS when using such nanoparticles and thus the strength of the SERS

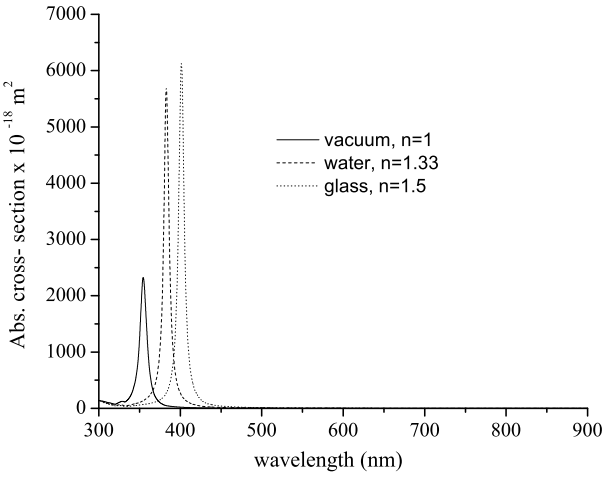

(a)

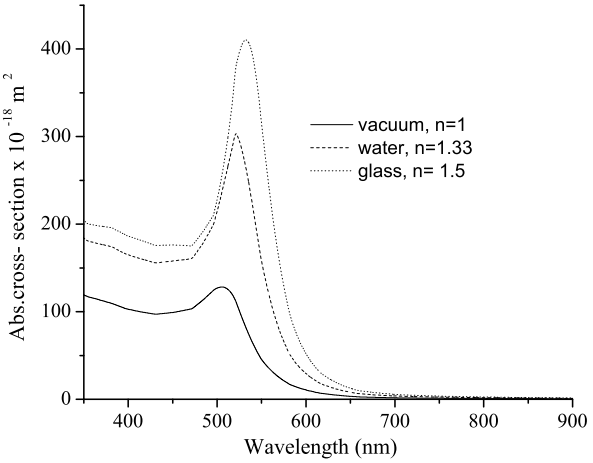

(b)

Figure A.2: Absorption cross section as a function of wavelength in vacuum, glass and water (a) for spherical silver particle with 20 nm diameter(b) for spherical gold particle with 20 nm diameter. Solid line: vacuum (n=1), Dashed line: water (n=1.33), Dotted line: glass (n=1.5).

enhancements also follow a similar trend where silver nanoparticles give much stronger enhancements than gold nanoparticles. For the real colloidal solutions the shapes of the nanoparticles will vary from perfect spheres broadening the

measured absorption resonance as shown in Fig 3.11 and also the formation of dimers (which give larger enhancements than single nanoparticles) will shift the resonant frequency to longer wavelengths as shown in Fig. 6.5. This shifts bring the resonant wavelength into the range of the excitation laser wavelength of 532nm used in the present experiments.

Appendix B

Matlab Code for Monte Carlo Simulation of Colloid Aggregation

```
%% 2D Brownian motion of particles: Limiting motion to one cell at a time
% Guided by the aggregation potential scheme defined using V_scheme
tic
% function 'potential_calc' used to calculate the interaction potential
%% Definitions
% Cell index = [x_coordinate_index , y_coordinate_index]
% Move = CHANGE IN POSITION (Δ_position)
% i.e., New position = Old position + Δ_position
% Feasible Moves: Δ_position can only assume 1, 0, −1 for each index
% Note: [0 0] not allowed since it means no movement

% RULES FOR THE PARTICLE MOVEMENT:
% (1) If the potential energy of the particle decreases, the move is
%     surely feasible and is deterministic
% (2) If not, the move is accepted based on some probability(Boltzman
%     factor)

clc; clear all; clear global; close all;

%Lattice size = L_size x L_size cells
L_size = 2500;

```

```
%No. of particles
N = 50;

% Empty matrix of L_sizexL_size cells and no particles (all zeros)
L_matrix = zeros(L_size);

L_matrix = sparse(L_matrix);%Converting to 'sparse' (Save memory)

%% V_scheme: The schematic potential definition (used in 'potential_calc')

V_scheme = [-40 5]; % THIS IS AN IMPORTANT TUNING PARAMETER FOR THE SIMULATION

% NOTE: The brownian motion will depend on this potential scheme

%% Initial Conditions: Uniformly allot particles in the 2500x2500 lattice

% Requires N randomly chosen UNIQUE CELL INDICES in the 2500x2500 lattice
% So, we need a (Nx2) matrix N cell indices in the range [1 to L_size]

U = unique(randi(L_size,N,2), 'rows'); % Rows are particles,
%columns represent cell index

% Assuming no initial aggregation: Remove and replace redundant cells

while (size(U,1) < N)
    U = [U;unique(randi(L_size, (N - size(U,1)), 2),'rows')];
    U = unique(U,'rows');
end


% Populate 'L_matrix' with particles according to random indices in 'U'
% function 'sub2ind' is used to assign values to indices stored in U
% sub2ind will convert row-column indices in U to linear indices.
% So, it will convert [i,j] to a linear position (j-1)*nrows + i

pos = sub2ind(size(L_matrix),double(U(:,1)),double(U(:,2)));
L_matrix(pos) = 1;

```

```
61 agg_max = 6; % Maximum level of aggregation (defines color ...
       coding accordingly)
62
63 L_matrix_frame = uint8(full(L_matrix(:))); % storing ...
       lattice matrix frame-by-frame
64
65 %% Perform Brownian motion choosing ONE particle at a time
66
67 %BROWNIAN MOTION FOR t_max TIME STEPS OF MONTE-CARLO ...
       SIMULATIONS
68 t_max = 6e8 ;
69
70 for i = 1 : t_max
71
72     i
73
74     [U_x U_y] = find(L_matrix); % Find non-zero cell ...
           locations in lattice
75
76     U = [U_x U_y];
77
78     % Effective number of particles will change due to ...
           aggregation
79     N_eff = size(U,1);
80
81     % Choose a random cell in L_matrix which contains ...
           atleast one particle
82     if N_eff > 1
83         dummy = randi(N_eff,1);
84     else
85         dummy = 1;
86     end
87     % The particle in this cell will move for this time step
88     U_this_move = U(dummy,:);
89
90     % Choose one move for at random from [1 0 -1]
91     U_delta = randi([-1 1],1,2);
92
93     % Remove [0 0] cases
94     while (sum(abs(U_delta)) == 0)
95         U_delta = randi([-1 1],1,2);
96     end
97
98     U_new = U_this_move + U_delta;
99
100    U_new(U_new < 1) = L_size;
101
102    U_new(U_new > L_size) = 1;
103
104    pos_new = sub2ind(size(L_matrix), U_new(1), U_new(2));
```

```
105     pos_this_move = sub2ind(size(L_matrix), U_this_move(1), ...
            U_this_move(2));
106
107     if pos_new == pos_this_move
108         % NO MOVEMENT  !!!!!
109         % This can happen at some point during the ...
                simulation !!!!!!
110         % For ex., when particle is constrained to an edge
111     else
112         %Brownian move: The particle appears in the ...
                adjacent cell and
113         %aggregates to the existing particle in that cell, ...
                if any
114
115         % Two-step simulation of the Brownian move: ...
                Limitting the
116         % maximum aggregation size to agg_max
117
118
119         NP_new = L_matrix(pos_new) + L_matrix(pos_this_move);
120
121         if NP_new ≤ agg_max % Limitting the maximum ...
                aggregation size
122
123             L_old = L_matrix; % Storing current lattice ...
                    (for recovering
124             %L_matrix from infeasible moves)
125
126             %First, the adjacent cell value in L_matrix ...
                    becomes NP_new
127             L_matrix(pos_new) = NP_new;
128
129             % Second, Initial cell of the particle becomes ...
                    null/empty
130             L_matrix(pos_this_move) = 0;
131
132             % Checking for potential energy feasibility
133
134             V_old = potential_calc_fast(U_this_move, L_old, ...
                    V_scheme);
135
136             V_new = potential_calc_fast(U_new, L_matrix, ...
                    V_scheme);
137             % Calculating the new potential
138
139             if V_new ≤ V_old
140
141                 % Accept the move deterministically,
142                 % i.e., do nothing to L_matrix as it is now
143
144             else % Probability based on BOLTZMAN FACTOR:
```

```
145                     %    Pr(V ≥ x) = exp(−x) OR  Pr(V < x) = ...
                            [1 − exp(−x)]
146                     % ie., the random number X can be ...
                            generated as
147                     % x = −ln(1 − U_rand),
148                     %U_rand is a uniform random no.in the ...
                            interval [0 1]
149
150                     % Generate a uniform random number in the ...
                            interval [0 1]
151                     U_rand = rand;
152
153                     % Note: The case of U_rand zero is NOT A ...
                            PROBLEM in MATLAB
154                     %       because ln(0)=−Inf
155
156                     % Based on the Boltzman probability:
157                     % If Vnew ≤ x, then ACCEPT the move,
158                     % else, REJECT the move
159
160                     x_rand = −log(U_rand);
161
162                     if V_new ≤ x_rand
163
164                         % Accept the move, i.e., do nothing to ...
                                L_matrix
165                     else
166
167                         % Reject(Restore the matrix to ...
                                previous state)
168                         L_matrix = L_old;
169                     end
170                 end
171             end
172         end
173
174         % Store the lattice every 50th time step of simulation only
175         % (down−sampling so that there is a significant change ...
                between frame
176         % snapshots for making movie)
177
178         if mod(i,60000000) == 0
179             L_matrix_frame(:,end+1) = uint8(full(L_matrix(:)));
180         end
181
182         if (sum(sum(L_matrix)) < N)
183             error('Error');
184         end
185     end
186
187     toc
```

```
188  npart = hist(full(L_matrix(:,2)),[0 :6]);
```

Potential Calculation

```
1  function V = potential_calc(U, L_matrix, V_scheme)
2
3  % Calculates the potential of a particle in a reference ...
       cell U of a matrix
4  % filled with  particles according to L_matrix and a given ...
       schematic
5  % potential V_scheme
6
7  %% Inputs:
8  % U : Cell index (row, column) for which potential is ...
       calculated
9  % L_matrix: Lattice matrix with the distribution of ...
       particles in each cell
10 % V_scheme: The schematic potential for a pair of particles ...
       defined as
11 % a discretised function of lattice unit distances(starting ...
       from 1.5).
12
13 %  Example: V_scheme = [-40 10 10] would mean the following
14
15 %        if 0 <= distance <= 1.5, then V (for a pair) = -40
16 %
17 %        if 1.5 < distance <= 2_/2, then V (for a pair) = 10
18 %
19 %        if 2_/2 < distance <= 3_/2, then V (for a pair) = 10
20
21 %        for all other distances, V (for a pair) = 0 .... ...
       and, so on
22
23 pos_U =  sub2ind(size(L_matrix), U(1), U(2)); % Converting ...
       subscripts to linear
24 % index (for easy reference)
25
26 if L_matrix(pos_U) == 0 % Avoiding calculation if the cell ...
       U is empty
27     error('The cell is empty');
28 end
29
30 L_size = size(L_matrix,1);
31
32 % Region of interest for calculations (potential is assumed ...
       to be zero
33 % beyond the number of lattice units in V_scheme)
34 ROI = min(length(V_scheme), L_size-1); % ROI <= Lattice size -1
```

```
35
36 L_ROI = L_matrix;
37 % Cropping the matrix according to ROI
38
39 L_ROI(pos_U) = NaN; % Marking the cell with NaN (to keep ...
       track later)
40
41 L_ROI = L_ROI(max(1,U(1)-ROI): min(L_size,U(1)+ROI),:);
42
43 L_ROI = L_ROI(:, max(1,U(2)-ROI):min(L_size,U(2)+ROI));
44
45 [U_new(1) U_new(2)] = find(isnan(L_ROI)); %Finding U in the ...
       cropped matrix
46
47 L_ROI(isnan(L_ROI))= L_matrix(pos_U); %Replacing the actual ...
       value back
48
49 V = 0; % Initialising
50
51 [r c] = size(L_ROI);
52
53 for i = 1 : ROI
54
55     dummy =  L_ROI; % Dummy for calculating potential at ...
           i-th neighborhood
56
57     dummy = dummy(max(1,U_new(1)- i): min(r,U_new(1) + i),:);
58
59     dummy = dummy(:, max(1,U_new(2)- i):min(c,U_new(2) + i));
60
61     % Counting particles at the i-th Neighbourhood lattice ...
           cells
62     % Note: This will also count the particle(s) inside the ...
           i-th
63     % neighbourhood. But we are only interseted in the ...
           boundary cells
64
65     N(i) = sum(dummy(:));
66
67     % Subtracting all the redundant particles
68
69     if i == 1
70
71     N_eff= ...
           (N(i)-L_ROI(U_new(1),U_new(2)))*L_ROI(U_new(1),U_new(2));
72
73     else
74         N(i) = N(i) - N(i-1);
75
76         %Effective # of contributions = N(i) x (# of ...
               particles in ref. cell)
```

```
77          N_eff = N(i) * L_ROI(U_new(1),U_new(2));
78      end
79      % Calculating potential of the i-th neighbourhood and ...
            adding up
80
81      V = V + V_scheme(i)*N_eff;
82  end
```

Bibliography

[1] C.H.Chung and Y.T. Chen. Raman scattering of L-tryptophan enhanced by surface plasmon of silver nanoparticles: vibrational assignment and structural determination. *Journal of Raman Spectroscopy*, 40(2):150–156, 2009.

[2] K. Kneipp, H. Kneipp, I. Itzkan, R. R. Dasari, and M. S. Feld. Surface-enhanced Raman scattering and biophysics. *Journal of Physics: Condensed Matter*, 14(18):R597–R624, 2002.

[3] J. J. Mock, S. M. Norton, S.-Y. Chen, A. A. Lazarides, and D. R. Smith. Electromagnetic enhancement effect caused by aggregation on SERS-active gold nanoparticles. *Plasmonics*, 6(1):113–124, 2010.

[4] A . Campion and P. Kambhampati. Surface-enhanced raman scattering. *Chemical society reviews*, 27:241–250, 1998.

[5] J. M. Senior. *Optical fiber communications Principles and practice*. Prentice Hall, 2009.

[6] S. V. Karpov, A. L. Bas'ko, A. K. Popov, and V. V. Slabko. Optical Spectra of Silver Colloids Within the Framework of Fractal Physics. *Colloid Journal*, 62(6):699–713, 2000.

[7] A. Smekal. Zur quantentheorie der dispersion. *Die Naturwissenschaften*, 11(43):873–875, 1923.

[8] C. V. Raman and K. S. Krishnan. A new type of secondary radiation. *Nature*, 121:501–502, 1928.

[9] D. A. Long. *Raman Spectroscopy*. McGraw-Hill, 1977.

[10] P. J. Hendra M.Fleischmann and A. J. McQuillan. Raman spectra of pyridine adsorbed at a silver electrode. *Chemical Physics Letters*, 26(2):163–166, 1974.

[11] D. L.jeanmaire and R. P. Van Duyne. Surface Raman spectroelectrochemistry part1.Heterocyclic,aromatic and aliphatic amines adsorbed on the anodized siver electrode. *Journal of electroanalytical chemistry*, 84:1–20, 1977.

[12] S.K.Kim, M.S.Kim, and S.W.Suh. Surface-enhanced raman scattering(sers) of aromatic amino acids and their glycyl dipeptides in silver sol. *Journal of Raman spectroscopy*, 18:171–175, 1987.

[13] J. S. Suh and M. Moskovits. Surface-enhanced Raman spectroscopy of amino acids and nucleotide bases adsorbed on silver. *Journal of the American Chemical Society*, 108(16):4711–4718, 1986.

[14] A.E. Aliaga, I. Osorio-Roman, C. Garrido, P. Leyton, J. Cárcamo, E. Clavijo, J.S. Gómez-Jeria, G. Díaz F., and M.M. Campos-Vallette. Surface enhanced Raman scattering study of l-lysine. *Vibrational Spectroscopy*, 50(1):131–135, 2009.

[15] E.Podstawka, Y.Ozaki, and L.M.Proniewicz. Part I: surface-enhanced Raman spectroscopy investigation of amino acids and their homodipeptides adsorbed on colloidal silver. *Applied spectroscopy*, 58(5):570–80, 2004.

[16] S.Stewart and P.M. Fredericks. Surface-enhanced Raman spectroscopy of amino acids adsorbed on an electrochemically prepared silver surface. *Spectrochimica Acta Part A: Molecular and Biomolecular Spectroscopy*, 55(7-8):1641–1660, 1999.

[17] E.Podstawka, Y.Ozaki, and L.M.Proniewicz. Part III: Surface-enhanced Raman scattering of amino acids and their homodipeptide monolayers deposited onto colloidal gold surface. *Applied spectroscopy*, 59(12):1516–26, 2005.

[18] T. Park, S. Lee, G. H. Seong, J. Choo, E. K. Lee, Y. S. Kim, W. H. Ji, S. Y. Hwang, D.G. Gweon, and S. Lee. Highly sensitive signal detection

of duplex dye-labelled DNA oligonucleotides in a PDMS microfluidic chip: confocal surface-enhanced Raman spectroscopic study. *Lab on a chip*, 5:437–42, 2005.

[19] G. L. Liu and L. P. Lee. Nanowell surface enhanced Raman scattering arrays fabricated by soft-lithography for label-free biomolecular detections in integrated microfluidics. *Applied Physics Letters*, 87(7):074101, 2005.

[20] R. Keir, E. Igata, M. Arundell, W. E. Smith, C. Graham, D.and McHugh, and J. M. Cooper. SERRS. In situ substrate formation and improved detection using microfluidics. *Analytical chemistry*, 74(7):1503–8, 2002.

[21] D. R. Meldrum and M.R. Holl. Microscale bioanalytical systems. *Science*, 297:1197, 2002.

[22] S. K. Sia and G. M. Whitesides. Microfluidic devices fabricated in poly(dimethylsiloxane) for biological studies. *Electrophoresis*, 24(21):3563–76, 2003.

[23] P. S. Dittrich and A. Manz. Single-molecule fluorescence detection in microfluidic channels–the Holy Grail in muTAS? *Analytical and bioanalytical chemistry*, 382(8):1771–82, 2005.

[24] F.T. Docherty, P. B. Monaghan, R. Keir, D. Graham, W. E. Smith, and J. M. Cooper. The first SERRS multiplexing from labelled oligonucleotides in a microfluidics lab-on-a-chip. *Chemical communications (Cambridge, England)*, (1):118–9, 2004.

[25] A. E. Aliaga, I. Osorio-Román, P. Leyton, C. Garrido, J. Cárcamo, C. Caniulef, F. Célis, G. Díaz F., E. Clavijo, J. S. Gómez-Jeria, and M. M. Campos-Vallette. Surface-enhanced Raman scattering study of L-tryptophan. *Journal of Raman Spectroscopy*, 40(2):164–169, 2008.

[26] H.I. Lee and S.W. Suh. Raman Spectroscopy of L-Tryptophan-Containing Peptides Adsorbed on a silver surface. *Journal of Raman Spectroscopy*, 19:491–495, 1988.

[27] D. Qi and A. J. Berger. Quantitative analysis of Raman signal enhancement from aqueous samples in liquid core optical fibers. *Applied spectroscopy*, 58:1165–71, 2004.

[28] R. Altkorn, I. Koev, R. P. Van Duyne, and M. Litorja. Low-loss liquid-core optical fiber for low-refractive-index liquids: fabrication, characterization, and application in Raman spectroscopy. *Applied optics*, 36(34):8992–8, 1997.

[29] M. Holtz, P. K. Dasgupta, and G. Zhang. Small-Volume Raman Spectroscopy with a Liquid Core Waveguide. *Analytical Chemistry*, 71(14):2934–2938, 1999.

[30] A. Kandakkathara, I. Utkin, and R. Fedosejevs. Surface enhanced Raman scattering of amino acids and peptides. *Physica Status Solidi (C)*, 6(S1):S27–S30, May 2009.

[31] M. G. Albrecht and J. A.Creighton. Anomalously intense raman spectra of pyridine at a silver electrode. *Journal of the American Chemical Society*, 99:5215–5217, 1977.

[32] H. Seki. Raman spectra of molecules considered to be surface enhanced. *Journal of Electron Spectroscopy and Related Phenomena*, 39:289–310, 1986.

[33] M. Moskovits. Surface-enhanced spectroscopy. *Reviews of Modern Physics*, 57:783, 1985.

[34] J. A. Dieringer, A.D. McFarland, N. C. Shah, D. A. Stuart, A. V. Whitney, C. R. Yonzon, M. A. Young, X. Zhang, and R.P. Van Duyne. Introductory lecture : Surface enhanced raman spectroscopy: new materials, concepts, characterization tools, and applications. *Faraday Discussions*, 132:9, 2006.

[35] H. Xu, J. Aizpurua, M. Kall, and P. Apell. Electromagnetic contributions to single-molecule sensitivity in surface-enhanced raman scattering. *Physical review. E, Statistical physics, plasmas, fluids, and related interdisciplinary topics*, 62:4318–24, 2000.

[36] M. Inouse and K. Ohtaka. Surface enhanced Raman scattering by metal spheres. 1. Cluster effect. *Jounral of the Physical Society of Japan*, pages 3853–3864, 1983.

[37] S. Nie. Probing Single Molecules and Single Nanoparticles by Surface-Enhanced Raman Scattering. *Science*, 275:1102–1106, 1997.

[38] K. Kneipp, Y. Wang, H. Kneipp, L. T. Perelman, R. R. Itzkan, I.and Dasari, and M.S. Feld. Single Molecule Detection Using Surface-Enhanced Raman Scattering (SERS). *Physical review letters*, 78:1667–1670, 1997.

[39] D.K. Lim, K. Jeon, J. H. Hwang, H. Kim, S. Kwon, Y. D. Suh, and J. M. Nam. Highly uniform and reproducible surface-enhanced raman scattering from DNA-tailorable nanoparticles with 1-nm interior gap. *Nature Nanotechnology*, 6:452–460, 2011.

[40] W. H. Park and Z. H. Kim. Charge transfer enhancement in the SERS of a single molecule. *Nano Letters*, 10:4040–4048, 2012.

[41] J. R. Ferraro, K. Nakamoto, and C. W. Brown. *Introductory Raman spectroscopy*. Academic Press, 2003.

[42] K. Kneipp, H. Kneipp, I. Itzkan, R. R. Dasari, and M. S. Feld. Ultra-sensitive chemical analysis by Raman spectroscopy. *Chemical reviews*, 99(10):2957–76, 1999.

[43] E. C. Le Ru and P. G. Etchegoin. *Principles of Surface-Enhanced Raman Spectroscopy and Related Plasmonic Effects*. Elsevier, 2009.

[44] W. L Barnes, A. Dereux, and T. W. Ebbesen. Subwavelength optics. *Nature*, 424:824–831, 2003.

[45] M. Moskovits. Surface-Enhanced raman spectroscopy: a brief perspective. In K. Kneipp, M. Moskovits, and H. Kneipp, editors, *Topics in Applied Physics*, volume 103, pages 1–17. Springer Berlin / Heidelberg, 2006.

[46] L.A.Bumm M. Kerker, O.Siiman and D.S.Wang. Surface enhanced Raman scattering (SERS) of citrate ion adsorbed on colloidal silver. *Applied optics*, 19:3253–3255, 1980.

[47] E. J. Zeman and G. C. Schatz. An Accurate Electromagnetic Theory Study of Surface Enhancement Factors for Ag, Au, Cu, Li, Na, AI, Ga, In, Zn, and Cd. 91(3):634–643, 1987.

[48] M. Kerker. Electromagnetic model for surface-enhanced raman scattering (SERS) on metal colloids. *Accounts of chemical research*, 17:271–277, 1984.

[49] I. Romero, J. Aizpurua, G. W Bryant, and F. J. Abajo. Plasmons in nearly touching metallic nanoparticles: singular response in the limit of touching dimers. *Optics express*, 14:9988–99, 2006.

[50] A.-S. Grimault, A. Vial, and M. L. Chapelle. Modeling of regular gold nanostructures arrays for SERS applications using a 3D FDTD method. *Applied Physics B*, 84:111–115, 2006.

[51] H. Xu, J. Aizpurua, M. Kall, and P. Apell. Electromagnetic contributions to single-molecule sensitivity in surface-enhanced raman scattering. *Physical Review E*, 62(3):4318–4324, 2000.

[52] E. Hao and G. C. Schatz. Electromagnetic fields around silver nanoparticles and dimers. *The Journal of Chemical Physics*, 120:357–366, 2004.

[53] L. V. Brown, H. Sobhani, J. B. Lassiter, P. Nordlander, and N. J. Halas. Heterodimers: Plasmonic properties of mismatched nanoparticle pairs. *ACS Nano*, 4(2):819–832, 2012.

[54] M. Rycenga, P. H. C. Camargo, W. Li, C. H. Moran, and Y. Xia. Understanding the SERS effects of single silver nanoparticles and their dimers, one at a time. *The Journal of the Physical Chemistry Letters*, 1(4):696–703, 2012.

[55] R. J. C Brown, J. Wang, R. Tantra, R. E Yardley, and M. J. T. Milton. Electromagnetic modelling of raman enhancement from nanoscale substrates: a route to estimation of the magnitude of the chemical enhance-

ment mechanism in SERS. *Faraday Discussions*, 132:201–213, 2006. PMID: 16833118.

[56] R. J. C. Brown, J. Wang, and M. J. T. Milton. Electromagnetic modelling of raman enhancement from nanoscale structures as a means to predict the efficacy of SERS substrates. *Journal of Nanomaterials*, 2007:1–10, 2007.

[57] G. C. Schatz and R. P. Van Duyne. *Electromagnetic Mechanism of Surface-enhanced Spectroscopy*. John Wiley & Sons, Ltd. Chichester, 2002.

[58] K. Kneipp, H. Kneipp, V. Kartha, R. Manoharan, G. Deinum, R. Itzkan, I.and Dasari, and M. Feld. Detection and identification of a single DNA base molecule using surface-enhanced Raman scattering (SERS). *Physical Review E*, 57:R6281–R6284, 1998.

[59] A. Otto. Theory of first layer and single molecule surface enhanced raman scattering (SERS). *physica status solidi (a)*, 188:1455–1470, 2001.

[60] P. Kambhampati, C. M. Child, M. C. Foster, and A. Campion. On the chemical mechanism of surface enhanced Raman scattering: Experiment and theory. *The Journal of Chemical Physics*, 108:5013, 1998.

[61] J. A. Creighton, C. G. Blatchford, and M. G. Albrecht. Plasma resonance enhancement of Raman scattering by pyridine adsorbed on silver or gold sol particles of size comparable to the excitation wavelength. *Journal of the Chemical Society, Faraday Transactions 2*, 75:790, 1979.

[62] P. C. Lee and D. Meisel. Adsorption and surface-enhanced Raman of dyes on silver and gold sols. *The Journal of Physical Chemistry*, 86:3391–3395, 1982.

[63] A. Henglein. Physicochemical properties of small metal particles in solution: "microelectrode" reactions, chemisorption, composite metal particles, and the atom-to-metal transition. *The Journal of Physical Chemistry*, 97(21):5457–5471, 1993.

[64] M. Prochazka, J. Stepaneka, B. Vickova, I. Srnova, and P. Maly. Laser ablation: Preparation of "chemically pure" Ag colloids for surface-enhanced Raman scattering spectroscopy. *Journal of Molecular Structure*, 410-411:213–216, 1997.

[65] M. Green and F. M. Liu. SERS substrates fabricated by island lithography: The Silver/Pyridine system. *Jounral of Physical chemistry B*, 107(47):13015–13021, 2011.

[66] E.C. LeRu, P.G. Etchegoin, J. Grand, N. Felidj, J. Aubard, G. Levi, A. Hohenau, and J. Krenn. Surface enhanced Raman spectroscopy on nanolithography-prepared substrates. *Current Applied Physics*, 8:467–470, 2008.

[67] N. Felidj, J. Aubard, G. Lvi, J. R. Krenn, M. Salerno, G. Schider, B. Lamprecht, A. Leitner, and F. R. Aussenegg. Controlling the optical response of regular arrays of gold particles for surface-enhanced raman scattering. *Physical Review B*, 65(7):075419, 2002.

[68] A. G. Brolo, E. Arctander, R. Gordon, B. Leathem, and K. L. Kavanagh. Nanohole-Enhanced raman scattering. *Nano Letters*, 4:2015–2018, 2004.

[69] N. Felidj, J. Aubard, G. Levi, J. R. Krenn, A. Hohenau, G. Schider, A. Leitner, and F. R. Aussenegg. Optimized surface-enhanced raman scattering on gold nanoparticle arrays. *Applied Physics Letters*, 82:3095 –3097, 2003.

[70] A. G. Brolo, R. Gordon, B. Leathem, and K. L. Kavanagh. Surface plasmon sensor based on the enhanced light transmission through arrays of nanoholes in gold films. *Langmuir*, 20(12):4813–4815, 2004.

[71] Y. Lu, G.L. Liu, and L. P. Lee. High-Density silver nanoparticle film with Temperature-Controllable interparticle spacing for a tunable surface enhanced raman scattering substrate. *Nano Letters*, 5:5–9, 2011.

[72] J. Aizpurua, P. Hanarp, D. S. Sutherland, M. Kall, G. W. Bryant, and F. J. Abajo. Optical properties of gold nanorings. *Physical Review Letters*, 90:057401, 2003.

[73] C. J. Murphy, T. K. Sau, A. M. Gole, C. J. Orendorff, J. Gao, L. Gou, S. E. Hunyadi, and T. Li. Anisotropic metal nanoparticles: synthesis, assembly, and optical applications. *Jounral of Physical chemistry B*, 109:13857–13870, 2005.

[74] S. J. Oldenburg, J. B. Jackson, S. L. Westcott, and N. J. Halas. Infrared extinction properties of gold nanoshells. *Applied Physics Letters*, 75:2897, 1999.

[75] M. G. Moffitt C. M. S. Izumi and A. G. Brolo. Statistics on Surface-Enhanced resonance raman scattering from single nanoshells. *Jounral of Physical chemistry C*, 115(39):19104–19109, 2012.

[76] A. Lee, G. F. S. Andrade, A. Ahmed, M. L. Souza, N. Coombs, E. Tumarkin, K. Liu, R. Gordon, Al. G. Brolo, and E. Kumacheva. Probing dynamic generation of Hot-Spots in Self-Assembled chains of gold nanorods by Surface-Enhanced raman scattering. *Jounral of American Chemical Society*, 133(19):7563–7570, 2011.

[77] J. B. Jackson, S. L. Westcott, L. R. Hirsch, J. L. West, and N. J. Halas. Controlling the surface enhanced raman effect via the nanoshell geometry. *Applied Physics Letters*, 82:257, 2003.

[78] E. Prodan, P. Nordlander, and N. J. Halas. Electronic structure and optical properties of gold nanoshells. *Nano Letters*, 3(10):1411–1415, 2003.

[79] M. Fan, G. F.S. Andrade, and A. G. Brolo. A review on the fabrication of substrates for surface enhanced raman spectroscopy and their applications in analytical chemistry. *Analytica Chimica Acta*, 693:7–25, 2011.

[80] M. Fan and A. G Brolo. Self-assembled au nanoparticles as substrates for surface-enhanced vibrational spectroscopy: optimization and electrochemical stability. *Chemphyschem: A European Journal of Chemical Physics and Physical Chemistry*, 9:1899–1907, 2008.

[81] G. F. S Andrade, M. Fan, and A. G Brolo. Multilayer silver nanoparticles-modified optical fiber tip for high performance SERS remote sensing. *Biosensors & Bioelectronics*, 25(10):2270–2275, 2010.

[82] R. R.Sato-Berru, R. Redon, A. Vaquez-Olmos, and J. M. Saniger. Silver nanoparticles synthesized by direct photoreduction of metal salts. application in surface-enhanced raman spectroscopy. *Journal of Raman Spectroscopy*, 40(4):376–380, 2009.

[83] O. Lyandres, N. C Shah, C.R.Yonzon, J. T Walsh, M. R Glucksberg, and R. P Van Duyne. Real-time glucose sensing by surface-enhanced raman spectroscopy in bovine plasma facilitated by a mixed decanethiol/mercaptohexanol partition layer. *Analytical Chemistry*, 77:6134–6139, 2005.

[84] A. Barhoumi, D. Zhang, F. Tam, and N. J. Halas. Surface-enhanced Raman spectroscopy of DNA. *Journal of the American Chemical Society*, 130(16):5523–9, 2008.

[85] H. Li, J. Sun, and B. M. Cullum. Label-Free Detection of Proteins Using SERS-Based Immuno-Nanosensors. *Proteins*, 2:17–28, 2006.

[86] X. X Han, H. Y Jia, Y. F Wang, Z. C Lu, C. X Wang, W.Q. Xu, B. Zhao, and Y. Ozaki. Analytical technique for label-free multi-protein detection based on Western blot and surface-enhanced Raman scattering. *Analytical chemistry*, 80(8):2799–804, 2008.

[87] R. M Jarvis and R. Goodacre. Characterisation and identification of bacteria using SERS. *Chemical Society reviews*, 37:931–6, 2008.

[88] A. Sengupta and E. J. Laucks, M. L .and Davis. Surface-enhanced Raman spectroscopy of bacteria and pollen. *Applied spectroscopy*, 59(8):1016–23, 2005.

[89] S. Shanmukh, L. Jones, J. Driskell, Y. Zhao, R . Dluhy, and R. A Tripp. Rapid and sensitive detection of respiratory virus molecular signatures using a silver nanorod array SERS substrate. *Nano letters*, 6:2630–6, 2006.

[90] T. Vo-Dinh and D.L. Stokes. *Biomedical Photonics Handbook*. CRC Press, 1 edition, 2003.

[91] S. C Pinzaru, I. Pavel, N. Leopold, and W. Kiefer. Identification and characterization of pharmaceuticals using raman and surface-enhanced raman scattering. *Journal of Raman Spectroscopy*, 35:338–346, 2004.

[92] K. Kneipp S. R. Emory, S. Nie and G. R. Harrison. Single-molecule raman spectroscopy - fact or fiction? *Chimia*, 53:35–37, 1999.

[93] M.S. Anderson. Locally enhanced raman spectroscopy with an atomic force microscope. *Applied Physics Letters*, 76:3130, 2000.

[94] B. Pettinger, G. Picardi, R. Schuster, and G.Ertl. Surface-enhanced and STM-tip-enhanced raman spectroscopy at metal surfaces. *Single Molecules*, 3:285–294, 2002.

[95] J. S. Schwegler, M. C. Knorz, I. Akkoyun, and H. Liesenhoff. Basic, not acidic fibroblast growth factor stimulates proliferation of cultured human retinal pigment epithelial cells. *Molecular Vision*, 3:10, 1997.

[96] http://www.britannica.com/EBchecked/topic/479680/protein.

[97] http://www.catalinasci.com/WEBPDF/SE200_1.pdf.

[98] http://riodb01.ibase.aist.go.jp/sdbs/.

[99] C. S. Seney, B. M. Gutzman, and R. H. Goddard. Correlation of size and Surface-Enhanced raman scattering activity of optical and spectroscopic properties for silver nanoparticles. *J. Phys. Chem. C*, 113:74–80, 2012.

[100] O. Siiman, L. A. Bumm, R. Callaghan, C. G. Blatchford, and M. Kerker. Surface-enhanced raman scattering by citrate on colloidal silver. *J. Phys. Chem.*, 87:1014–1023, 2012.

[101] R. L. Garrell. Probing Biomolecule-Surface Interactions with Surface-Enhanced Raman Spectroscopy. *Journal of Bioactive and Compatible Polymers*, 6(3):296–307, 1991.

[102] G. D. Chumanov, R. G. Efremov, and I. R. Nabiev. Surface-enhanced Raman spectroscopy of biomolecules. Part I.water-soluble proteins, dipeptides and amino acids. *Journal of Raman Spectroscopy*, 21(1):43–48, 1990.

[103] Z. Pan, S. H. Morgan, A. Ueda, R. Mu, Y. Cui, M. Guo, A. Burger, and Y. Yeh. Surface-enhanced Raman probing of biomolecules using Ag-coated porous glass-ceramic substrates. *Journal of Raman Spectroscopy*, 36(11):1082–1087, 2005.

[104] M. Ishikawa, Y. Maruyama, J. Ye, and M. Futamata. Single-Molecule Imaging and Spectroscopy Using Fluorescence and Surface-Enhanced Raman Scattering. *Journal of Biological Physics*, 28(4):573–585, 2002.

[105] E. Podstawka, Y. Ozaki, and L. M. Proniewicz. Adsorption of S-S containing proteins on a colloidal silver surface studied by surface-enhanced Raman spectroscopy. *Applied spectroscopy*, 58(10):1147–56, 2004.

[106] T. M. Herne, A. Ahern, and R. L. Garrell. Surface-enhanced Raman spectroscopy of peptides: preferential N-terminal adsorption on colloidal silver. *Journal of the American Chemical Society*, 113(3):846–854, 1991.

[107] A. Kandakkathara, I. Utkin, and R. Fedosejevs. Surface-enhanced Raman scattering detection of amino acids and peptides in a microfluidic device. *Proceedings of SPIE*, 7386:73860A–73860A–7, 2009.

[108] K. Walter and S. Hans. *L-Tryptophan: Current Prospects in Medicine and Drug Safety*. Walter de Gruyter, 1 edition, 1994.

[109] N. R. Yaffe and E. W. Blanch. Effects and anomalies that can occur in SERS spectra of biological molecules when using a wide range of aggregating agents for hydroxylamine-reduced and citrate-reduced silver colloids. *Vibrational Spectroscopy*, 48(2):196–201, 2008.

[110] J. I. Millan, J. V. Garcia-Ramos, S. Sanchez-Cortes, and R. Rodriguez-Amaro. Adsorption of lucigenin on Ag nanoparticles studied by surface-enhanced Raman spectroscopy: effect of different anions on the intensification of Raman spectra. *Journal of Raman Spectroscopy*, 34(3):227–233, 2003.

[111] E. Hobbs and E. Hass. *Vitamins For Dummies*. For Dummies; 1 edition, May 2011.

[112] S. D. Schwab and R. L. McCreery. Versatile, efficient raman sampling with fiber optics. *Analytical chemistry*, 56:2199–2204, 1984.

[113] S. D. Schwab and R. L. McCreery. Remote, Long-Pathlength cell for High-Sensitivity raman spectroscopy. *Applied Spectroscopy*, 41:126–130, 1987.

[114] K. Tsunoda, A. Nomura, J. Yamada, and S. Nishi. The possibility of signal enhancement in liquid absorption spectrometry with a long capillary cell utilizing successive total reflection at the outer cell surface. *Applied Spectroscopy*, 43:49–55, 1989.

[115] S. Tanikkul, J. Jakmunee, M. Rayanakorn, K. Grudpan, B. J. Marquardt, G. M. Gross, B. J. Prazen, L. W . Burgess, G. D Christian, and R. E Synovec. Characterization and use of a raman liquid-core waveguide sensor using preconcentration principles. *Talanta*, 59:809–816, 2003.

[116] M. J. Pelletier and R. Altkorn. Raman sensitivity enhancement for aqueous protein samples using a Liquid-Core Optical-Fiber cell. *Analytical Chemistry*, 73:1393–1397, 2001.

[117] R. Altkorn, I. Koev, and M. J. Pelletier. Raman Performance Characteristics of Teflon-AF 2400 Liquid-Core Optical-Fiber Sample Cells. *Applied Spectroscopy*, 53:1169–1176, 1999.

[118] G. M. Whitesides and A. D. Stroock. Flexible methods for microfluidics. *Physics Today*, 54(6):42, 2001.

[119] D. Lee, S. Lee, G. H. Seong, J. Choo, E. K. Lee, D. G. Gweon, and S. Lee. Quantitative analysis of methyl parathion pesticides in a polydimethylsiloxane microfluidic channel using confocal surface-enhanced Raman spectroscopy. *Applied spectroscopy*, 60:373–7, 2006.

[120] S. Lee, J. Choi, L. Chen, B. Park, J. B. Kyong, G. H. Seong, J. Choo, Y. Lee, K. H. Shin, E. K. Lee, S. W. Joo, and K. H. Lee. Fast and sensitive trace analysis of malachite green using a surface-enhanced Raman microfluidic sensor. *Analytica chimica acta*, 590:139–44, 2007.

[121] N. A. Abu-Hatab, J. F. John, J. M. Oran, and M. J. Sepaniak. Multiplexed microfluidic Surface-Enhanced raman spectroscopy. *Applied Spectroscopy*, 61:1116–1122, 2007.

[122] A. Walter, A. MarZ, W. Schumacher, P. Rosch, and J. Popp. Towards a fast, high specific and reliable discrimination of bacteria on strain level by means of SERS in a microfluidic device. *Lab on a chip*, 11:1013–21, 2011.

[123] L. M. Cabalin and J. J. Ruperez, A. Laserna. Flow-injection analysis and liquid chromatography: surface-enhanced Raman spectrometry detection by using a windowless flow cell. *Analytica Chimica Acta*, 318:203–210, 1996.

[124] G. T. Taylor, S. K. Sharma, and K. Mohanan. Optimization of a Flow Injection Sampling System for Quantitative Analysis of Dilute Aqueous Solutions Using Combined Resonance and Surface-Enhanced Raman Spectroscopy (SERRS). *Applied Spectroscopy*, 44:635–640, 1990.

[125] http://www.micralyne.com/microfluidic-chips/.

[126] http://www.biogeneral.com/teflon.html.

[127] F. Eftekhari, J. Irizar, L. Hulbert, and A. S. Helmy. A comparative study of raman enhancement in capillaries. *Journal of Applied Physics*, 109:113104, 2011.

[128] D. Qi and A. J Berger. Chemical concentration measurement in blood serum and urine samples using liquid-core optical fiber Raman spectroscopy. *Applied optics*, 46:1726–34, 2007.

[129] J. Irizar, J. Dinglasan, J.B. Goh, A. Khetani, H. Anis, D. Anderson, C. Goh, and A.S. Helmy. Raman spectroscopy of nanoparticles using Hollow-Core photonic crystal fibers. *IEEE Journal ofSelected Topics in Quantum Electronics*, 14:1214–1222, 2008.

[130] D. Yin J. Z. Zhang E. J. Lunt P. Measor, L. Seballos, A. R. Hawkins, and H. Schmidt. On-chip surface-enhanced raman scattering detection using

integrated liquid-core waveguides. *Applied Physics Letters*, 90:211107, 2007.

[131] M. C. J. Large F. M. Cox, A. Argyros and S. Kalluri. Surface enhanced raman scattering in a hollow core microstructured optical fiber. *Optics Express*, 15:13675–13681, 2007.

[132] C. Shi Y. Zhang, L. Seballos C. Gu, and J. Z. Zhang. Liquid core photonic crystal fiber sensor based on surface enhanced raman scattering. *Applied Physics Letters*, 90(19):193504, 2007.

[133] L. X. Quang, C. Lim, G. H. Seong, J. Choo, K. J. Do, and S.K. Yoo. A portable surface-enhanced Raman scattering sensor integrated with a lab-on-a-chip for field analysis. *Lab on a Chip*, 8(12):2214–9, 2008.

[134] I. H. Chou M. Wang, N. Jing, G. L. Cote, and J. Kameoka. An optofluidic device for surface enhanced raman spectroscopy. *Lab on a Chip*, 7:630, 2007.

[135] A. Kandakkathara, I. Utkin, and R.Fedosejevs. Surface-enhanced raman scattering (sers) detection of low concentrations of tryptophan amino acid in silver colloid. *Applied spectroscopy*, 65(5):507–513, 2011.

[136] B.Giese and D.McNaughton. Surface-Enhanced Raman Spectroscopic and Density Functional Theory Study of Adenine Adsorption to Silver Surfaces. *The Journal of Physical Chemistry B*, 106(1):101–112, 2002.

[137] E.Smith and G.Dent. *Modern Raman spectroscopy: a practical approach*. John Wiley and Sons, January 2005.

[138] G.D Fleming, J.J Finnerty, M. Campos-Vallette, F. Célis, C.Fredes A.E. Aliaga, and R. Koch. Experimental and theoretical Raman and surface-enhanced Raman scattering study of cysteine. *Journal of Raman Spectroscopy*, 40(6):632–638, 2009.

[139] R.C.Brown, J.Wang, R.Tantra, R.E. Yardley, and M.T.Milton. Electromagnetic modelling of Raman enhancement from nanoscale substrates: a route to estimation of the magnitude of the chemical enhancement mechanism in SERS. *Faraday Discussions*, 132(0):201, 2006.

[140] W. E. Doering and S. Nie. Single-Molecule and Single-Nanoparticle SERS: examining the roles of surface active sites and chemical enhancement. *Journal of Physical Chemistry B.*, 106:311–317, 2002.

[141] L. Sun, D. Zhao, M. Ding, Z. Xu, Z. Zhang, B. Li, and D. Shen. Controllable synthesis of silver nanoparticle aggregates for Surface-Enhanced raman scattering studies. *Journal of Physical Chemistry C.*, 115:16295–16304, 2011.

[142] A. Otto, A. Bruckbauer, and Y.X. Chen. On the chloride activation in SERS and single molecule SERS. *Journal of Molecular Structure*, 661-662:501–514, 2003.

[143] H. Wetzel and H. Gerischer. Surface ennhanced Raman scattering fom pyridine and halide ions adsorbed on silver and gold sol particles. *Chemical Physics Letters*, 76(3):460–464, 1980.

[144] C. Bengter, H. Tengroth and S. P. Jacobsson. New light on Ag-colloid preparation for surface-enhanced FT-Raman spectroscopy: the role of aggregation. *Journal of Raman Spectroscopy*, 36(11):1015–1022, 2005.

[145] M. Cyrankiewicz, T. Wybranowski, and S. Kruszewski. Study of SERS efficiency of metallic colloidal systems. *Journal of Physics: Conference Series*, 79:012013, August 2007.

[146] W. Grochala, A. Kudelski, and J. Bukowska. Anion-induced charge-transfer enhancement in sers and serrs spectra of rhodamine 6g on a silver electrode: how important is it? *Journal of Raman Spectroscopy*, 29(8):681–685, 1998.

[147] G. Levi, J. Pantigny, J. P. Marsault, and J. Aubard. Sers spectra of acridine and acridinium ions in colloidal silver sols. electrolytes and ph effects. *Journal of Raman Spectroscopy*, 24(11):745–752, 1993.

[148] S. T. Oh, K. Kim, and M. S. Kim. Adsorption and surface reaction of acridine in silver sol: surface-enhanced raman spectroscopic study. *The Journal of Physical Chemistry*, 95(22):8844–8849, 1991.

[149] Z. Zhou, I. Yang, G. G. Huang, and Y. Ozaki. Co-adsorption of electrolyte and protein to Ag colloid observed by surface-enhanced Raman scattering. *The Analyst*, 135(9):2372–6, 2010.

[150] P. Hildebrandt, S. Keller, A. Hoffmann, F. Vanhecke, and B. Schrader. Enhancement factor of surface-enhanced raman scattering on silver and gold surfaces upon near-infrared excitation. indication of an unusual strong contribution of the chemical effect. *Journal of Raman Spectroscopy*, 24(11):791–796, 1993.

[151] B. D. Howes, L. Guerrini, S. Sanchez-cortes, M. P Marzocchi, and G. Smulevich. The influence of pH and anions on the adsorption mechanism of rifampicin on silver colloids. *Journal of Raman Spectroscopy*, 38:859–864, 2007.

[152] S. Schneider, H. Grau, P. Halbig, P. Freunscht, and U. Nickel. Stabilization of Silver Colloids by Various Types of Anions and Their Effect on the Surface-Enhanced Raman Spectra of Organic Dyes. *Journal of Raman Spectroscopy*, 27(1):57–68, 1996.

[153] E. J. Liang and W. Kiefer. Chemical Effect ofSERS with Near-Infrared Excitation. *Journal of Raman Spectroscopy*, 27(12):879–885, 1996.

[154] L. Kvitek, R. Prucek, A. Panacek, R. Novotny, J. Hrbac, and R. Zboril. The influence of complexing agent concentration on particle size in the process of SERS active silver colloid synthesis. *Journal of Materials Chemistry*, 15(10):1099, 2005.

[155] Z. Darzynkiewicz. Differential Staining of DNA and RNA in Intact Cells and Isolated Cell Nuclei with Acridine Orange. *Methods in Cell Biology*, 33:285–298, 1990.

[156] G. S. Sakovich V. N. Konyukhov, T. N. Perekhozheva Z. V. Pushkareva, G. M. Anoshina, and A. S. Barybin. Derivatives of acridine orange and their biological activity. *Pharmaceutical chemistry journal*, 13:47–50, 1979.

[157] F. Zimmerman, B. Hossenfelder, J.-C. Panitz, and a. Wokaun. SERRS study of Acridine Orange and Its Binding to DNA Strands. *The Journal of Physical Chemistry*, 98(48):12796–12804, 1994.

[158] E. Koglin and M. J. Schwuger. In situ analysis of adsorbed molecules by microsurface-enhanced Raman scattering. *Faraday Discussions*, 94:213, 1992.

[159] K. Kneipp, Y. Wang, R. R. Dasari, and M. S. Feld. Approach to Single Molecule Detection Using Surface-Enhanced Resonance Raman Scattering (SERRS): A Study Using Rhodamine 6G on Colloidal Silver. *Applied Spectroscopy*, 49(6):780–784, 1995.

[160] A. M. Michaels and L. Brus. Ag Nanocrystal Junctions as the Site for Surface-Enhanced Raman Scattering of Single Rhodamine 6G Molecules. *The Journal of Physical Chemistry B*, 104(50):11965–11971, 2000.

[161] J. A. Dieringer, K. L. Wustholz, D. J. Masiello, J. P. Camden, S. L. Kleinman, G. C. Schatz, and R. P. Van Duyne. Surface-Enhanced raman excitation spectroscopy of a single rhodamine 6G molecule. *Jounral of American Chemical Society*, 131(2):849–854, 2009.

[162] K. Kim S. T. Oh and M.S. Kim. Adsorption and Surface Reaction of Acridine in Silver Sol: Surface-Enhanced Raman Spectroscopic Study. *Journal of Physical Chemistry*, pages 8844–8849, 1991.

[163] C. Fang, A. Agarwal, K. Devi, N. Mohamed, S. Mohamed, E. Widjaja, M. V. Garland, N. Balasubramanian, and D. Kwong. DNA detection using nanostructured SERS substrates with Rhodamine B as Raman label. *Biosensors and Bioelectronics*, 24:216–221, 2008.

[164] J. Xie, Q. Zhang, J. Y. Lee, and D. C. Wang. The Synthesis of SERS-Active Gold Nanoflower Tags for In Vivo Applications. *ACS nano*, 2(12):2473–2480, 2008.

[165] http://www.hagen.com/pdf/aquatic/Elite_LeafletUL_USA.pdf.

[166] R. Aroca. *Surface-Enhanced Vibrational Spectroscopy*. Wiley, 1 edition, 2006.

[167] B. Derjaguin and L. Landau. Theory of the stability of strongly charged lyophobic sols and of the adhesion of strongly charged particles in solutions of electrolytes. *Acta physicochim URSS*, 14:633, 1941.

[168] W. Verwey E. Johannes and J. T. G. Overbeek. *Theory of the Stability of Lyophobic Colloids*. Elsevier, 1948.

[169] M. Meyer, E. C. Le Ru, and P. G. Etchegoin. Self-limiting aggregation leads to long-lived metastable clusters in colloidal solutions. *The journal of physical chemistry. B*, 110(12):6040–7, 2006.

[170] M. Regier and H. P. Schuchmann. Monte carlo simulations of observation Time-Dependent Self-Diffusion in porous media models. *Transport in Porous Media*, 59(1):115–126, 2005.

[171] D. F. Evans and H. Wennerstrom. *The Colloidal Domain: Where Physics, Chemistry, Biology, and Technology Meet*. Wiley-VCH, 2 edition, 1999.

[172] K. L Wu and S. K Lai. Theoretical studies of the early stage coagulation kinetics for a charged colloidal dispersion. *Langmuir: The ACS Journal of Surfaces and Colloids*, 21:3238–3246, 2005.

[173] F. Grinberg and P. Heitjans. *Diffusion Fundamentals Leipzig 2005*. Leipziger Universittsverlag, 2005.

[174] H.Mehrer. *Diffusion in solids: fundamentals, methods, materials, diffusion-controlled processes*. Springer, 2007.

[175] P. B. Johnson and R. W. Christy. Optical constants of the noble metals. *Physical Review B*, 6(12):4370–4379, 1972.

[176] L. Novotny and B. Hecht. *Principles of nano-optics*. Cambridge University Press, 2006.